

AN EXPERIMENTAL STUDY OF BAROCLINIC INSTABILITY IN A
ROTATING ANNULUS OF LIQUID

by

Carl B. Ketchum

M.S., New York University

1967

B.S., Bates College

1962

SUBMITTED IN PARTIAL FULFILLMENT

OF THE REQUIREMENTS FOR THE

DEGREE OF DOCTOR OF

PHILOSOPHY

at the

MASSACHUSETTS INSTITUTE OF

TECHNOLOGY

May 1968

Signature of Author

Department of Geology and Geophysics

Certified by

Thesis Supervisor

Accepted by

Chairman, Departmental Committee
on Graduate Students

WITHDRAWN
FROM
MIT LIBRARIES

AN EXPERIMENTAL STUDY OF BAROCLINIC INSTABILITY IN A
ROTATING ANNULUS OF LIQUID

by

slurk
Carl B. Ketchum

M.S., New York University

1967

B.S., Bates College

1962

SUBMITTED IN PARTIAL FULFILLMENT

OF THE REQUIREMENTS FOR THE

DEGREE OF DOCTOR OF

PHILOSOPHY

at the

MASSACHUSETTS INSTITUTE OF

TECHNOLOGY

May 1968

Signature of Author

Department of Geology and Geophysics

Certified by

Thesis Supervisor

Accepted by

Chairman, Departmental Committee
on Graduate Students

To Beverly, Andrew and Todd

ABSTRACT

A detailed study of the flow regimes and internal temperature structure at 16 points in the convecting fluid in a rotating annulus of liquid with a gap width of 15.28 cm. has been made. The results have been analyzed with respect to the position of the regimes of flow on a Π_4 versus Π_5 diagram and the internal parameters of the fluid determined from the temperature structure. The primary emphasis of the study was placed on the temperature structure of the regular wave regime.

The results indicate that the value of Π_{4c}^* at the transition from the symmetric flow to the regular wave regime is 3.746 ± 0.360 for $2.750 \times 10^7 \leq \Pi_5 \leq 9.721 \times 10^7$. The value of Π_{4c}^* has a slight tendency to increase with increasing Π_5 . The vacillating flow did not occur until Π_5 was greater than 1.737×10^9 , and the irregular flow did not occur until Π_5 was greater than 7.259×10^9 .

The vertical stability of the fluid increases with increasing rotation rate in the symmetric regime and remains almost constant within the wave regime. The value of the Eady number exceeds the critical value for the observed wave number at several experimental points in the wave regime and always at the transition between the symmetric regime and the wave regime. The observed value of the wave number is seldom the wave number with the theoretical maximum growth rate as determined from Eady's theory.

The radial available potential energy of the fluid increases with increasing rotation rate in the symmetric,

vacillating and irregular regimes. This value decreases with increasing rotation rate in the wave regime, while the value of the zonal available potential energy increases. The total available potential energy increases with increasing rotation rate in the symmetric, vacillating and irregular regimes, while it is almost constant within the wave regime.

The maximum wave amplitude in the regular wave regime generally occurs in the upper half of the fluid, while the maximum amplitude of the disturbance in the vacillating and irregular regime is more likely to occur in the lower half of the fluid. The radially averaged phase of the regular waves in the upper half of the fluid leads that in the lower half, and the vertical difference in phase tends to decrease with increasing rotation rate. The phase period of the disturbance increases in the wave regime and increases more rapidly in the vacillating regime with increasing rotation rate. The periods of the disturbance in the irregular regime are more characteristic of that in the wave regime than in the vacillating regime except that the disturbance has at least two distinct and significant components.

TABLE OF CONTENTS

	<u>Page</u>
Abstract	
Acknowledgements	iii
List of figures	v
List of tables	viii
Range of parameters	ix
I Introduction	1
II Review of previous work	7
Previous experimental results	7
Previous numerical and theoretical results	11
III Description of the apparatus and the experimental procedure	32
Apparatus	32
Experimental procedure	35
IV Presentation and interpretation of the results	40
Flow regimes	41
Interior temperature structure	44
Spectral analysis	54
V Side wall boundary layers and the effect of the thermocouples on the flow	58
VI Summary and suggestions for future work	61
References	65
Appendices	
I Design and construction of the 42 inch annulus	71
Turntable and drive mechanism	72
Convection chamber and baths	73
Convection chamber thermocouples	77
Electrical recording and measuring systems	79
Discussion of error	80
Suggestions for future modifications	82

	<u>Page</u>
II Methods for the calculation of external and internal parameters, available potential energy and time series analysis	83
Autobiographical note	91

ACKNOWLEDGEMENTS

I am indebted to Professor Raymond Hide for his continuing support and encouragement throughout the period of this work. A large part of the results presented here is due either directly or indirectly to his suggestions, interpretations, and participation during the course of the construction of the apparatus and the collection and analysis of the data.

I would like to thank Professor Norman Phillips for his comments on the calculation of the available potential energy and his suggestion to calculate the cospectrum and coherency values for each of the sixteen thermocouple outputs for the experimental runs. I would also like to thank Professor Erik Mollo-Christensen for his suggestions concerning the apparatus.

Mr. Ken Harper made several valuable suggestions about the design and construction of the apparatus, and Mr. John Burke participated in the initial design considerations. The apparatus was constructed with the help of Mr. Tony Cieri. I am truly grateful for this assistance. I am also grateful to Mr. Bernie Grey who helped in the acquisition of the data.

I would like to express my appreciation to my several colleagues in the Rotating Fluid Dynamics Laboratory, Dr. Robert Beardsley, Mr. Richard Miller, Mr. Herbert McLease, Dr. Keith Aldridge and Dr. Tom Rossby for all their discussions and suggestions concerning this and related work within the laboratory.

Mr. William Whitamore provided the program and the time for transferring the digital data on the punch paper tape to

magnetic tape. This was accomplished on the Honeywell Computer at the M.I.T. Instrumentation Laboratory. Most of the data analysis was done at the M.I.T. Computation Center on the IBM 360/65. The balance of the analysis was done at the computation center at The State University of New York at Albany. Dr. Ralph Wiggins supplied the subroutine for the time series analysis. I am particularly grateful for the above assistance.

I would like to thank Mrs. Karin Henrikson for typing the final draft of this paper.

I would also like to thank the Tidewater Oil Company for their generous fellowship support during the year preceding the commencement of this study.

Part of this paper was written while the author was an assistant professor of atmospheric sciences at the State University of New York at Albany.

I would like to thank my parents for the guidance, support and encouragement they have always given. I am very grateful for the continuing support, help and encouragement of my wife throughout my graduate student life and for the unconscious support of my children during the last few years.

FIGURES

<u>Number</u>		<u>After Page</u>
1	Surface patterns of the convection flow in the annulus	6
2	Schematic of basic apparatus	6
3	$\overline{\Pi}_4$ versus $\overline{\Pi}_5$ plot of previous experimental points (Fowlis and Hide (1965))	6
4	$\overline{\Pi}_4$ versus $\overline{\Pi}_5$ plot of experimental points for this study	6
5	$G^{\frac{1}{2}}$ versus E^{-1} plot of experimental points for this study	6
6a	Phase variations; Eady normal mode	31
6b	Basic state; Eady solution	31
6c	Second order correction to mean state; Eady solution	31
7a	Detailed schematic of apparatus	39
7b	Schematic diagram of sampling procedure	39
8	Vertical variation of the wall temperature	39
9	Thermocouple array	39
10a	Temperature traces; wave regime	46
10b	Simultaneous temperature traces; Run 42, single vertical array	46
10c	Temperature traces; vacillating and irregular regimes	46
11a	Contours of mean temperature; symmetric regime	46
11b	Contours of mean temperature and standard deviation; wave regime	46
11c	Contours of mean temperature and standard deviation; vacillating and irregular regimes	46

FIGURES (Cont.)

<u>Number</u>		<u>After Page</u>
12a	σ_z versus E^{-1} ; $\Delta T \doteq 9.12^\circ\text{C}$	50
12b	σ_z versus E^{-1} ; $\Delta T \doteq 5.09^\circ\text{C}$	50
13a	σ_r versus E^{-1} ; $\Delta T \doteq 9.12^\circ\text{C}$	50
13b	σ_r versus E^{-1} ; $\Delta T \doteq 5.09^\circ\text{C}$	50
14a	σ_{rI} versus E^{-1} ; $\Delta T \doteq 9.12^\circ\text{C}$	50
14b	σ_{rI} versus E^{-1} ; $\Delta T \doteq 5.09^\circ\text{C}$	50
15	B versus E^{-1} ; $\Delta T \doteq 9.12^\circ\text{C}$	50
16	Standard deviation versus E^{-1} ; $\Delta T \doteq 9.12^\circ\text{C}$	50
17	Radial, zonal and total available potential energy per unit volume; $\Delta T = 9.12^\circ\text{C}$	53
18	Radial, zonal and total available potential energy per unit volume; $\Delta T \doteq 5.09$	53
19	Power spectrum; Run 42, thermocouple T(3,3)	55
20	Power spectrum; Runs 71 and 69, thermo- couple T(3,3)	55
21	Period at maximum power versus E^{-1} ; $\Delta T \doteq 9.12^\circ\text{C}$	55
22	Contours of maximum cospectrum values and phase; Runs 36, 42 and 38	57
23	Average vertical phase variation; wave regime, $\Delta T = 9.12^\circ\text{C}$	57
24	Contours of maximum cospectrum values and coherence; Runs 73, 71, and 69	57
25	Side wall boundary layer temperature; $\alpha = 0.0$, $\Delta T = 8.3^\circ\text{C}$, 1 cm. from bottom	60
26	Side wall boundary layer temperature;	60

FIGURES (Cont.)

Number

After Page

$\Omega = 0.549 \text{ sec}^{-1}$, $\Delta T = 8.8^\circ\text{C}$,
3.24 cm. from top

27

Stepping switch logic circuit

82

TABLES

Number		After Page
I a.	"Specification of system" (Fowlis and Hide (1965))	6
b.	"External dimensionless parameters measuring independent variables" (Fowlis and Hide (1965))	6
II a.	Experimental data for $\Delta T = 9.12^{\circ}\text{C}$	40
b.	Experimental data for $\Delta T = 5.09^{\circ}\text{C}$	40
c.	Experimental data for $\Delta T = 2.53^{\circ}\text{C}$	40
III	Experimental results for $\Delta T = 2.53^{\circ}\text{C}$	50
IV	Values of Σ and B_{crit} for the 42 inch annulus	50
V	Dimensions of the three copper cylinders constructed for the 42 inch annulus	82

RANGE OF PARAMETERS

Parameter	Range
Inner radius of convection chamber, a	23.105 cm.
Outer radius of convection chamber, b	38.445 cm.
Depth of fluid in convection chamber, d	15.14 ≤ d ≤ 15.3
Rotation rate, Ω	0.0 ≤ Ω ≤ 1.846 sec ⁻¹
Temperature difference, $\Delta T = T_b - T_a$	2.38 ≤ ΔT ≤ 9.86 °C
Kinematic viscosity, ν	10 ⁻² cm ² sec ⁻¹
Thermometric conductivity, k	1.4 × 10 ⁻³ cm ² sec ⁻¹

CHAPTER I
INTRODUCTION

The annulus experiments deal with the study of the thermal convection occurring in a fluid in the annular region between two concentric uniformly rotating cylinders which are maintained at different but constant temperatures. The resulting flow exhibits at least four distinct patterns whose presence depends on the rotation rate of the apparatus and the impressed temperature difference. These flow patterns are indicated in Figure 1. The flow is axisymmetric for low impressed temperature differences and/or low rotation rates. At higher rotation rates a regular wave pattern appears in the form of a jet with a large cross stream temperature gradient which progresses from the inner to the outer cylinder with a wave number, m . The wave number tends to increase with increasing rotation rate. Vacillation appears at higher rotation rates as a quasi-periodic oscillation in either the wave amplitude or wave shape. At even higher rotation rates the flow appears to be nonperiodic or irregular.

Previous experimental and theoretical results have indicated that the regular wave regime is probably due to the baroclinic instability of the basic axisymmetric flow. This type of instability was first discussed in relation to the long waves and cyclones in the atmosphere and the production of the kinetic energy of the atmospheric motions, Charney (1948) and Eady (1949). Recently, Schulman (1967) has discussed the problem of baroclinic instability in the mid-ocean circulation. Consequently, a quantitative study of the interior structure of the less

complex laboratory experiment could lead to some valuable insight into the nature of these processes in the oceans and the atmosphere. This paper presents the results of temperature measurements at 16 positions within the convecting fluid of the annulus.

The experimental apparatus, shown schematically in Figure 2, consists of two concentric cylinders of radius a , and b which are maintained at the temperatures T_a and T_b , respectively. The annular region thus formed is filled to a depth d , with a fluid of density, ρ ; kinetic viscosity, ν , and thermal conductivity, λ . The apparatus is mounted on a turntable with a variable but steady rotation rate, Ω . A complete list of the experimental parameters which define the convecting fluid are listed in Tables I_a and I_b.

Fowlis and Hide (1966) have reported results from their own and previous experiments which indicate that the transition from the axisymmetric flow to the regular wave regime is best characterized by a plot of Π_4 vs. Π_5 where

$$\Pi_4 = g \Delta e d / \Omega^2 \bar{e} (b-a)^2 \quad 1.1$$

$$\Pi_5 = 4 \Omega^2 (b-a)^5 / \bar{\nu}^2 d \quad 1.2$$

where $\Delta e = e(T_b) - e(T_a)$ for $T_b > T_a$ and $\bar{\quad}$ indicates the average value. The position of the various regimes can then be plotted as in Figure 3. Since the present study is more concerned with the interior structure of the fluid than with the position of the general transition curves, it was found convenient to introduce a different set of nondimensional parameters. These are the Grashof number:

$$G = g \Delta e (b-a)^3 / \bar{e} \bar{\nu}^2 \quad 1.3$$

and the Ekman number based on the horizontal length scale or an inverse Taylor number;

$$E = (\bar{v} / 2 \Omega (b-a)^2) (d / (b-a))^{1/2} \tag{1.4}$$

This choice of parameters has the advantage in that for fixed values of $\Delta T = T_c - T_a$, the variation of E with respect to a change in rotation rate is parallel to lines of constant G. The disadvantage is that the position of the flow regimes will not necessarily be independent of the other parameters of the experiment as in the Π_4 vs. Π_5 diagram. The data in this paper will generally be presented in terms of $G^{1/2}$ and E^{-1} .

The following parameters determined by the internal structure of the flow will also be used in this presentation. A non-dimensional measure of the vertical temperature difference is given by σ_z where:

$$\sigma_z = \frac{\overline{\partial T}}{\partial z} \frac{d}{\Delta T} \tag{1.5}$$

In a similar manner, the nondimensional radial temperature gradient σ_r is:

$$\sigma_r = \frac{\overline{\partial T}}{\partial r} \frac{(b-a)}{\Delta T} \tag{1.6}$$

where the over bar indicates a volume average of the quantity over the fluid volume not contained within the boundary layers.

Using these values, a Rossby number using the thermal wind equation for a horizontal velocity scale, can be written as

$$R_0 = (g \alpha \sigma_r \Delta T / 4 \Omega^2 d) (d / (b-a))^2 \tag{1.7}$$

where α is the coefficient of thermal expansion.

The Eady number or the ratio of the square of the Väisälä Brunt frequency to the square of the inertial period times an aspect ratio is:

$$B = (g \alpha \sigma_z \Delta T / 4 \Omega^2 d) \cdot (d^2 / (b-a)^2) \quad 1.8$$

The main distinction between this work and the previous experimental work is that the experiment was performed on an annulus with a much larger gap width, $(b-a)$, than used previously. This means that the viscous boundary layers in the apparatus are much thinner in relation to $(b-a)$, and consequently, the viscous effects should be less. The second distinction is that simultaneous temperature measurements have been made at 16 different points in the fluid throughout the range of the experiment. The position of the experimental points are plotted in a Π_4 versus Π_5 diagram in Figure 4 and in a plot of $G^{\frac{1}{2}}$ versus E^{-1} in Figure 5. The range of the experiment covers $0.4662 \times 10^4 \leq G^{\frac{1}{2}} \leq 0.9765 \times 10^4$ and $0.0 \leq E^{-1} \leq 0.9319 \times 10^5$, corresponding to $2.38 \leq \Delta T \leq 9.86 \text{ }^\circ\text{C}$ and $0.0 \leq \Omega \leq 1.846 \text{ sec}^{-1}$.

The results have been analyzed with respect to the transition lines at the large values of Π_5 , the mean temperature structure of the flow, the amplitude and position of the wave disturbance, the frequency content of the disturbance and the cospectrum amplitude, coherence and phase of the disturbance.

These results indicate that:

1. The mean value of Π_4 at the transition between the symmetric flow and the regular wave regime is $\Pi_4^* = 3.746 \pm 0.360$ for $2.750 \times 10^7 \leq \Pi_5 \leq 9.721 \times 10^7$. The value of Π_4^* has a slight but not significant tendency to increase with increasing Π_5

2. The vacillating flow did not occur in this range of

Π_4 until $\Pi_5 > 1.737 \times 10^9$. The irregular flow did not occur under these conditions until $\Pi_5 > 7.259 \times 10^9$.

3. The nondimensional vertical temperature gradient, σ_z , increases to a maximum value in the symmetric regime just at the transition to the regular wave regime. The value of σ_z is either constant, or it decreases slightly with increasing E^{-1} in the wave regime.

4. The value of the Eady number as defined above exceeds the maximum critical value for instability of the wave number occurring at the transition between the symmetric regime to the regular wave regime and also at a few selected points within the wave regime. The observed value of the wave number is seldom the wave number with the theoretical maximum rate of growth as determined from Eady's theory.

5. The total available potential energy per unit volume of the fluid increases rapidly with increasing E^{-1} in the symmetric flow. This value drops discontinuously at the transition between the symmetric regime and the regular wave regime. It has a slight tendency to decrease within the wave regime with increasing E^{-1} . It increases again with increasing E^{-1} in the vacillating and irregular regimes. The radial available potential energy per unit volume behaves in the same way except within the wave regime, where it decreases with increasing E^{-1} . The zonal available potential energy per unit volume increases with increasing E^{-1} in the regular wave, vacillating, and irregular regimes.

6. The position of the wave¹ disturbance occurs near the upper surface of the fluid near the cold wall at a point in the wave regime just beyond the transition from the symmetric flow. This disturbance broadens and progresses deeper into the fluid as E^{-1} increases in this regime. For the vacillating and irregular regime points, the disturbance is significantly more concentrated in the lower half of the fluid.

7. The radially averaged phase of the wave with respect to the radially averaged phase at the mid depth of the fluid leads in the upper half of the annulus and lags in the lower half. The maximum phase lead or lag occurs at the mid region of the respective layers. The vertical variation of the radially averaged phase tends to decrease with increasing E^{-1} in the wave regime.

8. The phase period of the waves with respect to the rotating annulus tends to increase in the wave regime with increasing E^{-1} . The period of the vacillation cycle increases rapidly with increasing E^{-1} . The periods of oscillation in the irregular flow are more characteristic of that in the regular wave regime. However, the oscillations are much less coherent, and there is an indication that there are at least two disturbances with slightly different frequencies.

1. The amplitude and phase of the wave as used in this text always refers to the amplitude and phase of the temperature wave in the convecting fluid

A major portion of the work involved in the presentation was the design of modifications to and consequent construction of the large 42 inch rotating annulus in the Rotating Fluid Dynamics Laboratory. This paper presents a synopsis of previous experimental, numerical and theoretical work related to the annulus. The synopsis leads to a description of the apparatus and the experimental procedure followed by a presentation and interpretation of the results. The report is concluded with a summary of the results and some suggestions for future work. This work is supplemented by two appendices, the first describes the apparatus in greater detail than presented in the main text, and the second describes the methods of calculations employed in obtaining the results.

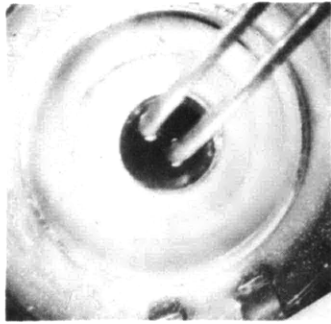
Figure 1. Surface patterns of the convective flow in the annulus. Reproduced and quoted with permission of Prof. R. Hide from Fowlis and Hide (1965).

Figure 2. Schematic of basic apparatus. Reproduced with permission of Prof. R. Hide from Fowlis and Hide (1965).

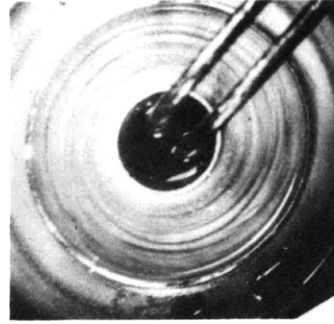
Figure 3. Π_4 versus Π_5 plot of previous experimental points "illustrating the positions of the upper symmetrical (A), steady waves (B), irregular (C) and lower symmetrical (D) flow regimes in a typical regime diagram. $\Pi_4 \equiv (gd\Delta\theta/\rho)/(\Omega^2(b-a)^2)$ and $\Pi_5 \equiv 4\Omega^2(b-a)^5/\bar{\nu}^2d$ (see Table 2). The heavy full lines are drawn through the middle of the transition regions; the length of the bar on each experimental point indicates the width of the region, and the number(s) indicate(s) the wave number(s) at the transition. Along each of the heavy broken lines, the indicated wave number occurred with maximum frequency. Each of the diagonal full lines sloping from upper left to lower right corresponds to a constant value of $\Delta T = T_b - T_a$. Experimental details: $-a = 3.48$ cm, $b = 6.02$ cm, $d = 10.0$ cm, $\bar{T} = 20.00$, $\bar{\nu} = 1.01 \times 10^2$ cm² sec⁻¹, $\bar{\rho} = 0.998$ gm cm⁻³; liquid used--water; upper surface--free. $\Pi_1 = 0.535$, $\Pi_2 = 3.94$, $\Pi_3 = 4.82 \times 10^{-4}$ to 1.49×10^{-1} , $\Pi_6 = 7.19$, $\Pi_7 = 3.4 \times 10^{-4}$ to 8.54×10^{-2} , $\Pi_8 = 1.12 \times 10^6$ to 3.46×10^8 ." Reproduced and quoted with permission of Prof. R. Hide from Fowlis and Hide (1965).

Figure 4. Π_4 versus Π_5 plot of the experimental points for this study.

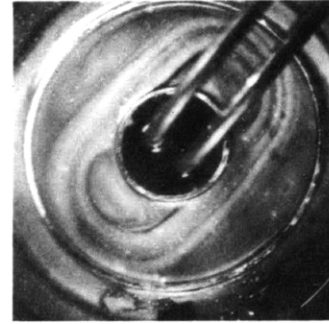
Figure 5. $G^{\frac{1}{2}}$ versus E^{-1} plot of the experimental points for this study.



(a)



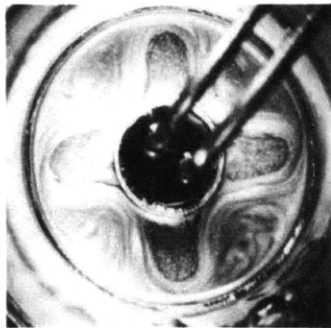
(b)



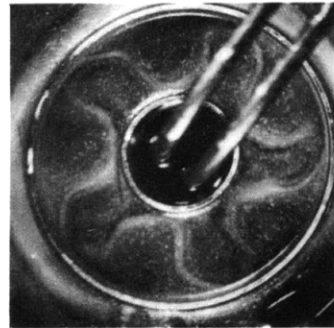
(c)



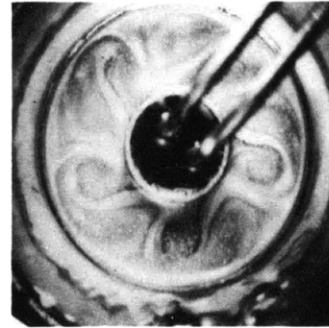
(d)



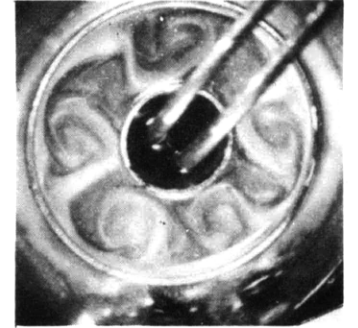
(e)



(f)



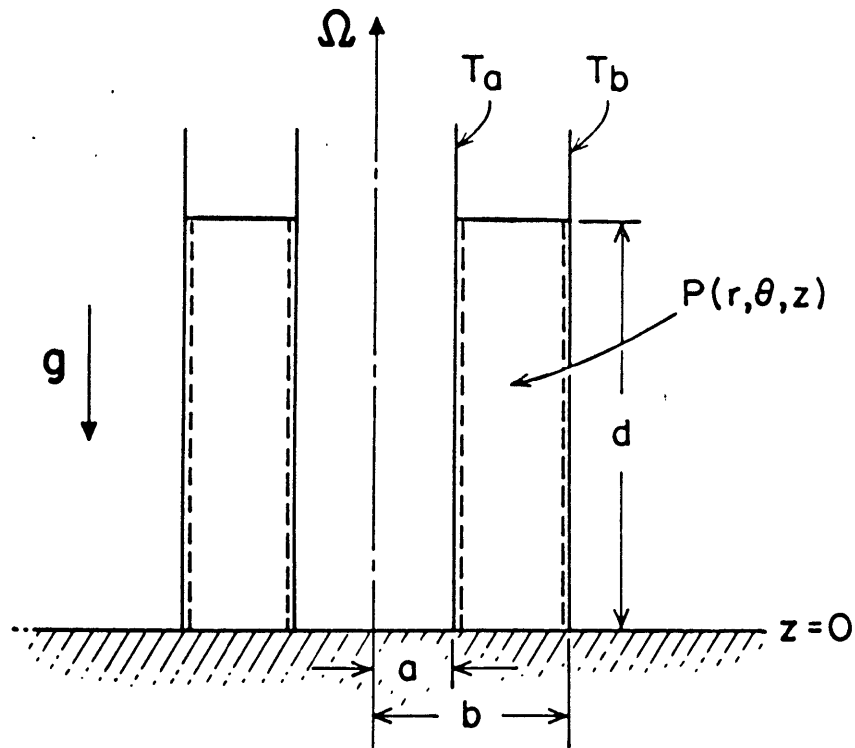
(g)



(h)

FIGURE

ILLUSTRATING FLOW REGIME CHANGES AS THE EFFECT OF ROTATION INCREASES
(a) and (b) – symmetrical; (c), (d), (e), (f) – steady waves; (g) – vacillation; (h) – irregular
(After R. Hide, Ph.D. dissertation, 1953, Cambridge; also 1958, Philos. Trans. Royal Soc.
Lond. 250 A, 441-478).



P - General point having cylindrical polar coordinates (r, θ, z) in frame rotating with the apparatus

$\Omega = (0, 0, \Omega)$ - rotation vector

$g = (0, 0, -g)$ - acceleration of gravity

b, a, d - fluid occupies region

$$a < r < b, 0 < z < d \left[1 + \frac{\Omega^2 (r^2 - 1/2(b^2 + a^2))}{2gd} \right] \approx d$$

$T(r, \theta, z, t)$ - temperature at general point P and time t

T_a, T_b - $T(a, \theta, z, t); T(b, \theta, z, t)$ respectively

FIGURE 2 SCHEMATIC DIAGRAM ILLUSTRATING ROTATING FLUID ANNULUS

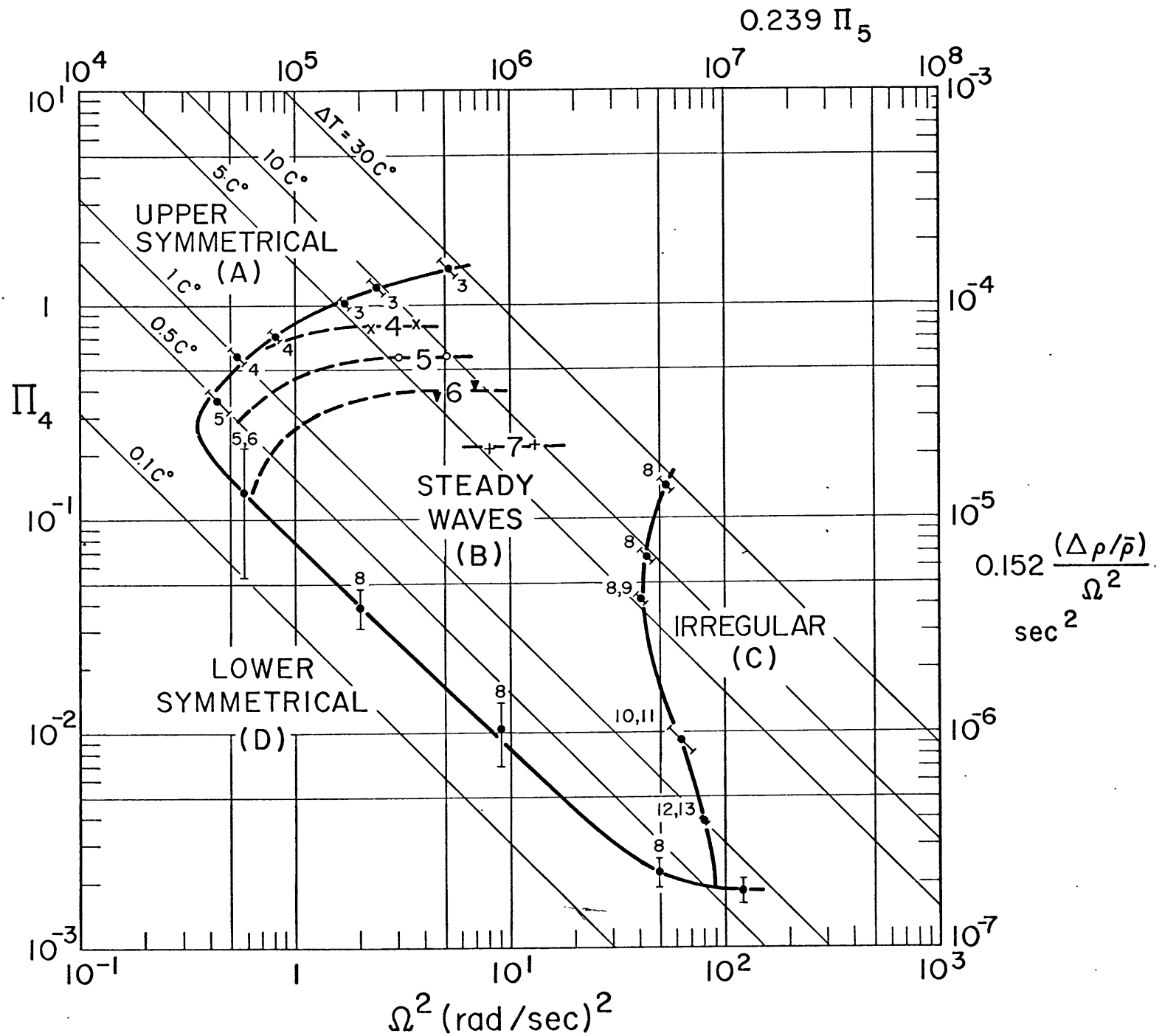


Figure 3

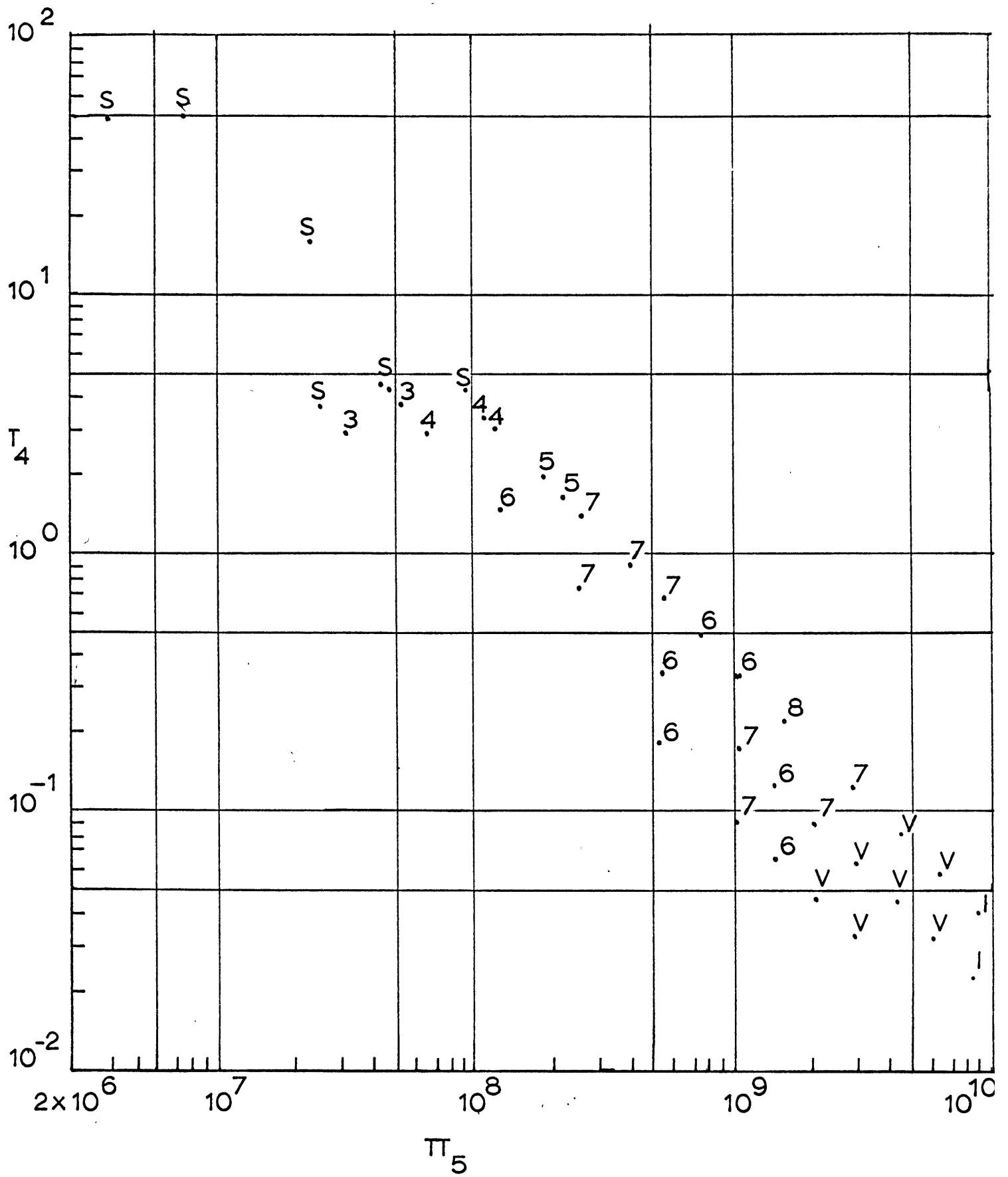


Figure 4

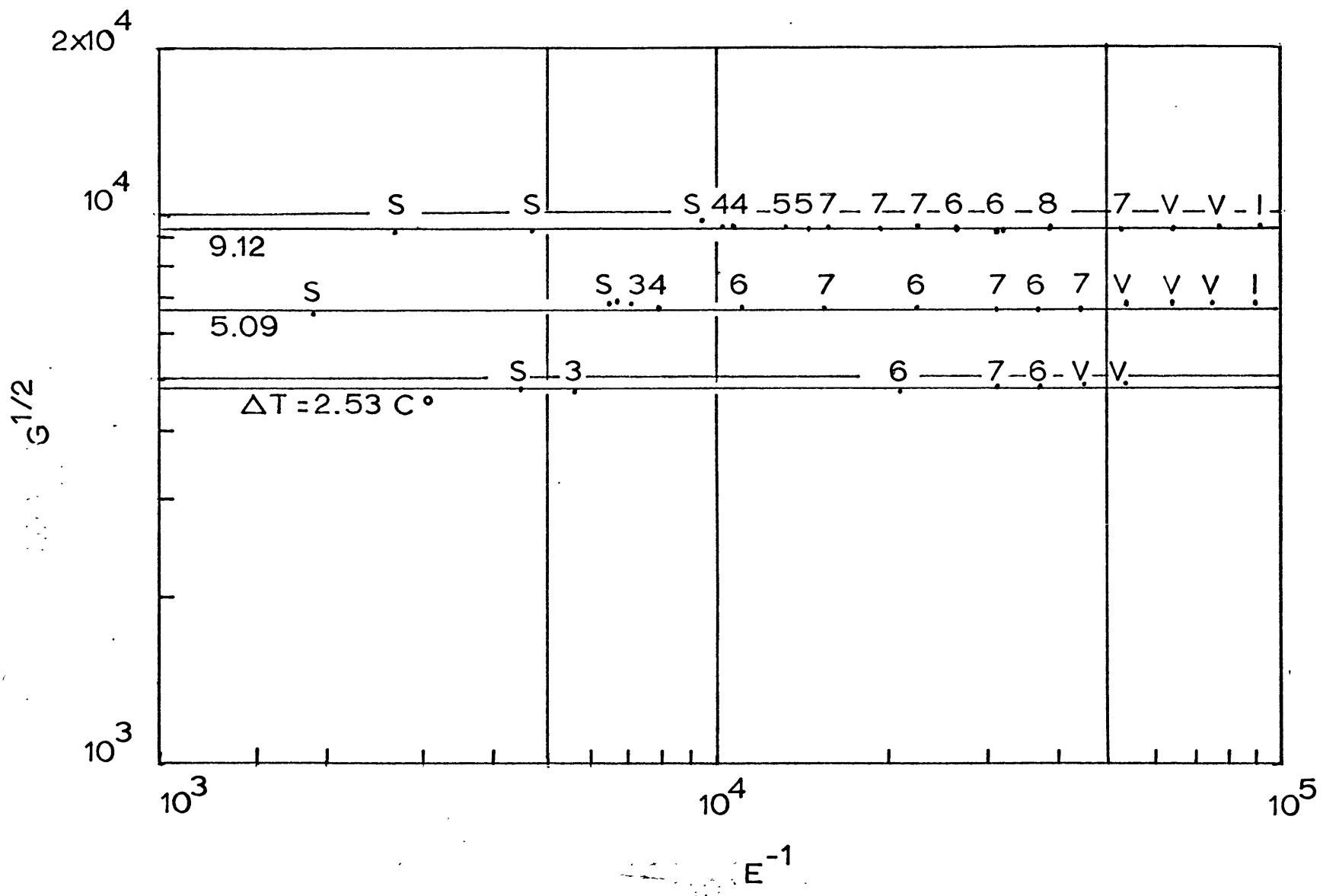


FIGURE 5

TABLE I a*

Specification of System

Definition of Symbols

<u>Symbol</u>	<u>Units</u>	<u>Definition</u>
(1) (r, θ, z)	cm, rad, cm	cylindrical polar coordinates of general point P (see Figure 2)
(2) t	sec	time
(3) $g = (0, 0, -g)$	cm sec ⁻²	acceleration of gravity; taken as 980 cm sec ⁻²
(4) $\vec{\omega} = (0, 0, \omega)$	rad sec ⁻¹	uniform angular velocity of rotation of apparatus
(5) a, b	cm, cm	$a \leq r \leq b$ is horizontal extent of liquid in convection chamber
(6) d	cm	volume of liquid is $(b^2 - a^2)d$ cm ³ ; see legend to Figure 1
(7) $T = T(r, \theta, z, t)$	°C or °K	temperature at point P and time t
(8) $\rho = \rho(T)$	gm cm ⁻³	density of liquid at temperature T
(9) $\eta = \eta(T)$	gm cm ⁻¹ sec ⁻¹	coefficient of viscosity of liquid (usually strongly dependent on T)
(10) $\nu = \nu(T)$	cm ² sec ⁻¹	kinematic viscosity, η/ρ
(11) $c = c(T)$	erg gm ⁻¹ (C°) ⁻¹	specific heat of liquid (depends only weakly on T)
(12) $\chi = \chi(T)$	erg cm ⁻¹ sec ⁻¹ (C°) ⁻¹	thermal conductivity of liquid (depends weakly on T)
(13) $\kappa = \kappa(T)$	cm ² sec ⁻¹	thermometric conductivity
(14) T_a, T_b	°C or °K	$T(r = a, \theta, z; t),$

<u>Symbol</u>	<u>Units</u>	<u>Definition</u>
(14) Cont.		$T(r = b, \Theta, z, t)$; each held substantially uniform and constant in typical experiment
(15) \bar{T}	$^{\circ}\text{C}$ or $^{\circ}\text{K}$	$\frac{1}{2}(T_a + T_b)$
(16) ΔT	$^{\circ}\text{C}$	$(T_b - T_a)$
(17) Δe	gm cm^{-3}	$e(T_a) - e(T_b)$
(18) \bar{e}	gm cm^{-3}	$[e(T_a) + e(T_b)]/2$
(19) \bar{v}	$\text{cm}^2 \text{sec}^{-1}$	$[v(T_a) + v(T_b)]/2$
(20) \bar{k}	$\text{cm}^2 \text{sec}^{-1}$	$[K(T_a) + K(T_b)]/2$
(21) \bar{c}	$\text{erg gm}^{-1} (^{\circ}\text{C})^{-1}$	$[c(T_a) + c(T_b)]/2$
(22) Δv	$\text{cm}^2 \text{sec}^{-1}$	$v(T_a) - v(T_b)$
(23) ΔK	$\text{cm}^2 \text{sec}^{-1}$	$K(T_a) - K(T_b)$
(24) Δc	$\text{erg gm}^{-1} (^{\circ}\text{C})^{-1}$	$c(T_a) - c(T_b)$
(25) χ_i	$\text{erg cm}^{-1} \text{sec}^{-1} (^{\circ}\text{C})^{-1}$	thermal conductivity of inner cylinder
(26) χ_o	$\text{erg cm}^{-1} \text{sec}^{-1} (^{\circ}\text{C})^{-1}$	thermal conductivity of outer cylinder
(27) χ_b	$\text{erg cm}^{-1} \text{sec}^{-1} (^{\circ}\text{C})^{-1}$	thermal conductivity of base of convection chamber
(28) χ_u	$\text{erg cm}^{-1} \text{sec}^{-1} (^{\circ}\text{C})^{-1}$	effective thermal conductivity of region in contact with upper surface of convecting liquid
(29) $S(T)$	dyne cm^{-1}	surface tension at free upper surface of fluid in contact with air
(30) ΔS	dyne cm^{-1}	$S(T_a) - S(T_b)$

TABLE I b*

External Dimensionless Parameters

Measuring Independent Variables

<u>Symbol</u>	<u>Definition</u>	<u>Symbol</u>	<u>Definition</u>
π_1	$(b-a)/\frac{1}{2}(b+a)$	π_9	$\Delta c / \bar{c}$
π_2	$d / b - a$	π_{10}	$\Delta v / \bar{v}$
π_3	$\omega^2 (b^2 - a^2) / 2gd$	π_{11}	$\Delta k / \bar{k}$
π_4	$gd \Delta \epsilon / \bar{\epsilon} \omega^2 (b-a)^2$	π_{12}	$\chi_i / \chi(T_a)$
π_5	$4\omega^2 (b-a)^5 / \bar{v}^2 d$	π_{13}	$\chi_o / \chi(T_b)$
π_6	\bar{v} / \bar{k}	π_{14}	$\chi_e / \frac{1}{2}(\chi(T_a) + \chi(T_b))$
π_7	$\Delta T / \bar{T}$	π_{15}	$\chi_w / \frac{1}{2}(\chi(T_a) + \chi(T_b))$
π_8	$\bar{c} \bar{T} / \omega^2 (b+a)^2$	π_{16}	$\Delta S / \frac{1}{2}(S(T_a) + S(T_b))$

* Tables Ia and Ib were reproduced with permission of R. Hide, from Fowles and Hide (1965).

CHAPTER II

REVIEW OF PREVIOUS WORK

Previous experimental results.

The transition from the upper symmetrical regime (A), Figure 3, to the regular wave regime (B), Figure 3, is generally quite well defined. Hide (1953, 1958) found that in the range of $10^6 < \Pi_5 < 1.3 \times 10^7$ the critical value of Π_4 is $\Pi_4^* = 1.58 \pm 0.05$ (standard error) where the flow was always symmetric for $\Pi_4 > \Pi_4^*$. Subsequent work by Smith (1958), Hide (1953) and Fowlis and Hide (1965) indicate that Π_4^* varies rapidly with Π_5 for $1.85 \pm 0.08 \times 10^5 < \Pi_5 < 10^6$ and that the flow is always symmetric for all values of $\Pi_5 < \Pi_5^*$ where $\Pi_5^* = 1.85 \pm 0.08 \times 10^5$ (standard error). Lambert and Snyder (1966) have further found that when the aspect ratio $\Pi_2 = d/L - a$ is varied over the range $2 < \Pi_2 < 27$ the critical value of Π_4 also depends slightly on Π_2 .

The lower transition from the symmetrical regime (D), Figure 3, to the wave regime (B) was first discovered with very low heating rates by Fultz, et al. (1959). Fowlis and Hide (1965) have since found that this transition for $\Pi_5 > 2\Pi_5^*$ obeys the equation:

$$\text{Log } \Pi_4 \Pi_6 = -(0.864 \pm 0.043) \text{Log } (\Pi_2 \Pi_5) + 5.05 \pm 0.30$$

(standard errors)

The wave numbers Ma, Mc, and Md at the transition from the regime A to B, C to B, and D to B have been noted by Hide (1953, 1958), Fultz, et al. (1959), and Fowlis and Hide (1965). These results indicated that the wave number is not a unique function of the non-dimensional parameters. However, there does

exist a value of $\Pi_4(m)$ for which M is the most likely wave number. The variations of $\Pi_4(m)$ have been stated succinctly by Fowles and Hide (1965) and appear below.

"Conclusion 4. $\Pi_4(m)$ decreases with increasing m , the variation with Π_4 of the probability of m waves occurring being roughly symmetrical about $\Pi_4 = \Pi_4(m)$.

When Π_5 exceeds $2\Pi_5^*$, $\Pi_4(m)$ is independent of Π_5 except perhaps at the largest values of m (see Fig. 3).

Conclusion 5. When Π_5 is less than about $2\Pi_5^*$, the dependence of $\Pi_4(m)$ on Π_5 is evidently more complicated than when Π_5 exceeds $2\Pi_5^*$. (These complications have yet to be examined thoroughly.)

Conclusion 6. Within the limitations imposed on m by the fact that this quantity must be an integer, the quantity

$$\sigma_A = m_A (\zeta - \alpha) / \pi (\zeta + \alpha) \quad (4.3)$$

depends mainly on $\Pi_2\Pi_5$; moreover, when $\Pi_2\Pi_5$ exceeds about 3×10^6 this dependence is weak, σ_A having a value of between 0.2 and 0.3. When $\Pi_2\Pi_5$ is less than 3×10^6 , σ_A increases with decreasing $\Pi_2\Pi_5$, a variation due largely, though perhaps not entirely, to the dependence of Π_4 (A,B) on Π_5 .

Conclusion 7. Except at the highest values of Ω , when a slow increase of m_c with decreasing Π_4 occurs (see Fig. 3), the quantity m_c is independent of Π_4 ; the dependence of m_c on the other parameters of the problem may be summarized by the statement that

$$\sigma_c = m_c (\zeta - \alpha) / \pi (\zeta + \alpha) \quad (4.4)$$

is equal to about 0.7.

Conclusion 8. The quantity

$$\sigma_D = m_D (\zeta - \alpha) / \pi (\zeta + \alpha) \quad (4.5)$$

depends on $\Pi_2\Pi_5$, this variation being largely associated with the form of the transitional curve for the lower symmetrical regime. 1)

Results of experiments designed specifically for the study of the heat transfer indicate the following for the Nusselt number N . (Bowden (1961), Hide, et al. (1961), Bowden and Eden (1965).)

- a. N is greater for a rigid lid than for a free surface
- b. N varies between 9 and 3
- c. In the axisymmetric regime N decreases with increasing Ω and decreasing ΔT until the transition to the regular wave regime is reached where N increases abruptly by approximately 20%.
- d. N is nearly independent of d in both the symmetric and regular wave regimes.
- e. There is no strong dependence of N on Ω in the wave regime.

Smith (1957) has made detailed temperature measurements at two parameter points in the symmetric regime and three parameter points in the wave regime for values of $1.49 \times 10^6 \leq \Pi_5 \leq 1.80 \times 10^7$, $\Pi_2 = 3.28$ and ΔT approximately 20°C . These results when combined with results from four temperature probes at other values of Π_4 and Π_5 indicate that the slope of the isotherms σ_z/σ_r is proportional to $\Omega^2/\sigma_r \Delta T$ in the symmetric regime and proportional to $\Delta T \sigma_z/\Omega^2$ in the wave regime. The vertical temperature differences for these experiments is always greater than the horizontal temperature difference by a factor of two or more. Bowden and Eden (1965) indicate the same type of temperature dependence for the symmetric regime.

The temperature structure of the side wall boundary layers has been examined by Bowden and Eden (1965) and Eden and Piacsek (1967). These measurements indicate that there is a region with very strong horizontal temperature gradients near each wall and as rotation increases this region concentrates

nearer to the lower part of the hot wall and the upper part of the cold wall. This indicates that the heat source has been lowered and the heat sink raised. Outside this region the isotherms reverse direction forming a hump and then reverse direction, again, entering the interior region, and sloping upwards towards the cold wall. The amplitude of the hump increases with height on the hot wall and decreases with height on the cold wall.

Hide (1953, 1958) and Smith's (1957) results also indicate that the wave jet is a region of very strong cross stream temperature gradients with a zonal velocity which roughly satisfies the thermal wind equation. Thus, it flows in opposite directions at the upper and lower surfaces. The width of the stream increases with the square root of the impressed temperature difference and decreases with increased rotation, Smith (1957). Smith (1957) also noted a discontinuous phase lag of $1/3$ to $1/2$ the wave length between the lower and upper portion of the wave at the mid layer of the fluid.

Detailed temperature measurements at one point in the wave regime in a dishpan type annulus have been made by Riehl and Fultz (1957, 1958). The results of the geostrophically computed velocities indicate that the waves are quasi-geostrophic and tend to carry warm water upwards and cold water down.

Related experiments using modified annuli may also increase the understanding of these regimes. Specifically, Fultz, et al. (1964) have imposed an independent vertical temperature difference in an annulus, and consequently, showed that the transition value of $\overline{\Pi}_4$ decreases with increased vertical stability, all other factors

being constant. Also, Lambert and Snyder (1966) have shown that the effect of an impressed horizontal shear on the annulus regime is to increase the stability of the symmetric flow.

Previous numerical and theoretical results.

The theoretical work has concentrated mainly on determining the structure of the symmetric regime and the stability of this flow with respect to small amplitude wave disturbances. In order to facilitate a discussion of these processes the relevant equations for the hydrodynamic flow in the annulus are presented below. These will be followed by a discussion of the numerical experiments and the analytic theories for the symmetric regime. Then, a discussion of the theoretical work on the wave regime will be presented.

The equation of motion for the flow in an annulus can be written in cylindrical polar coordinates as:

$$\frac{du}{dt} - \frac{v^2}{r} - 2\Omega v = -\frac{1}{\rho} \frac{\partial p}{\partial r} + \nu \left(\nabla^2 u - \frac{2}{r^2} \frac{\partial v}{\partial \theta} \frac{u}{r} \right) \quad 2.1$$

$$\frac{dv}{dt} + \frac{uv}{r} + 2\Omega u = -\frac{1}{\rho r} \frac{\partial p}{\partial \theta} + \nu \left(\nabla^2 v + \frac{2}{r^2} \frac{\partial u}{\partial \theta} - \frac{v}{r^2} \right) \quad 2.2$$

$$\frac{d\omega}{dt} = -\frac{1}{\rho} \frac{\partial p}{\partial z} - g + \nu \nabla^2 \omega \quad 2.3$$

further $\frac{dT}{dt} = \kappa \nabla^2 T \quad 2.4$

$$\rho = \rho_0 (1 - \alpha (T - T_0)) \quad 2.5$$

$$\frac{1}{r} \frac{\partial}{\partial r} (r^2 u) + \frac{1}{r} \frac{\partial v}{\partial \theta} + \frac{\partial \omega}{\partial z} = 0 \quad 2.6$$

where

$$\frac{d}{dt} = \frac{\partial}{\partial t} + u \frac{\partial}{\partial r} + \frac{v}{r} \frac{\partial}{\partial \theta} + \omega \frac{\partial}{\partial z}$$

and

$$\nabla^2 = \frac{1}{r} \frac{\partial}{\partial r} r \frac{\partial}{\partial r} + \frac{1}{r^2} \frac{\partial^2}{\partial \theta^2} + \frac{\partial^2}{\partial z^2}$$

and u , v , and w are the components of velocity in the r , θ , and z directions, respectively.

In the case of steady axisymmetric flow, the problem is reduced to that of finding a solution to the $\hat{\theta}$ component of the vorticity equation, the zonal momentum equation and the temperature equation. The continuity equation can be satisfied identically with the use of a stream function, ψ , such that

$$u = +\frac{1}{r} \psi_z$$

$$w = -\frac{1}{r} \psi_r$$

These equations are respectively:

$$\frac{1}{r} \psi_z (\omega_r - \frac{\omega}{r}) - \frac{1}{r} \psi_r \omega_z = \nu (\nabla_1^2 \omega - \omega/r^2) - g \alpha T_r + 2 v_z (\omega + v/r) \quad 2.7$$

$$\frac{1}{r} \psi_z (v_r + v/r) - \frac{1}{r} \psi_r v_z = \nu (\nabla_1^2 v - v/r^2) - 2 \frac{\Omega}{r} \psi_z \quad 2.8$$

$$\frac{1}{r} \psi_z T_r - \frac{1}{r} \psi_r T_z = \kappa \nabla_1^2 T \quad 2.9$$

where

$$\nabla_1^2 = \frac{\partial^2}{\partial r^2} + \frac{1}{r} \frac{\partial}{\partial r} + \frac{\partial^2}{\partial z^2} \quad 2.9$$

and the $\hat{\theta}$ component of the vorticity is:

$$\omega = \frac{1}{r} \left(\frac{\partial^2}{\partial r^2} - \frac{1}{r} \frac{\partial}{\partial r} + \frac{\partial^2}{\partial z^2} \right) \psi$$

A further simplification can be introduced when the horizontal length scale of the annulus $L \sim (b - a)$ is much smaller than the mean radius $\bar{r} = \frac{1}{2} (b + a)$. The equations can

then be written in equivalent cartesian form by letting $x = r - a$ and $y = r\theta$ as;

$$\psi_z \omega_x - \psi_x \omega_z = \nu \nabla_H^2 \omega - g \alpha T_x + 2\Omega v_z \quad 2.10$$

$$\psi_z v_x - \psi_x v_z = \nu \nabla_H^2 v - 2\Omega \psi_z \quad 2.11$$

$$\psi_z T_x - \psi_x T_z = k \nabla_H^2 T \quad 2.12$$

where

$$\nabla_H^2 = \frac{\partial^2}{\partial x^2} + \frac{\partial^2}{\partial y^2}$$

and terms of order ν/\bar{r} have been neglected with respect to terms of order ν/L . The stream function is now defined as;

$$\omega = -\psi_x$$

$$v = \psi_y$$

These latter approximations are certainly valid in the side wall boundary layers where $1/\bar{r}$ is of order 10^{-2} , and they are also used without a large loss in accuracy in most of the analytical theories for the interior flow.

The numerical experiments of Piacsek (1966) and Williams (1966) have solved the complete set of Equations 2.7, 2.8, and 2.9, for the temperature distribution, zonal velocity and stream functions. The results also indicate the main balance in these equations occurring in the boundary layers and the interior flow.

These studies indicate that the boundary layer thickness tends to increase with increasing height on the warm cylinder and decrease on the cold. They are distinguished by two regions, one near the wall where the conduction of heat from the wall is balanced by the vertical convection, and one further out from

the wall where horizontal and vertical convection balance. The isotherms leaving the warm wall rise sharply and reach a maximum in height within the boundary layer. This forms a small hump in the temperature structure near the wall. The amplitude of this hump is largest at zero rotation rate and tends to increase with height on the warm cylinder and decrease with height on the cold cylinder. It also tends to decrease with increasing rotation rate.

In the case of a free upper surface, Piacsek (1966) and Williams (1966) both indicate that the upper region of fluid near the warm wall is almost isothermal. The flow is a basic Hadley type meridional circulation which releases potential energy by flowing at a small angle across the isotherms. A narrow secondary meridional circulation forms near the cold boundary wall but tends to decrease in strength as the rotation rate and/or temperature difference is increased. The zonal velocity has a maximum occurring at or near the free surface near the inner wall. The ^{maximum} ~~value~~ value of the zonal velocity at any height occurs on a conical surface sloping upwards towards the inner cylinder. There is a marked ~~axi~~ symmetric variation with depth for both the temperature field and the meridional and zonal velocity fields, due, mainly, to the fact that the free surface cannot support the same convective mass and heat transport as the rigid lower surface. The fields are much more symmetric for a rigid surface, except that at large values of ΔT there is still a region of isothermal fluid near the upper surface of the warm cylinder.

Piacsek (1966) has computed the interior parameters of the flow and found that the Rossby number of the zonal flow varied for 0.15 to 0.30 as the rotation rate increased. σ_z varied from 0.8 to 0.76 in the symmetric flow as rotation increased and reached a value of 0.55 when the symmetric solution obtained would probably have been unstable. σ_r varied from 0.06 to 0.22 in the symmetric regime as the rotation increased and reached a value of 0.42 at the possible unstable solution.

These experiments indicate that the main balance in the interior is between the buoyancy term and coriolis term. Further, the meridional circulation and the heat transport occurs mainly in the boundary layers except for the presence of an inertial circulation flowing upwards across the upper region of the annulus in the case of an upper free surface. The net result of increasing ΔT or decreasing Ω is to increase the meridional circulation. The Nusselt number decreases with increasing rotation rate and is larger for the annulus with a rigid lid.

The results at low heating rates by Williams (1966), corresponding to the lower and middle symmetrical regimes, indicate that the isotherms are almost vertical in the interior. Here, a secondary meridional cell forms near the boundary layers and the cells are asymmetrical in z being very slightly lower on the warm cylinder. The interior velocity field is viscously driven through the boundary layers and the heat transfer is largely by conduction.

Robinson (1959) has found an analytical solution for the flow in the lower symmetric regime with a rigid upper and lower

surface by assuming that the temperature field is determined by thermal conduction. Hunter (1966) has corrected this result by carefully matching the boundary layer flux to that in the vertical boundary layer. Hunter has also extended the results to the case of a free upper surface and solved for the first order correction associated with a small additional convective temperature balance for a rigid upper and lower surface.

The horizontal boundary layers on the rigid surface are Ekman layers with a thickness given by $\delta = (\nu/\Omega)^{1/2}$. The interior zonal velocity has a linear vertical shear and is zero at the midlayer, $z = \frac{1}{2}$. The flux through the Ekman layer is closed by the side wall boundary layers which for two rigid surfaces are Stewartson layers with a single structure of order $E^{1/3}$. The meridional circulation occurs in the boundary layers. An estimate for the Nusselt number when small convection effects are considered is given as:

$$N - 1 = \frac{1}{32} 0.136 \cdot P^2 \Pi^2 \left(\frac{\delta}{d} \right)^2 \frac{d}{(b-a)}$$

for $\frac{d}{b-a} > 1$

When the upper surface is free, the Ekman boundary layer associated with it is weakened and can only support a mass flux of order $E^{1/2}$ times that occurring in the rigid surface case (Hide 1964b). This complicates the analysis of the side wall boundaries and they now have a double structure comparable to the Stewartson layers of order $E^{1/3}$ and $E^{1/4}$. As in the case of the rigid upper surface the meridional circulation occurs mainly in the boundary layer.

Hide (1967) has indicated how the Nusselt number and vertical temperature contrast (proportional to σ_z) will vary in the symmetric regime. He derives the results for a free upper and lower surface (usf/l_sf), a free upper surface and ^arigid lower surface (usf/l_sr) and a rigid upper and lower surface (usr/l_sr). These are considered for either a large Peclet number (UL/K), indicative of convection dominated flow as in the upper symmetric regime, or a small Peclet number, or conduction dominated flow as in the case of the lower symmetric regime. The method of approach is to assume an appropriate temperature distribution and realize that most of the convective heat transfer occurs via the meridional circulation in the boundary layers.

Under these conditions the results for the case of both surfaces rigid and low Peclet number predict that

$$\sigma_z = Y/12$$

and
$$N - 1 = \frac{1}{2} (Y/\beta)^2$$

where
$$\beta = \frac{d}{b-a}, \text{ and } Y = 1/8 \pi_4 P \delta/d, =$$

and
$$P = \nu/K$$

The results for a free upper surface and ^arigid lower surface or a free upper and lower surface are:

$$\sigma_z = Y d/g$$

$$N - 1 = 2(Y/\beta \frac{\xi}{d})^2$$

In the case of a high Peclet number with both bounding surfaces rigid, the additional assumption is used that most of

the heat is conducted to or from the fluid near the lower part of the warm wall or the upper part of the cold wall, respectively. The results indicate that a reasonable estimate of σ_z and N will be:

$$\sigma_z = 2/3 (1 - (Y/\beta^2)^{-1} (1 + (4/3)\beta^2))$$

$$N = (1 - \sigma_z) (1 + \sigma_z Y/\beta^2)$$

These are the "agnostic" values of σ_z and N recorded by Hide (1967), determined by setting the small correction factors occurring in the original expression to zero. Since the case for high Peclet numbers with an upper free surface must have some form of inertial boundary layer to complete the circulation and convective heat transfer, it could not be readily solved in this manner.

McIntyre (1967) has presented a scaling analysis for the upper symmetric regime and a similarity solution for the boundary layers in the case of rigid upper and lower surfaces. The scaling assumptions are that $\frac{1}{4} \Pi_4$, P, $\frac{d}{b-a}$, and b/a are all of order unity; P is much greater than 1; there are single scale thicknesses for each of the vertical and horizontal boundaries; thermal convection is as important as conduction in the boundary layers; and the meridional velocities in the boundary layer are at least as large as those in the interior. The relevant equations are then Equations 2.7, 2.8, and 2.9 with the additional assumption of the boundary layer approximation.

Under these conditions the primary balance in the side wall boundary layers is between the viscous torque $\nu \omega_{\varphi r}$ and the

bouyancy torque (See Equation 2.10) $g \alpha T_r$. This coupled with the assertion that the horizontal conductive and vertical convective heat transports must also balance, i.e.:

$$\omega T_z = K T_{rr}$$

gives a scale factor of:

$$l^4 = \frac{\nu K d}{g \alpha \Delta T}$$

for the side wall boundary layers. The reason for the hump in the isotherms (See page 10) can be found by integrating ^{the} Equation: ~~2.10~~ $\nu \omega_{rr} = \nu \omega_{rrr} = g \alpha T_r$ from the side wall to the edge of the boundary layer at $r = r_L$, i.e.:

$$\nu \omega_{rr} = g \alpha (T - T(r_L, z))$$

Thus, since the vertical velocity has maximum value within the boundary layer on the warm wall, the temperature must have a minimum value between the wall and the edge of the boundary layer. The upper and lower boundary layers are non-divergent Ekman layers which carry the total mass flux from the side boundaries.

The scaling on the interior equations indicates that the zonal velocity is determined by the thermal wind equation.

$$U_z = g \alpha T_r / 2 \Omega$$

A further result of the scaling is that the meridional velocities (u, w) in the interior are viscously controlled and are smaller than in the boundary layers. This also means that both the

convective and conductive transport in the heat equation are important in the interior flow.

The solution to the side boundary layer equations leads to certain restrictions on the temperature distribution at the edge of the layer. The form of the temperature distribution just outside these layers is:

$$T_1(z) = B_1^4 / (z_1 - z)^3$$

where $B_1 = \psi_I / 0.36$ and ψ_I is the volume flux per radian in the boundary layer. A similar form is valid for the dependence near the hot wall. Since the Ekman layer flux ψ_I is related to the zonal velocity at the edge of the boundary layer, ψ_I must also be related to the interior temperature field through the thermal wind equation. The small meridional velocities in the interior help maintain the zonal flow against viscous dissipation and also maintain the temperature field necessary for the thermal wind against conductive dissipation. The largest discrepancy between this theory and the numerical models appears to be in the condition of zero entrainment in the side boundary layers.

The wave regime was initially proposed by Lorenz (1953) to be the result of an instability in the axisymmetric zonal flow. Under this assumption the symmetric flow is always a possible mathematical solution to the equations of motion, but it may be unstable such that it would not exist in the physical experiments. This instability is baroclinic since the energy for its growth is derived from the potential energy of the fluid. The original studies of this process were made independently by Charney (1947) and Eady (1949) in an effort to understand the nature of

the long waves and cyclones in the atmosphere. Eady's study is more relevant to the annulus due to the neglect of the variation of the coriolis parameter. For this reason it is reviewed below.

The relevant equation is the inviscid and non-conductive parts of Equations 2.1 to 2.6. With the assumption for the annulus that $2(b-a)/(b+a) \ll 1$ and the consequent introduction of cartesian coordinates, with the boussinesq approximation, these are:

$$\frac{\partial u}{\partial t} + u \frac{\partial u}{\partial x} + v \frac{\partial u}{\partial y} + w \frac{\partial u}{\partial z} - 2\Omega v = -\frac{1}{\rho_0} \frac{\partial p}{\partial x} \quad 2.13$$

$$\frac{\partial v}{\partial t} + u \frac{\partial v}{\partial x} + v \frac{\partial v}{\partial y} + w \frac{\partial v}{\partial z} + 2\Omega u = -\frac{1}{\rho_0} \frac{\partial p}{\partial y} \quad 2.14$$

$$\frac{\partial w}{\partial t} + u \frac{\partial w}{\partial x} + v \frac{\partial w}{\partial y} + w \frac{\partial w}{\partial z} = -\frac{1}{\rho_0} \frac{\partial p}{\partial z} + g \alpha T \quad 2.15$$

$$\frac{\partial T}{\partial t} + u \frac{\partial T}{\partial x} + v \frac{\partial T}{\partial y} + w \frac{\partial T}{\partial z} = 0 \quad 2.16$$

$$\frac{\partial u}{\partial x} + \frac{\partial v}{\partial y} + \frac{\partial w}{\partial z} = 0 \quad 2.17$$

where, contrary to the previous case discussed on page 10, we have set $x = r\theta$ $y = b - r$ so that y goes from zero at the outer wall to $(b-a)$ at the inner wall. This is the form in which the experimental results will be presented. u is now the zonal velocity. These can be scaled by setting

$$(x, y) = (b - a) (x^1, y^1)$$

$$z = d z^1$$

$$T = \Delta T T^1 = (T_b - T_a) T^1$$

$$t = \frac{(b-a)}{U} t^1$$

The horizontal velocity U can then be scaled on the basis of

the thermal wind, i.e.

$$u = \left(\frac{g \alpha \Delta H^T d}{2 \Omega (b-a)} \right) u'$$

where $\Delta H^T = \sigma_y \Delta T$. The Rossby number is then

$$R_0 = \frac{g \alpha \sigma_y \Delta T d}{4 \Omega^2 (b-a)^2} \quad 2.18$$

where σ_y in this equation corresponds to σ_y in Equation 1.7.

The Eady number is the same as in Equation 1.8.

$$B = \frac{g \alpha \sigma_z \Delta T d}{4 \Omega^2 (b-a)^2} \quad 2.19$$

Eady considered the problem of baroclinic instability under the conditions:

- a. Both viscous and conductive effects are negligible.
- b. The flow is quasi-geostrophic so that $R_0 \ll 1$.
- c. The basic flow has uniform vertical and radial temperature gradients.
- d. The slope of the isotherms is of the order of the Rossby number, or $\sigma_y / \sigma_z \sim R_0$.
- e. The wave amplitude is small enough so that a perturbation theory can be applied.

The basic symmetric state is then given as:

$$T_0 = -\lambda y + B/R_0 z \quad 2.20$$

where λ is a parameter of order unity. The first order geostrophic velocity field is then:

$$U_0 = \lambda z \quad 2.21$$

Using the above assumption and the basic first order state, the quasi-geostrophic equation for the flow can be found by expanding the variables, u' , v' , w' , T' and P' , in the scaled set of

equations derived from Equations 2.13 to 2.17, in powers of Rossby number and equating terms of equal order. This is to first order in Ro , letting $T_1 = \psi z$, $u = -\psi_y$ and $v = \psi_x$

$$\left(\frac{\partial}{\partial t} + \lambda z \frac{\partial}{\partial x}\right) (\nabla_H^2 \psi + B^{-1} \psi_{zz}) = 0 \quad 2.22$$

where the primes have been dropped from the scaled variables.

The boundary condition of $w = 0$ at $z = 0, 1$ is:

$$\left(\frac{\partial}{\partial t} + \lambda z \frac{\partial}{\partial x}\right) \psi_z - \lambda \psi_x = 0 \quad 2.23$$

and the boundary condition $v = 0$ at $y = 0, 1$ is:

$$\psi_x = 0 \text{ at } y = 0, 1 \quad 2.24$$

The more general case of these equations for the atmosphere has been derived by Charney and Stern (1962) and Pedlosky (1964).

To test for the stability we seek a solution of the form

$$\psi = \text{Re } \phi(z) e^{k(x-ct)} \sin(n\pi y) \quad 2.25$$

Any solution with $\text{Im}(kc) > 0$ will grow exponentially with time and thus constitute an unstable condition. The boundary condition at $y = 0, 1$ is identically satisfied. The boundary condition at $z = 0, 1$ leads to a quadratic equation for C whose roots are:

$$kc = \frac{k\lambda}{2} \pm \frac{k\lambda}{2} \left((\delta/2 - \tanh \delta/2) (\delta/2 - \coth \delta/2) \right)^{\frac{1}{2}}$$

and

Thus, kc has a positive imaginary part when $\coth \delta/2 > \delta/2$ or

$$\delta < \delta_c \quad \text{where } \delta_c = 2 \coth \delta_c/2 = 2.399$$

This implies that the flow will be unstable for all wave numbers

$k < k_n$ when

$$B (k_n^2 + \pi^2 n^2) \leq 5.73 \quad 2.27$$

Marginal stability will occur for $k = 0$, $n = 1$ when $B_c = 0.581$. Thus, all wave numbers are stable if $B > B_c$. This condition, when applied to the annulus results indicates that if

$$\Delta v^T = \sigma_z \Delta T = 2/3 \Delta T$$

then the flow should be stable for all values of $\pi_4 < \pi_{4c}$ when $\pi_{4c} = 6 \times B_c = 3.5$. This, of course, will only apply when the flow can be considered inviscid and is most likely to occur when $E \ll 1$ or equivalently for large gap widths.

There is a vertical phase variation implicit in the solution for ϕ when $\text{Im}(c) > 0$. In this case $\phi(z)$ can be rewritten in the polar form as:

$$\phi(z) = |\phi(z)| e^{i\Theta(z)}$$

where

$$\phi(z) = \left[(\sinh(\gamma z) - \frac{\gamma \text{Re}(c)}{\lambda} \cosh(\gamma z))^2 + (\frac{\gamma \text{Im}(c)}{\lambda} \cosh(\gamma z))^2 \right]^{\frac{1}{2}}$$

and

$$\Theta(z) = \tan^{-1} \left(\frac{\text{Im}(c) \cosh(\gamma z)}{\sinh(\gamma z) - \frac{\gamma \text{Re}(c)}{\lambda} \cosh(\gamma z)} \right)$$

These vertical phase variations for the pressure, ψ , and temperature ψ_z have been calculated by Eady and are indicated in Figure 6a. This indicates that the temperature at the upper

surface should lead to that at the bottom.

The kinematics of these waves indicate that the colder fluid flowing towards the warm boundary descends and, ^{the} converse is true for the warm fluid. Thus, the waves carry heat upwards and maintain themselves at the expense of the potential energy of the flow. Since there is no horizontal shear in the basic velocity state, no kinetic energy is converted from the basic state.

A solution to the second order problem by Pedlosky (1966) indicates how the instability initially affects the basic symmetric state. Under the above assumption we can write:

$$\psi = \psi_0 + Ro\psi_1 + Ro^2\psi_2$$

where $\psi_0 = B/Ro z^2/2 - \lambda yz$ and ψ_1 is the solution to Eady's problem. The equation for ψ_2 is then

$$\left(\frac{\partial}{\partial t} + \lambda z \frac{\partial}{\partial x}\right) (\nabla_H^2 \psi_2 + B^{-1} \psi_{2zz}) = -J(\psi_1, \nabla_H^2 \psi_1 + B^{-1} \psi_{1zz}) \quad 2.31$$

where J is the Jacobian with respect to x and y and is equal to zero, since ψ_1 is the solution to Equation 2.22. The boundary conditions are then: $v = 0$ or $\psi_{2x} = 0$ at $y = 0, 1$ and $w = 0$ at $z = 0, 1$

$$\left(\frac{\partial}{\partial t} + \lambda z \frac{\partial}{\partial x}\right) \psi_{2z} - \lambda \psi_{2x} = -J(\psi_1, \psi_{1z})$$

The solution to this problem which modifies the basic state with the previous solution for ψ_1 and initial conditions of $\psi_2 = 0$ at $t = 0$ is:

$$\Psi_2 = -(\gamma^2 (e^{2k \operatorname{Im}(k)t} - 1) / B^{1/2} \lambda \sinh(2n\pi\beta)) \cdot \sinh(n\pi\beta) \cdot \sinh(2n\pi\beta(z - 1/2)) \sin 2n\pi y$$

The changes to the initial temperature and velocity distribution are indicated in Figure 6c. The absolute magnitude of the zonal flow is decreased in the center and increased near the edges of the channel for $z = 0$, and 1. The vertical shear is similarly decreased in the center and increased near the edges. These effects, in turn, mean that the horizontal slope of ^{the} initial isotherms must decrease in the center and increase near the edges.

Davis (1956) has obtained a solution to the quasi-geostrophic equation in an annular region with the curvature term retained. The basic state is assumed as:

$$T = \frac{\Delta_H T}{d} z + \frac{\Delta_r T}{(b^2 - a^2)} r^2$$

The stability criteria is then given as:

$$d^2 \gamma_{sm} B \beta^{-2} (1 + \frac{1}{2} \operatorname{Ro} C_1)^2 < (2.399)^2$$

where γ_{sm} is the s 'th zero of the equation:

$$J_m(\gamma b) Y_m(\gamma a) - J_m(\gamma a) Y_m(\gamma b) = 0$$

$$\beta = \frac{d}{b-a} \quad \text{and} \quad C_1 = \frac{(b-a)}{\frac{1}{2}(b+a)}$$

The first zero is obtained by asymptotic expansion as:

$$\gamma_{1m} = \frac{\pi}{b-a} \left(1 + \frac{(4m^2 - 1)(b-a)^2}{8\pi^2 ab} + \dots \right)$$

Thus, the criteria is:

$$B \left(1 + \frac{1}{2} R_0 C\right)^2 \left(1 + \frac{(4m^2 - 1)}{8} \frac{(b-a)^2}{2ab}\right) < 0.581 \quad 2.32$$

This reduces to the Eady criterion when the curvature term, c , is small.

Several authors have tried to ascertain the manner in which viscous forces modify these results. Kuo (1956 a, b, 1957) has considered the case with the conductive terms replaced by a spatial heating function and the viscous terms treated as proportional to the velocity. These assumptions eliminate the possibility of boundary layer formations. However, the qualitative results do predict the correct form of the stability curve.

Barcelon (1964) has solved the Eady problem for the annulus with the neglect of the horizontal boundaries for a rigid upper and lower surface. In a similar manner Brindley (1960) has extended Davies' solution in cylindrical coordinates for the case of a free upper surface and a rigid lower surface. In each case the horizontal boundary layer is either a rigid surface Ekman layer or a free surface Ekman layer. Thus, the boundary layer problem can be reduced to that of finding the interior solution which has the correct vertical velocity prescribed by these layers; i.e., the vertical velocity at the upper and lower boundaries are:

$$w = -\frac{1}{2} \hat{k} \cdot \hat{\ell} \delta \hat{k} \cdot (\nabla \times W) \quad \text{rigid surface}$$

$$w = -\frac{1}{2} \delta^2 \frac{\partial}{\partial z} (\hat{k} \cdot \nabla \times W) \quad \text{free surface (Hide 1965)}$$

where $\hat{\ell}$ is the normal to the surface. Hide (1963) has used this

approach to solve the Eady problem in cartesian coordinates with a rigid upper and lower surface, a free upper and lower surface, and a free upper surface and rigid lower surface.

Brindley (1960), Barcelona (1964), and Hide (1963) obtained the correct form for the stability curve and the approximate wave number near the knee of the curve. However, the value of E for the position of the knee, i.e., that point at which for larger values of E the flow is symmetric, is an order of magnitude larger than the experimental results. This indicates that the side wall boundary conditions play an essential role in the determination of the viscous cut off.

Since the side wall boundary layers may affect the shape of the velocity profile in the Eady model, it is relevant to consider the effect of introducing a small deformation in the basic Eady velocity profile. Pedlosky (1965) has considered the stability of the flow when the basic zonal velocity is of the form $U_0 = \lambda z + u_g(y, z)$ where $u \ll 1$.

"The change of stability of the flow at the neutral curve of the zero order problem depends only on that part of g which is odd about $z = \frac{1}{2}$ and even about $y = \frac{1}{2}$ "

This has been investigated experimentally with slightly inconclusive results by Lambert and Snyder (1966).

Lorenz (1962) has obtained a numerical solution for the wave regime in the annulus with a two layer model. He employs a simplified set of equations reduced to indicate the basic physical processes. In this manner the nonlinear convective heat transport terms are retained while the angular momentum transport terms are neglected. The heating and viscous effects are parameterized by linear formulae acting at the boundary of the

two fluids. Thus, the solution can demonstrate the effect of the waves on the mean temperature field, but barotropic instability and boundary layer formation are suppressed. The results show remarkably well the qualitative structure of the stability regime. Direct comparison with the experiments is not feasible, however, due to the unknown parameters for the heating and viscous effects.

The structure of the jet stream in the wave regime has been investigated by Rogers (1959). In this case the jet is treated as a free thermal boundary layer phenomenon. By neglecting the viscosity entirely and assuming that the heat conduction across the stream is balanced by the convection of heat along the stream she was able to show that:

1. The temperature difference across the stream and the velocity along the stream both decrease in the downstream direction.
2. There is net outflow of ascending motion on the warm side and descending motion on the cold side of the stream
3. The width of the stream is

$$3 Y_0 = 3 \left(\frac{8 \pi \omega \rho_0}{g_m \Delta e} (b + a) k \right)^{\frac{1}{2}}$$

where ω is the phase speed and m is the number of lobes of the wave.

The point of contact of this solution with the wall acts like a discontinuity.

Davis (1959) has obtained an analytical solution to the nonlinear heat equation under quasi-geostrophic conditions without the boundary layer assumption. Using cylindrical coordinates he obtains a unique wave solution by assuming a form for the angular momentum transport and then stating that the most likely

wave to occur will be the one that carries the most heat. This analysis is valid when the vertical temperature gradient is not significantly larger than the horizontal temperature gradient or equivalently in a deep annulus where

$$\Delta_V T \sim \frac{d}{(G-a)} \Delta_H T$$

Rogers (1961) has extended this solution to include the side wall viscous boundary conditions with the neglect of the horizontal boundaries. The boundary layers tend to increase the horizontal velocity of the jet at the outer walls and decrease it at the inner wall. The equation also permitted an oscillating solution such that the results could lead to an explanation for the wave shape vacillation in the annulus.

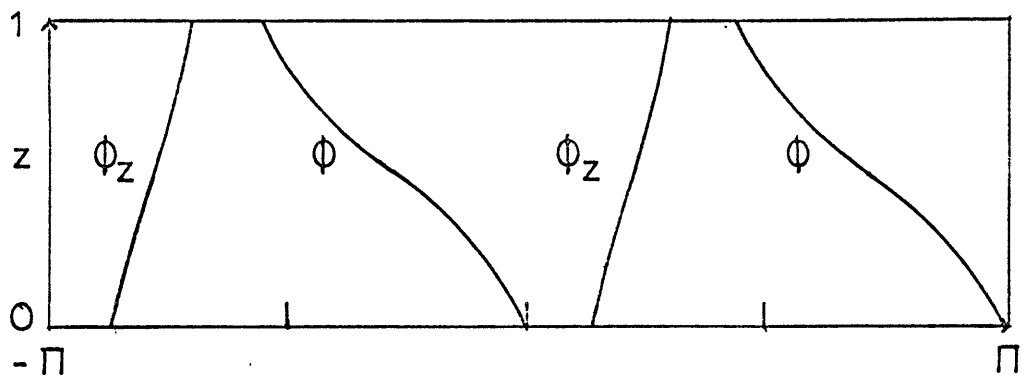
Lorenz (1963) has used slightly less simplified equations than those in Lorenz (1962) to explain the existence of vacillation and nonperiodic flow in the annulus. The variables of the two layer model are expanded in a truncated fourier series. Further, only two modes in the cross channel direction are allowed. The author then postulates that the Rossby circulation of the first mode, corresponding to $n = 1$ in Equation 2.25 are always possible solutions when the symmetric flow is unstable, but may be unstable with respect to Rossby circulations of the second mode, i.e. $n = 2$. The numerical solution of the resulting set of equations indicates that as the rotation rate is increased for a fixed ΔT , the symmetric flow first becomes unstable with respect to the first mode. At slightly higher rotation rates both the first and second modes may occur without changing their individual shape. This is called the mixed mode. The mixed

mode, in turn, can be unstable with respect to symmetric and nonsymmetric vacillation. Symmetric vacillation has the distinction of not changing the statistical properties of the fully developed solution. Lorenz(1963) also finds a nonperiodic region with more than two degrees of freedom. Further extension is not possible without considering the interaction of the higher modes previously eliminated.

Figure 6a. Phase variation; Eady normal mode. (Eady 1949)

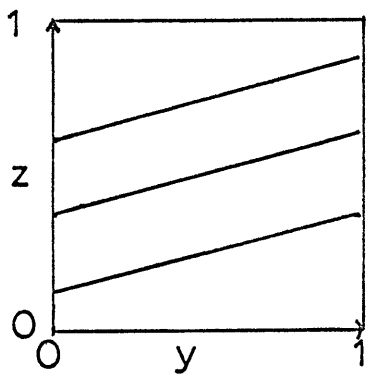
Figure 6b. Basic state; Eady solution.

Figure 6c. Second order convection to mean state; Eady solution. (Pedlosky 1966)

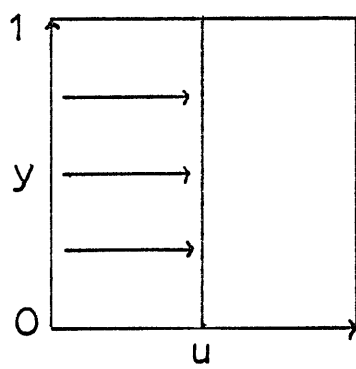


VERTICAL PHASE

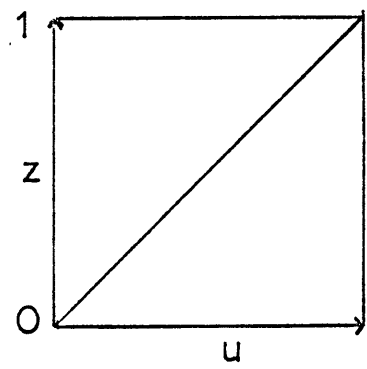
Figure 6a



ISOTHERMS

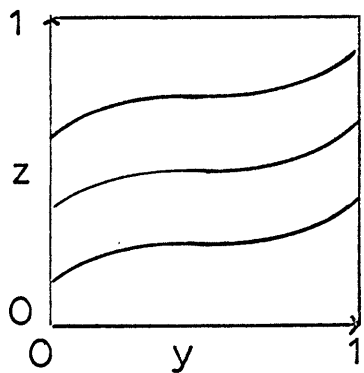


$U_0(z)/z = \text{const.}$

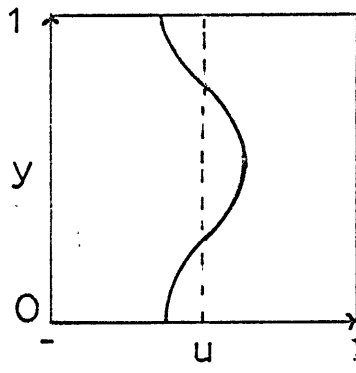


$U_0(z)$

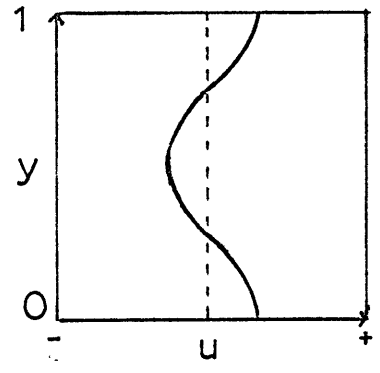
Figure 6b



ISOTHERMS



$U_2(z=0)$



$U_2(z=1)$

Figure 6c

CHAPTER III

Description of the apparatus and the experimental procedure

Apparatus

The basic apparatus is shown schematically in Figure 2, and in greater detail in Figure 7a. A detailed description of the construction and operation of the apparatus is given in Appendix 1.

The convection chamber is the annular region between the outer and inner cylinders of radii $b = 38.445 \text{ cm.} \pm 0.01 \text{ cm.}$ (maximum deviation) and $a = 23.105 \pm 0.002 \text{ cm.}$ (maximum deviation). These cylinders are fastened to a phenolic plate with O ring seals under each cylinder. The resulting gap width $(b-a)$ after careful alignment is $15.280 \pm 0.016 \text{ cm.}$ (maximum deviation). The bottom of the convection chamber is formed with a 1 inch thick plexiglas false bottom supported 15 cm. above the phenolic base. It is flat to within ± 0.005 inches. Grid lines are marked over 120 degrees on the underside of the false bottom and three 9 inch fluorescent lights are mounted directly below to supply lighting for dye studies. The resulting chamber is filled with water to a depth of 15.28 cm. A plexiglas lid is placed on the top of the cylinders, not in contact with the water, to reduce the effects of evaporation.

The outer bath is formed by mounting a 1 inch wide by 18 inches high plexiglas cylinder with a 38 inch inside diameter on the phenolic base outside of the outer cylinder. The inside

bath is the inner volume of the smaller cylinder. The top of each bath is sealed by a 3/4 inch plexiglas top with side ring seals. In this experiment the outer bath was always kept at a warmer temperature than the inner bath.

A Haake circulator model NBS maintains the temperature and flow rate of the circulating water in each bath. The inflow temperature is held constant in time to $\pm 0.05^{\circ}\text{C}$. with a flow rate of 2.4 gallons/minute. Due to the large heat flux in the annulus, the difference in temperature between the inflow and outflow of the bath is about 8% of the resulting impressed temperature difference. This drop tends to occur in the thermal boundary layer near the lower part of the warm wall and the upper part of the cold wall where most of the heat is extracted from or added to the bath. Consequently, there is a vertical variation of mean temperature in each wall. This was reduced to some extent by directing the circulating water at the walls and increasing the local turbulent transfer in the boundary layer. The circulating water is forced through four porous circulation tubs located at different heights and released such that the maximum temperature control is applied to the lower region of the hot wall and the upper region of the cold wall. The temperature of each wall is monitored with 24 thermocouples, 12 of which span the 15.28 cm. height of the convection chamber.

The vertical variation of the deviation of wall temperature from the mean wall temperature in the region of the convecting fluid is shown in Figure 8. This was determined from an azimuthal average of the 12 thermocouples spanning the chamber on the outer wall for Run 34 in the symmetric regime where the

vertical variation should be largest. The local temperature at each point on the wall may also vary by $\pm 2.5\%$ of the impressed temperature difference as a wave passed that point.

The phenolic base holding the convection chamber and the baths is mounted 4 inches above the turntable which is a 42 inch diameter by $\frac{1}{2}$ inch thick ground steel plate. This plate is supported by a $22\frac{1}{2}$ inch diameter ring bearing mounted on a triangular stand with three adjustable leveling legs. A hollow stainless steel shaft fastened to the underside of the plate supports a Browning notched gear, the fluid slip rings and the eight coin silver power slip rings. The turntable is driven with a $\frac{1}{2}$ h.p. synchronous motor and a variable speed Graham transmission. This is coupled to the table via a Browning gear and belt system. The rotation rate of the table would be varied over the range of 0 to 20 rpm. with a mean stability of $\pm 0.089\%$ of the rotation rate.

The temperature of the convecting fluid is determined with four vertical arrays of four thermocouples each. (See Figures 9a, 9b and 9c.) These are constructed from 5/1000 inch copper constantan thermocouple wire. Each junction is positioned vertically to within ± 0.025 cm. of 1.04, 5.44, 9.84 and 14.24 cm. from the false bottom. The four arrays are then positioned with the same spacing from the outer wall and separated by 60° in a counter clockwise direction from each other with decreasing distance to the axis of rotation. Thus, the net result is an array of 16 thermocouples, the outer edge being separated from each vertical and horizontal boundary by 1.04 cm. with the inner points being separated by 4.4 cm. and 60° in azimuth.

Each thermocouple is referenced to a single thermocouple in an ice bath located on the turntable. The signals are carried to the recording equipment via a set of 36 silver-plated low noise level slip rings. The output from either the wall thermocouples or the thermocouple array can be recorded on either a four channel Beckman Dynograph type SII recorder or in digital form on punched paper tape using a digital data acquisition system. The recorder has a response time of 100 cps. and a noise level of 1 uv rms. The digital data acquisition system consists of a Sigma Cohn stepping switch, a timing circuit, a Dana D.C. data preamplifier, a digital voltmeter, and a paper tape punch. The sampling rate is variable, but in the experiment it was generally set to sample 16 thermocouples and three zero references every 9.8 sec. The maximum sampling time, determined by the length of the paper tape, is two hours with this sampling rate. The schematic of the sampling sequence is indicated in Figure 7b. After calibration and the noise level is considered the relative accuracy of the temperature measurements is $\pm 0.068^{\circ}\text{C}$ for all thermocouples except the four near the free upper surface where the error, due to larger calibration errors, is $\pm 0.085^{\circ}\text{C}$.

Experimental procedure

The experimental data collected for each run in Figure 5 consisted of the following:

1. The mean temperature of the baths determined from the thermometers recording the temperature of the inflow and outflow from each bath.

2. The corresponding flow rates through each bath.
3. The mean temperature difference across the annulus determined from the mean of the difference between the 12 thermocouples in each wall.
4. The mean rotation period determined from ten periods measured with a Beckman counter.
5. The state of the flow determined by surface observation when possible.
6. A Beckman chart record of at least four of the convection chamber thermocouples.
7. A digital sample of the 16 array thermocouples and three reference positions for at least 15 minutes in the symmetric regime and at least the minimum of ten wave periods or two hours in the regular wave regime, vacillating regime or irregular regimes.

This data was collected at a set of predetermined grid points in $G^{1/2}$ and E^{-1} . The minimum increment in rotation rate was set by choosing a logarithmic interval equivalent to a change in rotation period of four sec. at the transition from the symmetric regime to the regular wave regime with an impressed temperature difference of 5°C . This determines the values of E^{-1} . The corresponding logarithmic intervals for G were set by choosing 9.3°C and 2.6°C as the maximum and minimum impressed temperature differences. These limits correspond to the maximum easily controllable temperature difference between the baths and the minimum temperature difference necessary to produce reliable and meaningful thermocouple output, respectively.

In the acquisition of the data it was not possible to maintain the impressed temperature difference at these levels due to the variation of the Nusselt number throughout the range of E^{-1} covered. Consequently, the experimental runs will be characterized by the mean value of ΔT for each set of runs at

that temperature difference. The actual values of ΔT are indicated in Tables IIa, IIb, and IIc, for each run. The corresponding mean values of ΔT for each set of runs are 9.12, 5.09, and 2.53 C°. Each set of runs will be referred to in the text by these characteristic mean values. C. E. Preliminary experiments were run for each temperature at several multiples of the intervals in E^{-1} . Data was then collected at the smaller intervals in E^{-1} near the regime transition points and near some of the wave transition points until all of the experimental points in Figure 5 were completed. The order in which each point was sampled is indicated by the run number in Table IIa, IIb, and IIc.

The experimental procedure followed was to set the inflowing temperature for each bath to give approximately the required impressed temperature difference between the convection chamber walls. The mean temperature between the baths was chosen to be as close as possible to room temperature. The apparatus was then allowed to reach equilibrium for at least 48 hours with no rotation. The state of the fluid at $\Omega = 0$ was also used as a reference check to be sure that all systems were behaving well. The rotation rate was then changed successively to the new experimental points. The minimum setup time allowed between experiments was five hours, and in most cases it exceeded ten hours in the wave regime, and was always greater than 15 hours in the symmetric regime. In all cases no data was recorded until the thermocouple output indicated on the Beckman recorder showed no detectable variations for a period of at least 1.5 hours.

During the setup time the thermocouples along the diagonal in radius and depth from the lower part of the cold wall and the upper part of the cold wall were recorded. After Run No. 36 the average wall temperature was also recorded for at least 15 min. just prior to the start of the digital sample. The 16 array thermocouples were then recorded with the digital data acquisition system. The number of waves noted on Figure 5 was obtained from observation of the surface flow pattern made visible with aluminum flakes. This was not possible at very high rotation rates and/or small temperature differences because the surface patterns were not visible.

The resulting digital data matrix was then transferred to magnetic tape and converted to a nondimensional temperature matrix by dividing the converted temperature differences centered at the mean temperature of the baths by the actual impressed temperature difference. At the same time, the mean value, and standard deviation for each element in the array were calculated. Contour plots of mean temperature and standard deviation were drawn and the values of σ_r , σ_z and available potential energy calculated for each run. In addition to this a calcomp plot for each temperature vector was made in order to determine the position and occurrence of incorrectly sampled data (which occurred very seldom). In addition to this, time series analysis for power spectrum, complex cospectrum, and coherence was made for each run in the wave, vacillating and irregular regimes for $\Delta T = 9.12^\circ\text{C}$ and for the last six runs on Figure 5 with $\Delta T = 5.09^\circ\text{C}$.

Some of the runs are not indicated in the results because

no internal temperature measurements were made. Thus, Run Nos. 1 through 17 were made in the process of checking and correcting various mechanical and electrical problems of the apparatus. Run Nos. 19, 43, and 57 were calibration runs for the thermocouples.

During some of the runs one thermocouple was broken. When this occurred the output of the thermocouple was replaced by a linear interpolation between the adjacent vertical thermocouples for each sample time. This process generally underestimates the temperature at that point because the vertical temperature gradient increases with decreasing height. However, the observations of the data indicate that the additional error due to the interpolation is not greater than +2.7% of ΔT . Thermocouple T (2,2) was broken for Runs 24 to 26, and thermocouple T (1,3) was broken during Runs 69 to 73.

Figure 7a. Detailed schematic of apparatus.

- | | |
|--------------------------------|----------------------------------|
| a. reference thermocouple | p. outflow tube |
| b. ice bath and dewar flask | q. copper cylinder; inner |
| c. wall thermocouples | r. copper cylinder; outer |
| d. plexiglas false bottom | s. plexiglas outer bath cylinder |
| e. thermocouple plug | t. phenolic base plate |
| f. vertical thermocouple array | u. support blocks |
| g. circulation tubes | v. steel turntable |
| h. outflow tubes | w. electrical power slip rings |
| i. thermocouple mounting block | x. browning gear |
| j. cannon plug and mount | y. steel shaft |
| k. electrical slip rings | z. fluid slip rings |
| l. plexiglas slip rings | A. adjustable foot screw |
| m. O ring seal | B. leg |
| n. plexiglas cover | C. turntable bearing |
| o. copper mounting fins | |

Figure 7b. Schematic diagram of the sampling procedure.

Figure 8. Vertical variation of the wall temperature.

Figure 9. Thermocouple array.

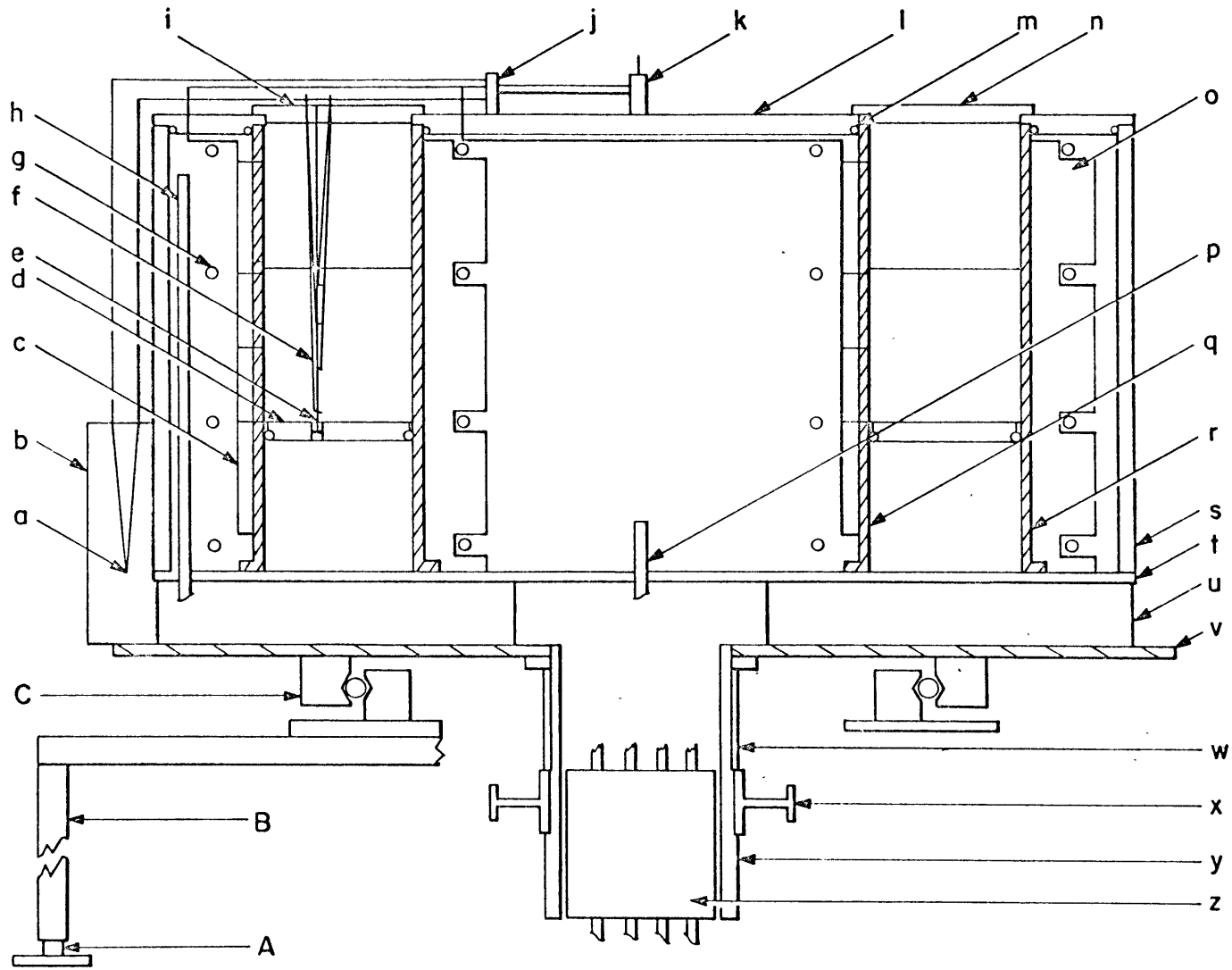


Figure 7a

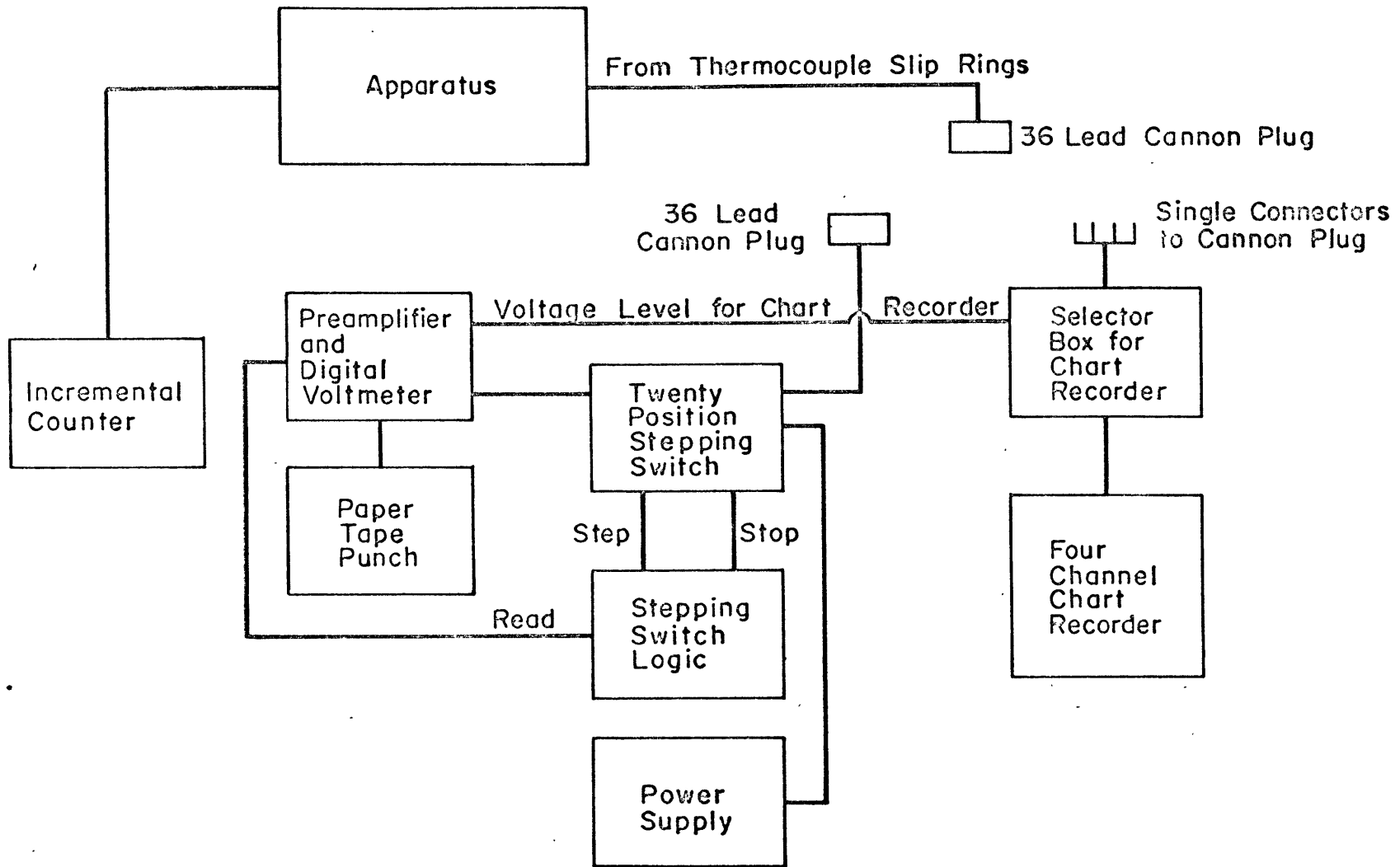


Figure 7b

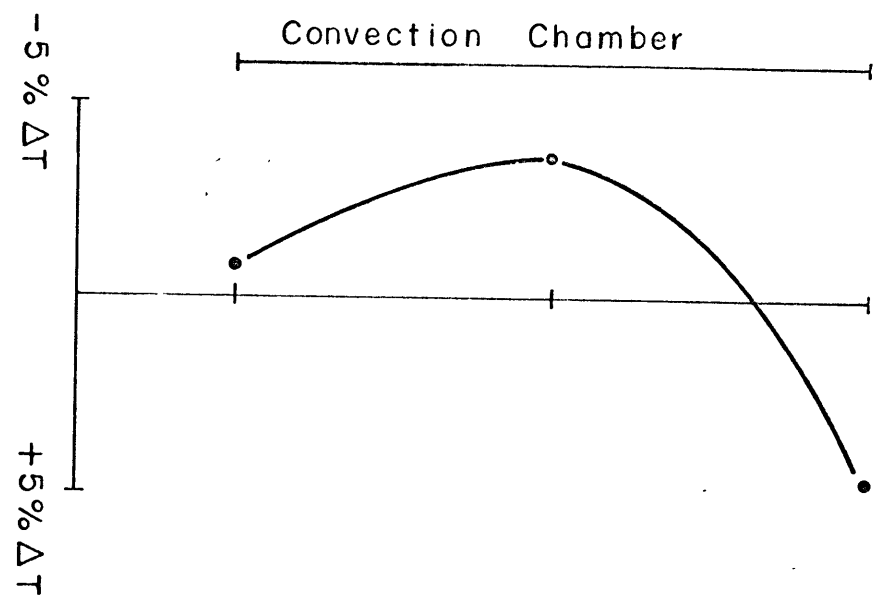
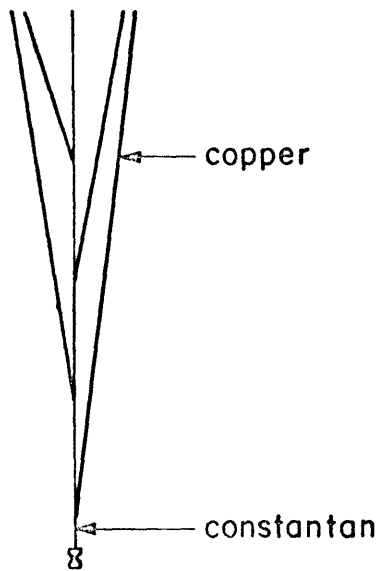
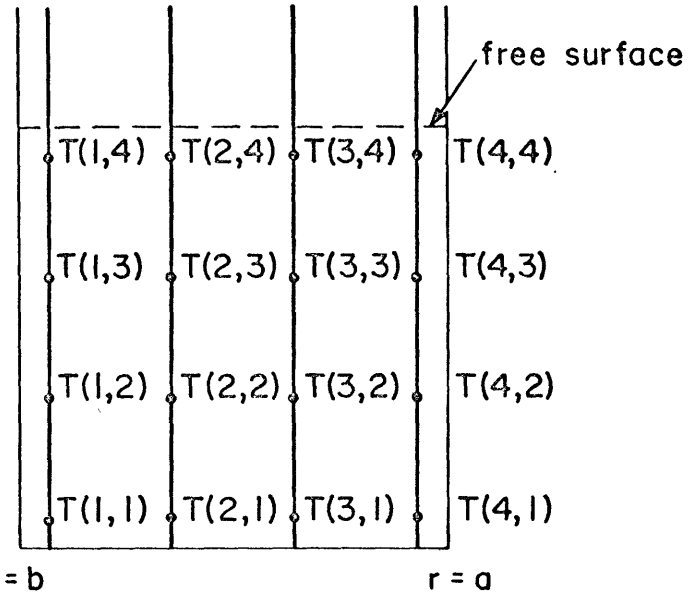


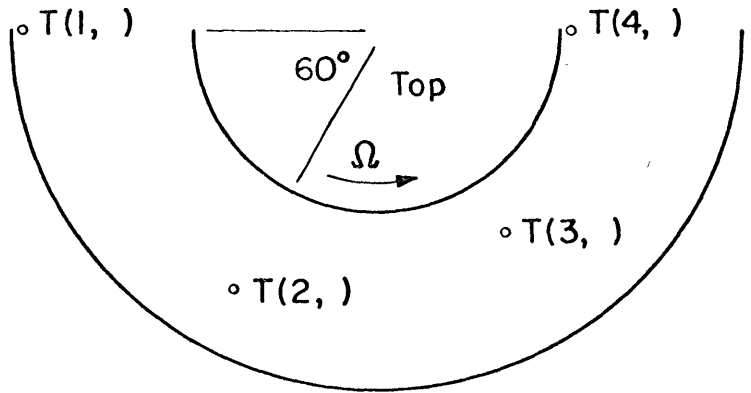
Figure 8



Vertical Thermocouple Array



Radial Position of Vertical Arrays



Azimuthal Position of Vertical Arrays

Figure 9

CHAPTER IV

PRESENTATION AND INTERPRETATION OF THE RESULTS

The experimental results will be discussed in three sections. This first section formulates a description of the temperature traces and surface flow patterns used to determine the annulus regimes and an indication of the transition points between the regimes. Secondly, the mean temperature structure of the flow, the variation of the internal parameters, the variation of wave amplitude, and the available potential energy of the fluid will be presented. The third section will discuss the power spectrum, cospectrum, coherence and phase of the disturbance. In the foregoing discussion contour data from a few selected runs, mostly at $\Delta T = 9.12 \text{ C}^\circ$, are indicated as characteristic of the basic pattern involved. Any experimental run which is at variance with these examples will be mentioned. A discussion of the technique used to calculate the following results is presented in Appendix 2.

The location of the experimental points is shown in Figure 5. The experimental parameters $\Delta T, \omega$, the state of the flow, $G^{\frac{1}{2}}$ and E^{-1} are listed in Tables IIa, IIb, and IIc for the set of runs at 9.12 C° , 5.09 C° and 2.53 C° , in order of increasing E^{-1} for each set. This should facilitate identification of the plotted points in Figure 5 with the correct run numbers as they are referred to in the text. This table along with the wave numbers indicated on each of the graphs should also enable the reader to identify each point on the graphs with the correct run number.

TABLE II a

Experimental Data for $\Delta T = 9.12^\circ\text{C}$

Run No.	State	ΔT $^\circ\text{C}$	ω sec^{-1}	E^{-1} $\times 10^{-4}$	$G^{\frac{1}{2}}$ $\times 10^{-3}$	B	1 B_{crit}	2 M_p
31	S	8.86	0.0	0.0	9.293			
72	S	8.72	0.0	0.0	9.186			
32	S	8.86	0.053	0.266	9.286	8.890		
47	S	9.06	0.094	0.468	9.367	3.118		
34	S	9.86	0.188	0.942	9.771	0.943		
36	4	9.27	0.205	1.028	9.475	0.690	0.415	-
39	4	9.10	0.215	1.077	9.437	0.618	0.415	-
44	5	9.08	0.267	1.338	9.408	0.392	0.357	3
46	5	9.09	0.292	1.462	9.403	0.326	0.357	4
45	7	9.11	0.317	1.587	9.413	0.281	0.260	5
35	7	9.08	0.392	1.968	9.419	0.180	0.260	7
41	7	9.11	0.458	2.298	9.433	0.130	0.260	8
42	6	9.08	0.536	2.697	9.407	0.093	0.305	10
40	6	9.05	0.639	3.187	9.309	0.066	0.305	12
37	6	9.03	0.640	3.211	9.379	0.067	0.305	12
70	8	9.10	0.771	3.916	9.419	0.042	0.223	15
38	7	9.04	1.055	5.290	9.396	0.026	0.260	20
73	V	9.22	1.296	6.566	9.440	0.016		
71	V	9.38	1.550	7.867	9.549	0.012		
69	I	9.41	1.846	9.319	9.534	0.008		

1. B_{crit} is the critical value of B for the observed wave number.

2. M_p is that wave number which should theoretically have the maximum growth rate as calculated from the observed value of B.

TABLE IIb

Experimental Data for $\Delta T = 5.09$

Run No.	State	ΔT °C	ω sec ⁻¹	E^{-1} x10 ⁻⁴	$G^{\frac{1}{2}}$ x10 ⁻³	B	Bert.	M_p
28	S	4.86	0.0	0.0	6.593			
56	S	4.86	0.0	0.0	6.675			
64	S	4.90	0.0	0.0	6.667			
21	S	4.84	0.039	0.189	6.589	8.756		
20	S	5.20	0.132	0.642	6.825	1.009		
61	S	5.28	0.135	0.664	6.896	0.889		
59	3	5.18	0.143	0.703	6.824	0.736	0.472	-
22	4	5.01	0.161	0.789	6.708	0.589	0.415	-
60	6	5.03	0.224	1.105	6.751	0.275	0.305	5
62	7	5.01	0.317	1.558	6.740	0.136	0.260	8
63A	6	5.07	0.465	2.281	6.740	0.064	0.305	12
24	7	5.02	0.646	3.179	6.725	0.035	0.260	15
25	6 ³	5.07	0.768	3.756	6.685	0.025	0.305	20
26	7 ³	5.10	0.911	4.471	6.751	0.018	0.260	24
65	V	5.22	1.093	5.391	6.858	0.013		
63B	V	5.28	1.310	6.469	6.919	0.009		
66	V	5.30	1.550	7.646	6.916	0.007		
67	I	5.32	1.849	9.120	6.905	0.005		

3. This wave number was inferred from the phase information obtained from the spectral analysis of the thermocouple data.

TABLE IIc

Experimental Data for $\Delta T = 2.530^\circ$

Run No.	State	ΔT °C	ω sec ⁻¹	E^{-1} x10 ⁻⁴	$G^{\frac{1}{2}}$ x10 ⁻³	B	Bert.	M_p
55	S	2.38'	0.00	0.00	4.662			
48	S	2.53	0.101	0.497	4.804	0.800		
49	3	2.47	0.111	0.551	4.731	0.594	0.474	-
50	6 ⁴	2.49	0.448	2.228	4.794	0.035	0.306	17
51	7 ⁴	2.55	0.643	3.186	4.827	0.018	0.261	24
53	6 ⁴	2.58	0.767	3.777	4.867	0.013	0.306	28
54	V	2.62	0.917	4.524	4.897	0.010		
52	V	2.59	1.073	5.331	4.888	0.007		

4. This wave number was inferred from the phase of the wave at the different vertical thermocouple arrays determined from a calcomp plot of the data.

Flow regimes

The typical temperature oscillations at thermocouple T (3.3) in the wave regime for Runs 36, 42 and 38 with $\Delta T \dot{=} 9.12 \text{ C}^\circ$ are shown in Figure 10a. Run 36 is a four wave pattern near the transition from the symmetric flow. The slightly irregular wave pattern has persisted for at least 12 hours. At higher rotation rates the wave pattern becomes much more even as in Run 42. Run 38 denotes a regular wave pattern with some slight irregularities. Figure 10b indicates the typical temperature trace from each thermocouple in the vertical array. T (2, J) J = 1, 4 for Run 38. It is obvious that the wave form passing the upper and lower thermocouples near the boundaries is less regular than the interior ones. This structure also appears in the traces from thermocouples near the cylinder walls. There was a clearly discernable regular wave pattern on the surface of the fluid for each of these runs. The characteristic temperature trace in the symmetric regime consists of much higher frequencies whose amplitudes are at least one order of magnitude below those in Figure 10 (a, b).

Figure 10c illustrates the temperature traces which are more characteristic of the vacillating regime, Runs 73 and 71, and irregular regime, Run 69. The transition between the regular wave regime and the vacillating regime is not as clear as the transition from the symmetric flow to the regular wave flow. However, there is a distinct appearance of a higher frequency oscillation in the wave pattern and an increase in the wave period. The higher frequency oscillations are probably due to

a wavering of the wave shape as it passes the probe. The third trace in Figure 10c is indicative of the irregular flow in that there is no real discernable regular wave pattern. The trace appears more like the results of an interaction between several uncorrelated long waves coupled with some wavering in each wave shape which produces the high frequency component. The transition from the vacillating to irregular flow is also not as clear as from the symmetric to regular wave flow. These conclusions, with the exception of the wavering, also seem to be substantiated by the power spectrum results discussed in a later section.

Treating the above temperature traces as characteristic of each regime along with the observations of the free surface, the regimes can be labelled as in Figures 4 and 5. The position of the transition is taken as the midpoint between the two nearest points with the different characteristics of each regime. The three points representing the transition from the symmetric regime to the wave regime have a mean value of $\overline{\Pi}_4 = 3.746 \pm 0.360$ for $2.750 \times 10^7 \leq \Pi_5 \leq 9.721 \times 10^7$. A line of best fit between the three points is given as:

$$\text{Log } \overline{\Pi}_4 = (-0.1977 \pm 0.9107) + (0.1000 \pm 0.1182) \text{Log } \Pi_5$$

(standard error)

Consequently, with only three points, it is not significantly different from being independent of Π_5 .

The transition between the regular wave regime and the vacillating regime is determined in the same manner for the three corresponding points as:

$$\text{Log } \Pi_4 = (-9.1111 \pm 0.3685) + (0.6515 \pm 0.0392) \text{Log } \Pi_5$$

(standard errors) for $1.737 \times 10^9 \leq \Pi_5 \leq 3.554 \times 10^9$

This transition line indicates that points to the right of this line have the characteristics of vacillation or irregular flow. It does not indicate that vacillation will not occur to the left of the line, but only that this did not occur in this series of experiments. Previous results on smaller annuli indicate that vacillation may occur at several points within the wave regime.

The transition from the vacillating to the irregular regime is determined from only two points to be given by:

$$\Pi_5 = 7.259 \times 10^9$$

$$\text{For } 2.783 \times 10^{-2} \leq \Pi_4 \leq 5.040 \times 10^{-2}$$

This is significant because previous results indicated that the irregular flow at large values of Π_5 might occur at values of Π_4 of order unity (see Figure 3). These results also indicate that very high rotation rates will have to be used in order to study the irregular flow in annuli with large gap widths. The rotation period for Run 69, for example, is 3.4 sec.

Finally, one must note that the wave numbers on Figure 5 do not increase monotonically with increasing rotation. This has been investigated at the surrounding points near, for example, Run 35, where at a later time Runs No. 41, 42, 44, 46, 45 were taken to verify the result of 35. The phenomenon appears to be repetitive, though not necessarily unique, since the point

determined by Run 62 at $\Delta T \doteq 5.09 \text{ C}^\circ$, wave number 7, was found on a previous run to be 5 waves.

Interior temperature structure

In the presentation of the time averaged data it is implicitly assumed that the time average has replaced the azimuthal average. In this manner the averaged value of the quantities can be plotted and contoured as if the vertical thermocouple arrays were all in the same azimuthal position. The implied assumption is that the temperature field is advected by each thermocouple. This is probably true in the wave regime where the phase of the wave is propagated at an apparently uniform rate at all levels. In the symmetric regime, the presence of the vertical shear means that there is at least one stationary surface which is not advected by the probe. However, since the main characteristic of this regime is its azimuthal symmetry this should not prove to be a poor assumption.

The contour plots presented here are drawn using a modified computer program, the original of which was written by the Geophysical Fluid Dynamics section at E.S.S.A. in Washington, D.C. and supplied to the author by Dr. Stephen Piascek. This program plots a given number of contours between the maximum and minimum points in an array. This means that some care must be exercised in the comparison between plots of the same parameter because the contour interval will vary slightly. In order to aid the comparison, the contour interval, the maximum value, and the minimum value of each plot in the figure are given in the

caption. The advantage of this display is that the structure of each matrix is displayed clearly, even when the mean values of the matrix vary from one run to another. In these plots the warm outer cylinder is on the left side of the contour plot. The gap between the edges of each contour represents, approximately, the distance between the convection chamber boundaries and the thermocouple array.

Figures 11a, 11b, and 11c show the contour plots of mean temperature for $\Delta T = 9.12^\circ \text{C}$ in the symmetric regime, the wave regime and the vacillating and irregular regimes, respectively. They are presented in order of increasing rotation rate.

The contour interval for Figure 11a changes from 0.059 at Run 31 to 0.087 at the transition point, Run 34. This fact along with the characteristics of the actual plots indicates that the vertical stratification is increasing in this region with increasing rotation rate. This figure also indicates that the radial temperature gradient is increasing with increasing rotation rate. Further, there is an increase in the area of relatively isothermal fluid near the upper surface of the warm cylinder from Run 31 to Run 34. The contours of mean temperature for Run 31 with $\Omega = 0.0$ also compare favorably with the results of the numerical work discussed previously.

The isotherms for Run 36 (Figure 11b) in the wave regime have a much smaller slope than those appearing in the symmetric flow. This indicates that the waves have released some potential energy from the fluid. Since the contour intervals are almost the same for each run in Figure 11b, it appears that the vertical stability of the flow in the wave regime does not

- Figure 10a. Temperature traces; wave regime
- Figure 10b. Simultaneous temperature traces; Run 42, single vertical array.
- Figure 10c. Temperature traces; vacillating and irregular regimes.
- Figure 11a. Contours of mean temperature; symmetric regime.

Run No.		Min. Value*	Max. Value*	Contour Interval
31	Mean Temp.	-0.154	0.438	0.059
47	Mean Temp.	-0.240	0.449	0.069
34	Mean Temp.	-0.334	0.535	0.087

Figure 11b. Contours of mean temperature and standard deviation; wave regime.

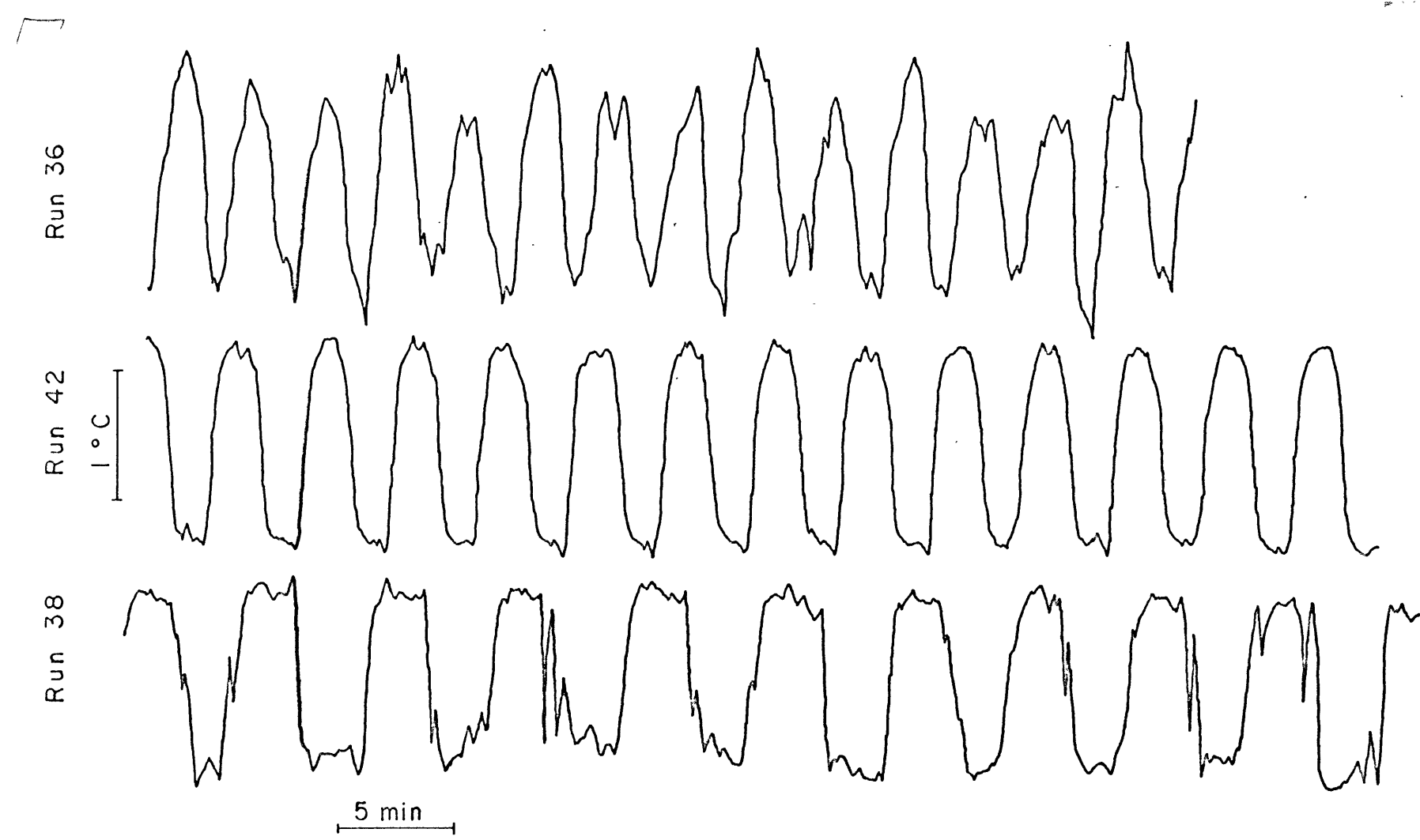
Run No.		Min. Value*	Max. Value*	Contour Interval
36	Mean Temp.	-0.269	0.523	0.079
	Stand. Dev.	0.012	0.077	0.013
42	Mean Temp.	-0.262	0.500	0.076
	Stand. Dev.	0.014	0.084	0.014
38	Mean Temp.	-0.292	0.494	0.079
	Stand. Dev.	0.022	0.076	0.011

Figure 11c. Contours of mean temperature and standard deviation; vacillating and irregular regimes.

Run No.		Min. Value*	Max. Value*	Contour Interval
73	Mean Temp.	-0.300	0.461	0.076
	Stand. Dev.	0.019	0.076	0.011
71	Mean Temp.	-0.315	0.469	0.078
	Stand. Dev.	0.020	0.085	0.013
69	Mean Temp.	-0.341	0.463	0.080
	Stand. Dev.	0.023	0.089	0.013

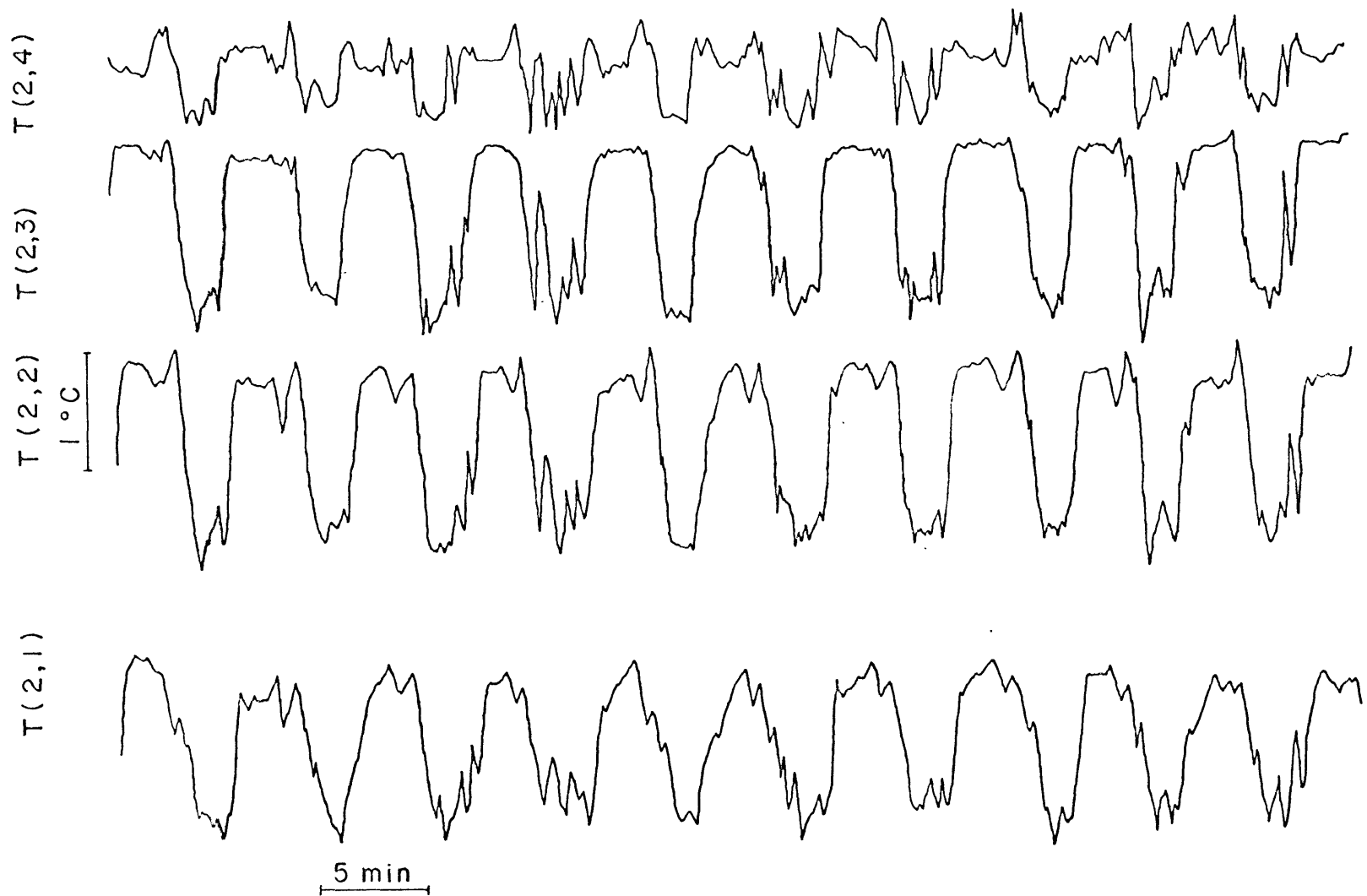
*The maximum and minimum values are the nondimensional maximum and minimum values of temperature and standard deviations determined from the nondimensional temperature defined as:

$$T = (T - \bar{T}_m) / \Delta T$$



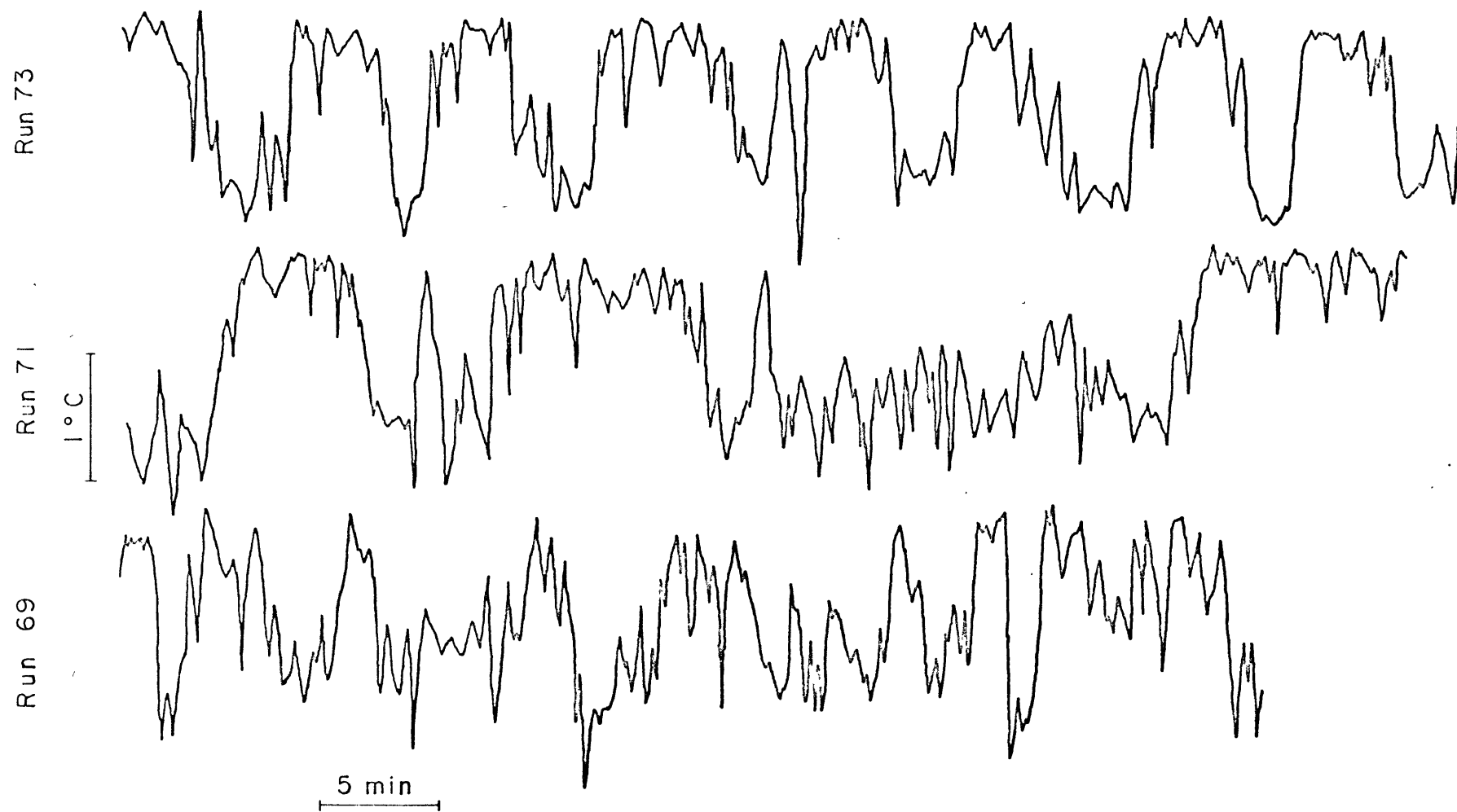
Temperature Traces from Thermocouple T(3,3)

Figure 10a



Temperature Traces from a Vertical Array of Thermocouples for Run 38

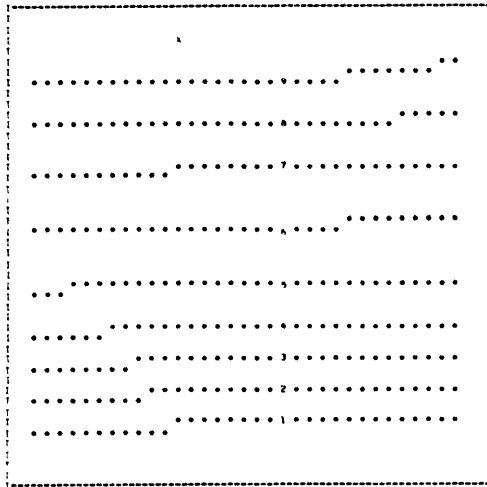
Figure 10b



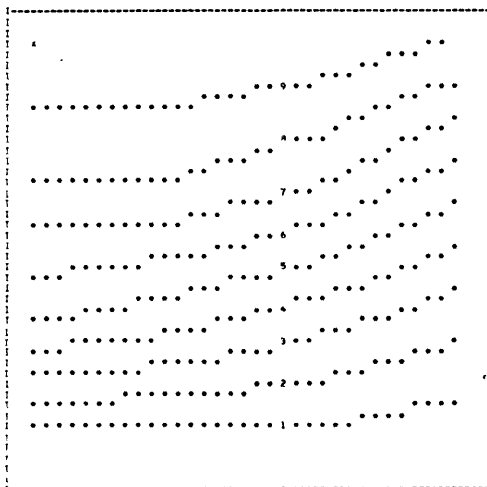
Temperature Traces from Thermocouple T(3,3)

Figure 10c

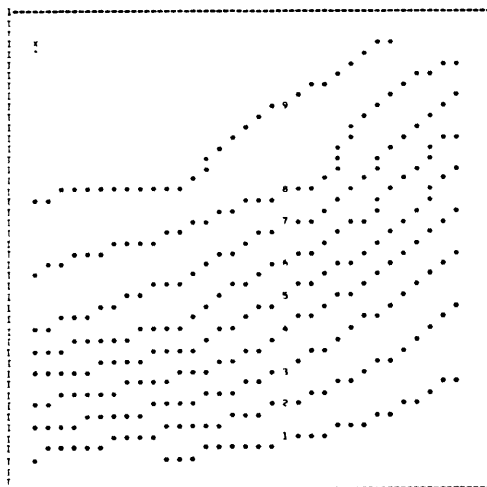
Mean Temperature



Run 31



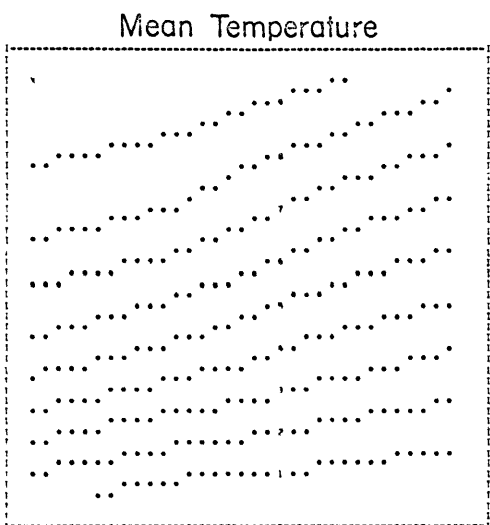
Run 47



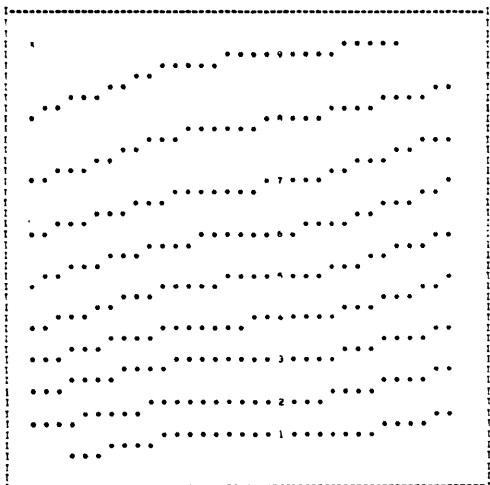
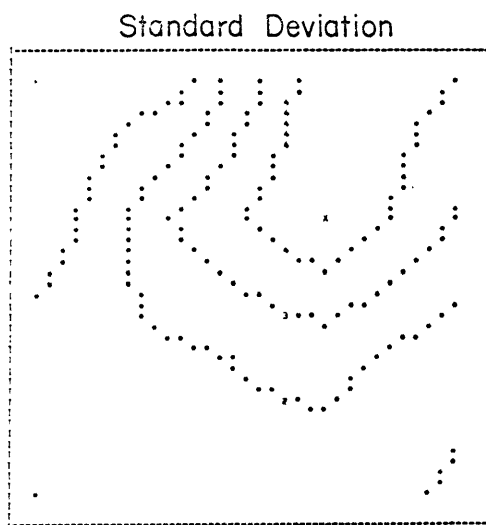
Run 34

Figure 11a

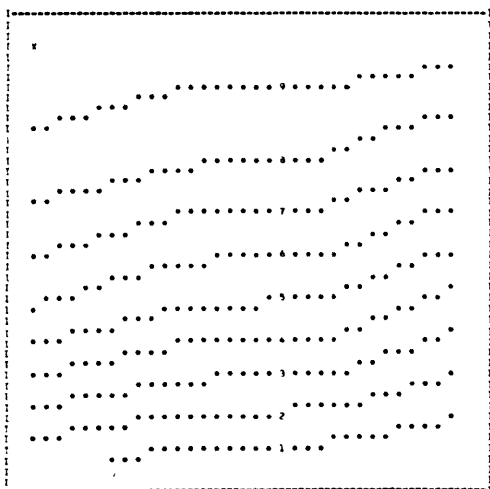
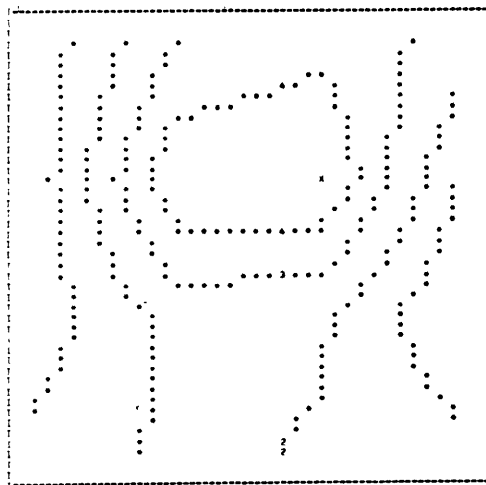
10226



Run 36



Run 42



Run 38

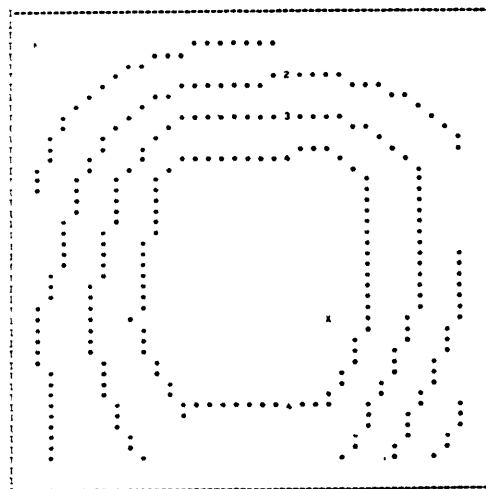
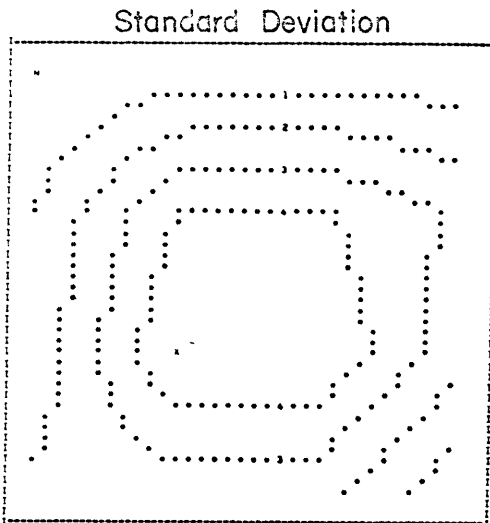
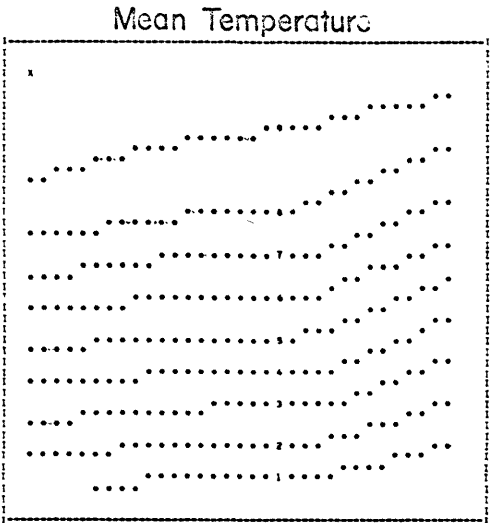
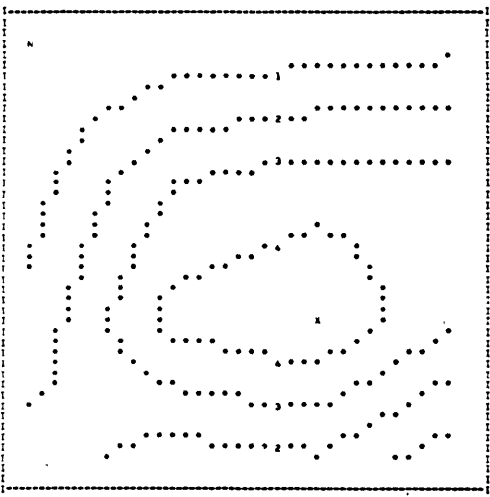
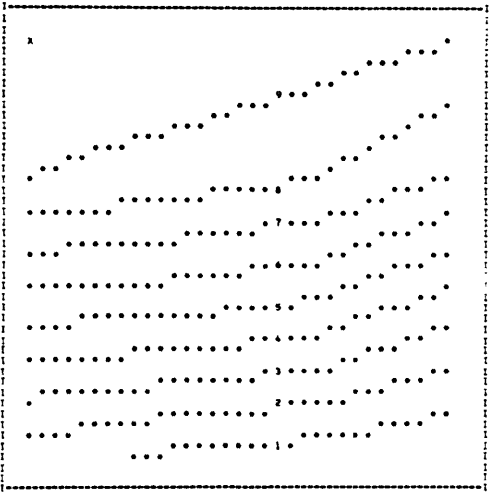


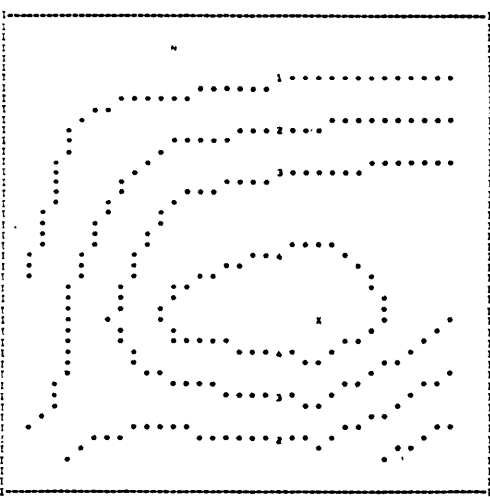
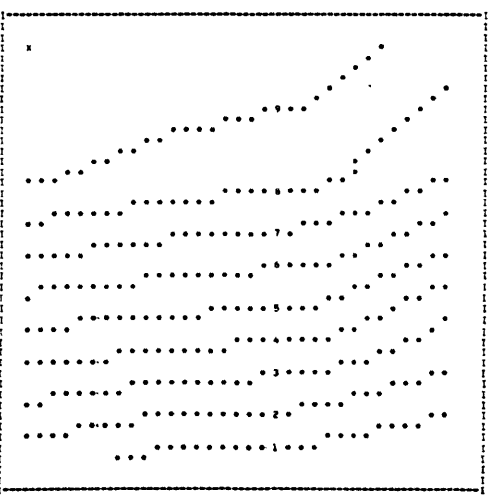
Figure 11b



Run 73



Run 71



Run 69

Figure 11c

change very much from Run 36 to Run 38. The radial temperature difference has a slight tendency to decrease with increasing rotation rate.

The differences in the isotherm plots between the vacillating and irregular flows in Figure 11c are not so obvious. There is an appearance of a larger region of isothermal fluid near the upper region of the warm wall^{as} compared to the temperature structure in the wave regime. This region tends to increase with increasing rotation rate, i.e.: from Run 73 to 69. There is also an increase in the slope of the isotherms near the cold wall as compared to those in the wave regime. The mean temperature structure seems to resemble that of the symmetric flow more than that of the regular wave regime.

A discussion of the internal parameters for the runs leads to a more quantitative interpretation of these characteristics. In the calculation of the parameters σ_r and σ_z the limits of integration were set at the edges of the thermocouple array. These nondimensional estimates of the vertical and the radial temperature differences are extended to the respective boundaries by multiplying the result by the actual depth or gap width, respectively, as in Equations 1.5 and 1.6. It should also be noted that since this quantity is measured over the thermocouple array but extended to the edges of the annulus, the sum of σ_r and σ_z is not necessarily less than unity.

Figures 12a, 12b, 13a and 13b show the values of σ_z and σ_r for the set of runs at 9.12°C and 5.09°C , respectively. The values for the set of runs at 2.53°C were not plotted since they are so few in number. However, they are listed in Table III.

The estimate of the vertical temperature difference, σ_z , tends to increase in the symmetric regime and then decrease just before the transition for the set of runs at 5.09C° and just after the transition to the regular wave regime for the runs at 9.12C° and 2.53C°. σ_z does not vary as much in the wave, vacillating and irregular wave regimes for all the runs, and with the exception of the three low values for the runs at 5.09C°, it is almost constant. The mean values for σ_z in the wave regime are 0.783 ± 0.026 , 0.770 ± 0.033 and 0.784 ± 0.050 for the runs at 9.12, 5.09, and 2.53C° respectively. A least square fit to the points in the wave regime for $\Delta T = 9.12$ is:

$\sigma_z = 0.983 \pm 0.144 - (0.046 \pm 0.033) \log E^{-1}$. This also indicates that σ_z decreases very slightly with increasing rotation rate or E^{-1} .

The value indicative of the radial temperature difference, σ_r , seems to behave in a strikingly similar manner to that of σ_z for each set of runs. However, some care must be exercised in the interpretation of this value because, if the limits of integration were extended to the cylinder walls, σ_r would be identically equal to 1.0. Since the edges of the thermocouple array may be affected to some extent by the side wall boundary layers, a more reasonable estimate of the radial temperature difference would be the value of σ_{rI} , calculated from the four internal thermocouples of the array. This value of σ_{rI} is given for each set of runs in Figures 14a, 14b, and Table III. The value of σ_{rI} defined in this way decreases significantly within the wave regime for each set of runs. It has a tendency to increase within the vacillating regime and then decrease

again to the irregular regime. The net result is that, while the temperature difference across the fluid just outside the side boundary layers remains the same, the slope of the isotherms in the center must decrease. This is the result predicted by the second order Eady theory.

The value of σ_z can also be used to calculate the Eady number for each of the runs. The value of B in the wave regime for the runs at 9.120° is plotted in Figure 15. Since the value of σ_z tends to be rather constant in this regime, the variation of B is dominated by the variation in Ω with E^{-1} . A best fit to these points is given by,

$$\log B = (7.9789 \pm 0.0823) - (2.0317 \pm 0.0189) \times \log(E^{-1})$$

for $G^{\frac{1}{2}} \doteq 9.411 \times 10^3$

The values of the nondimensional wave number $\sum = \frac{m}{\pi} \frac{(b-a)}{(b+a)}$ are tabulated in Table IV. Using these values, the critical value of the Eady number for the observed wave number can be computed for each run number in the wave regime. The values of B_{crit} along with the wave number, m_p , which should have the maximum rate of growth for the observed value of B are contained in Tables IIIa, IIIb, and IIIc. These results indicate that waves will occur when the flow is theoretically stable, i.e.: $B > 0.581$ for Runs 36, 39, 59, 22, and 49. In addition to this the value of B also exceeds the critical value of B for the observed wave number at Runs 44 and 45. The value of B for each of these runs has also been calculated using the temperature difference between T (3,4) and T (3,3), i.e. where the wave amplitude is

a maximum. This value of B is not sufficiently smaller to change the above results except at Run 45.

The decrease in the stability of the flow cannot be explained with the addition of the curvature to Eady's model. Equation 2,32 indicates that the critical value of B decreases with increasing curvature. Further, the experimental results of Lambert and Snyder (1966) indicate that a linear velocity shear will also act to stabilize the flow. However, the results of the numerical solutions indicate that the velocity in the symmetric state, in addition to a linear horizontal shear, may have some component which is even about the radius $\bar{r} = \frac{a+b}{2}$. This effect could act to destabilize the flow so that the waves would still develop at values of B greater than 0.581. One further effect may be due to the fact that the measured values of B are determined from the fully developed wave state and not from the initial state.

The most probable wave number, i.e., that ^{one}with the maximum growth rate, becomes much larger than the observed value at higher rotation rates. This is probably the result of the fact that while the wave number increases in a limited channel, such as the annulus, the interior viscous dissipation must increase and act to counterbalance the larger growth rates of these waves. Consequently, the inviscid Eady theory should not be interpreted strictly in this range.

When the wave disturbance represents a single mode of the Eady theory, the standard deviation of the temperature will be a measure of the wave amplitude. These values have been calculated for each element of the thermocouple array for each

run. Contour values have been drawn and a volume average computed for the standard deviation at each run. The results for the average value of the standard deviation at $\Delta T = 9.12C^\circ$ are plotted in Figure 16. This indicates that the amplitude of the disturbance increases discontinuously at the transition between the symmetric flow to the regular wave regime. This amplitude has a tendency to increase within each wave number and to increase with increasing rotation in the regular wave, vacillating and irregular regimes.

Extending this interpretation, the contours of constant standard deviation indicate the strength of the wave over the thermocouple array. These contours are reproduced for Runs 36, 42 and 38 in Figure 11b. The position of the maximum disturbance starts for low values of E^{-1} near the upper free surface near the cold wall. As the rotation rate increases, the steady state wave amplitude becomes more centered over the upper regions of the fluid. At even higher rotation rates, Run 38, the disturbance is distributed much more evenly throughout the fluid. The fact that the contour interval is less for Run 38 than for Runs 36 and 42 strengthens this interpretation, indicating that the wave amplitude is more uniform over the array for Run 38 than in the previous runs. A study of these contours and the radially averaged values ^{of σ_z} indicates that the maximum amplitude of the wave generally occurs near or in the upper half of the fluid.

The contours of constant standard deviation for the vacillating and irregular regimes are indicated in Figure 11c. These indicate that the area of the disturbance decreases in size and

Figure 12a. σ_z versus E^{-1} ; $\Delta T = 9.12^\circ\text{C}$.

Figure 12b. σ_z versus E^{-1} ; $\Delta T = 5.09^\circ\text{C}$.

Figure 13a. σ_r versus E^{-1} ; $\Delta T = 9.12^\circ$.

Figure 13b. σ_r versus E^{-1} ; $\Delta T = 5.09^\circ\text{C}$.

Figure 14a. σ_{rI} versus E^{-1} ; $\Delta T = 9.12^\circ\text{C}$.

Figure 14b. σ_{rI} versus E^{-1} ; $\Delta T = 5.09^\circ\text{C}$.

Figure 15. B versus E^{-1} ; $\Delta T = 9.12$.

Figure 16. Standard deviation versus E^{-1} ; $\Delta T = 9.12^\circ\text{C}$.

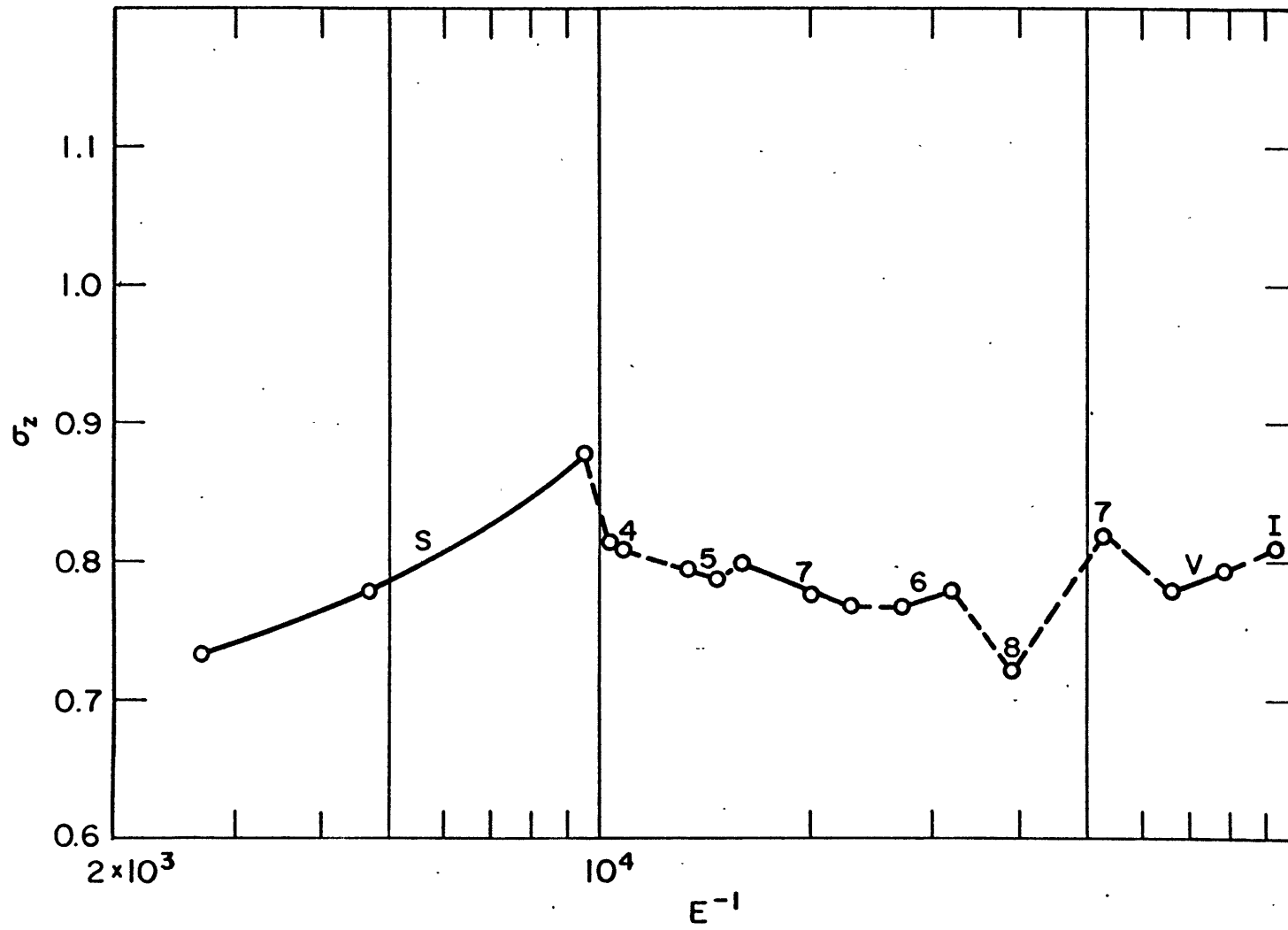


Figure 12 a

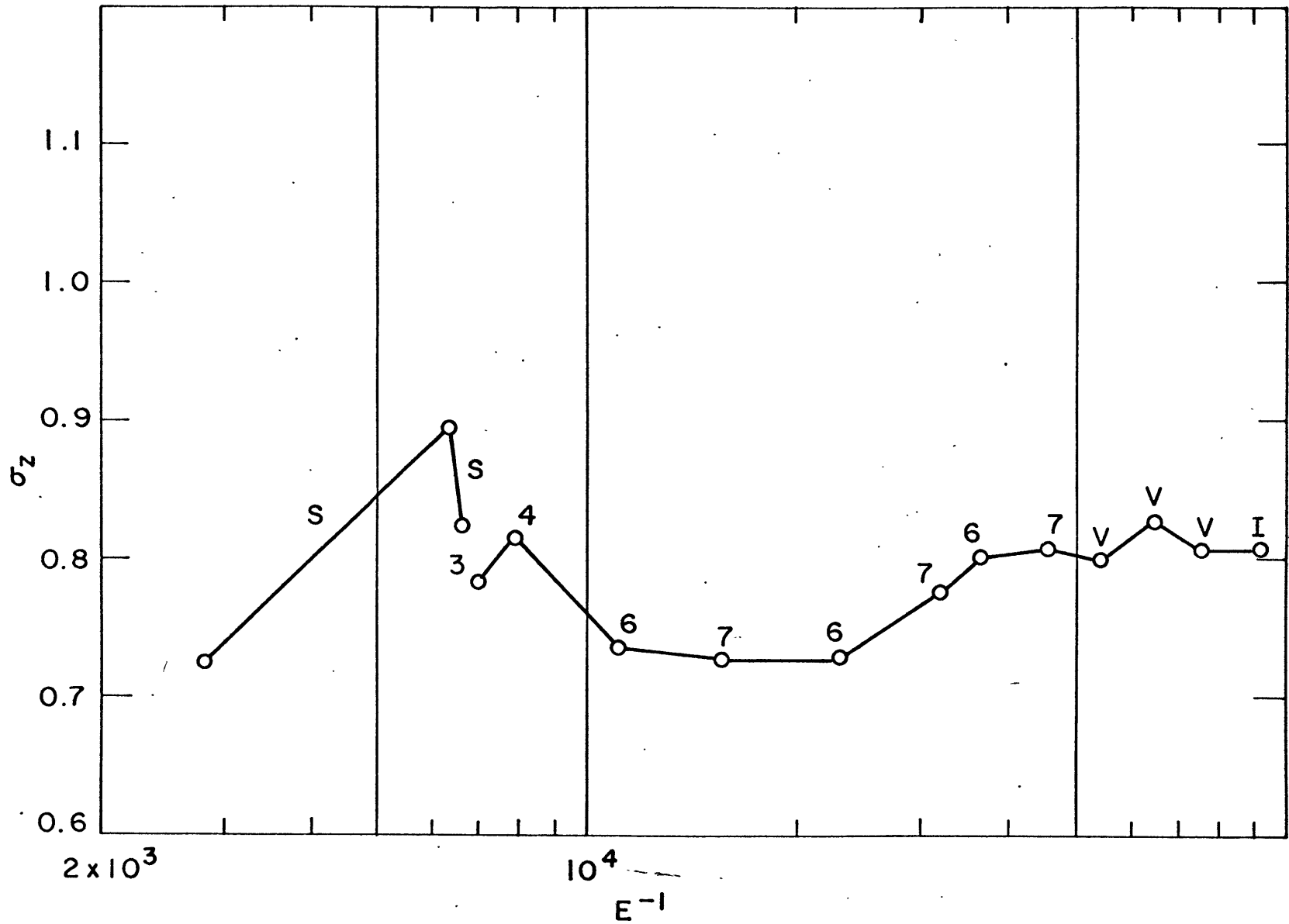


Figure 12b

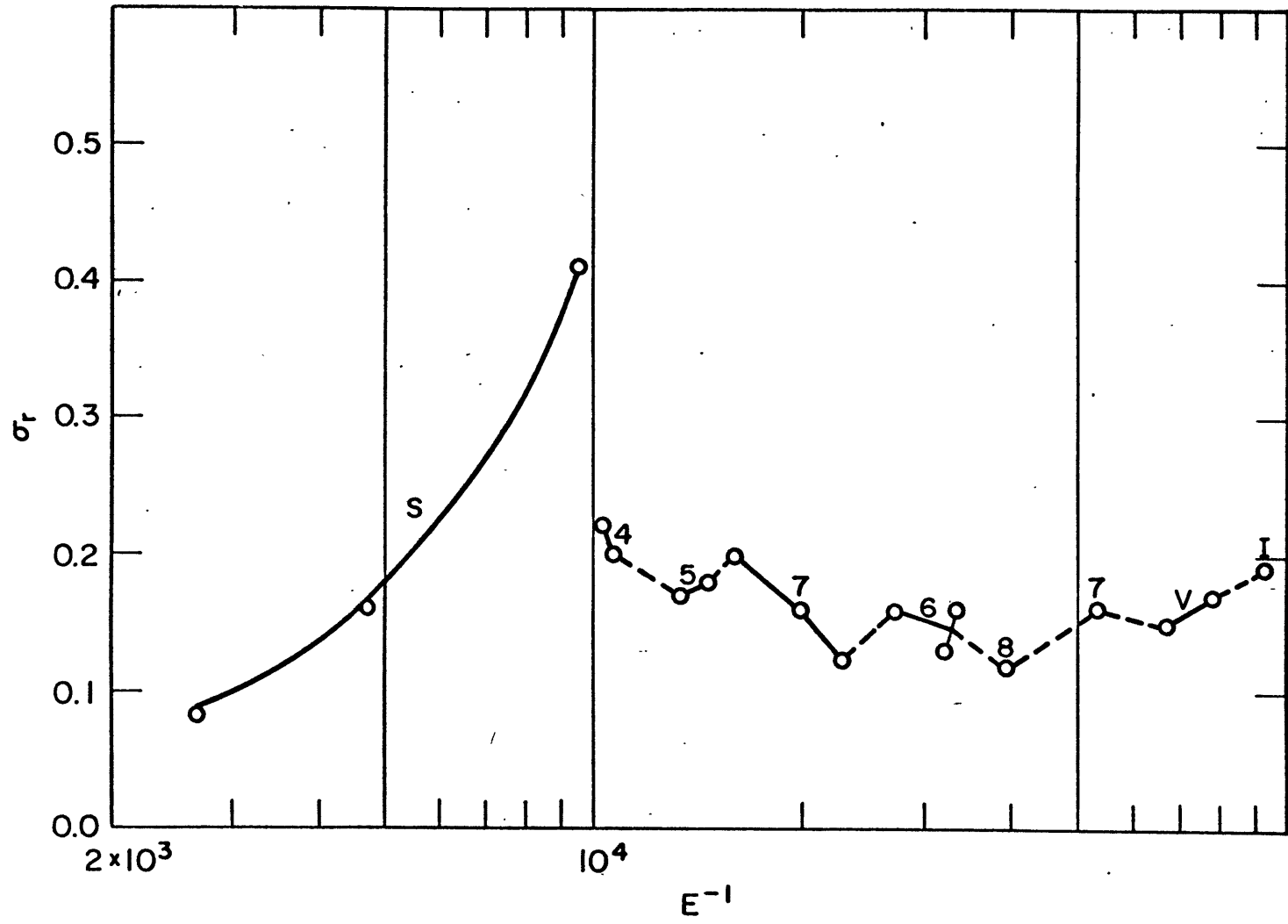


Figure 13a

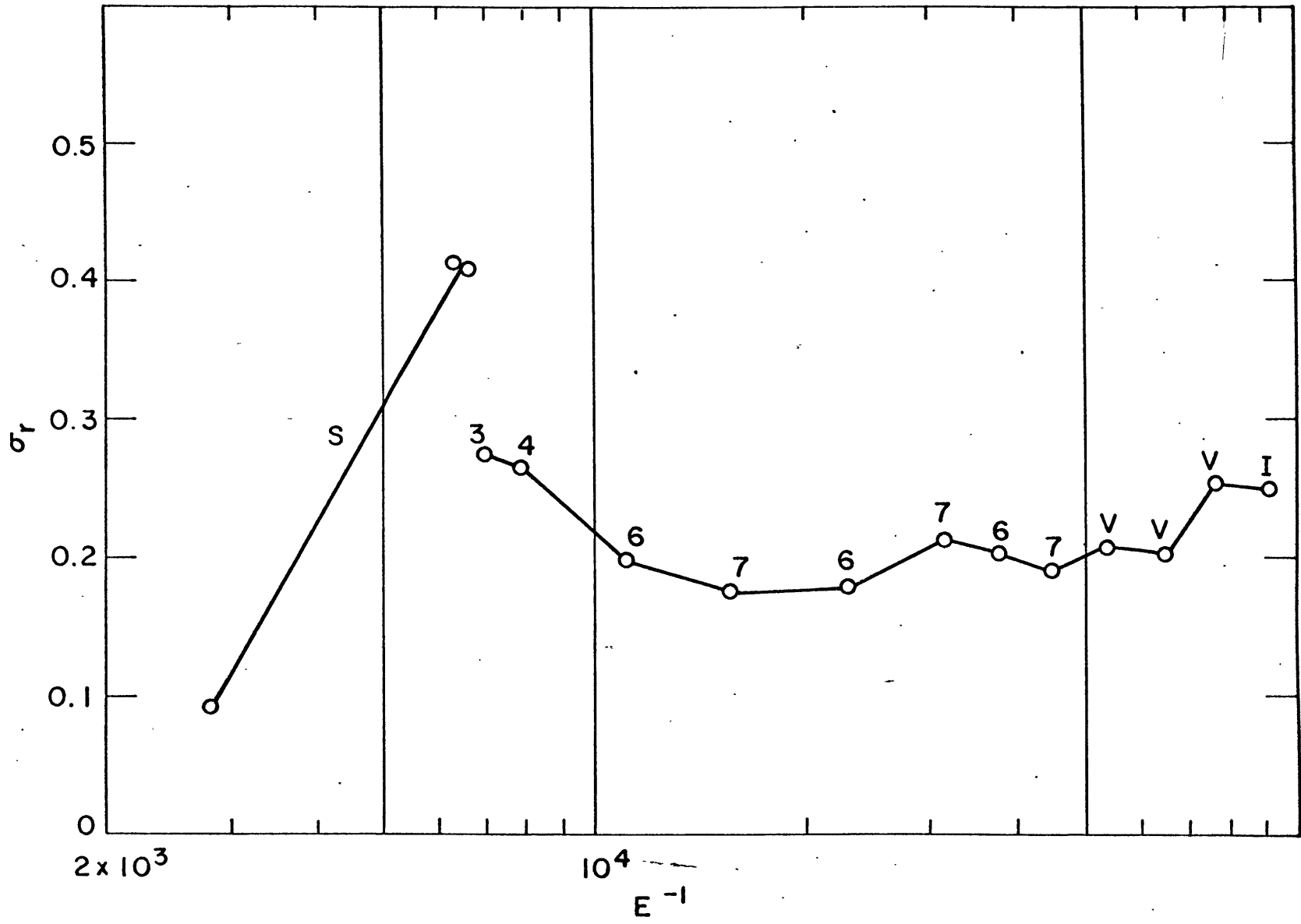


Figure 13b

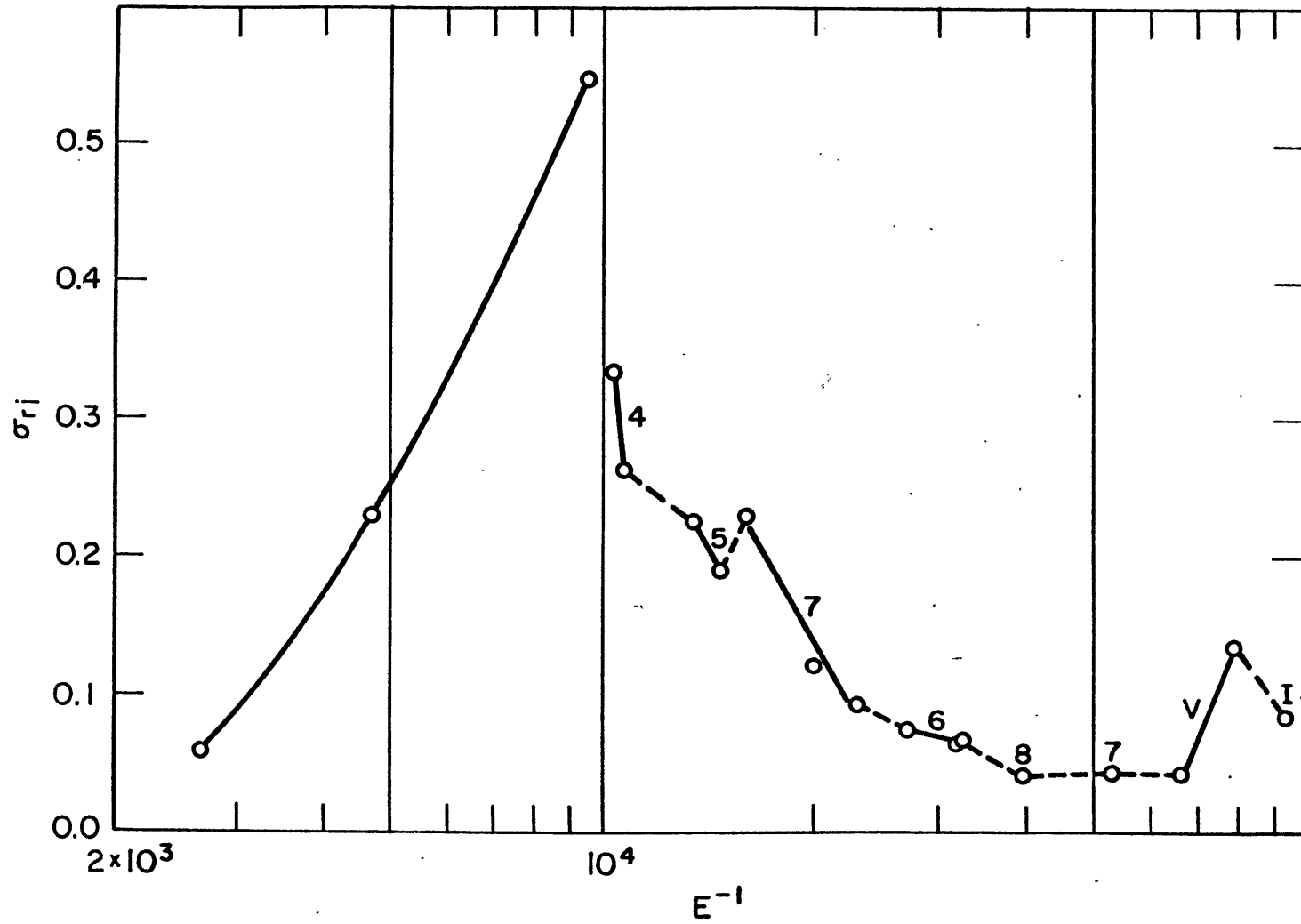


Figure 14a

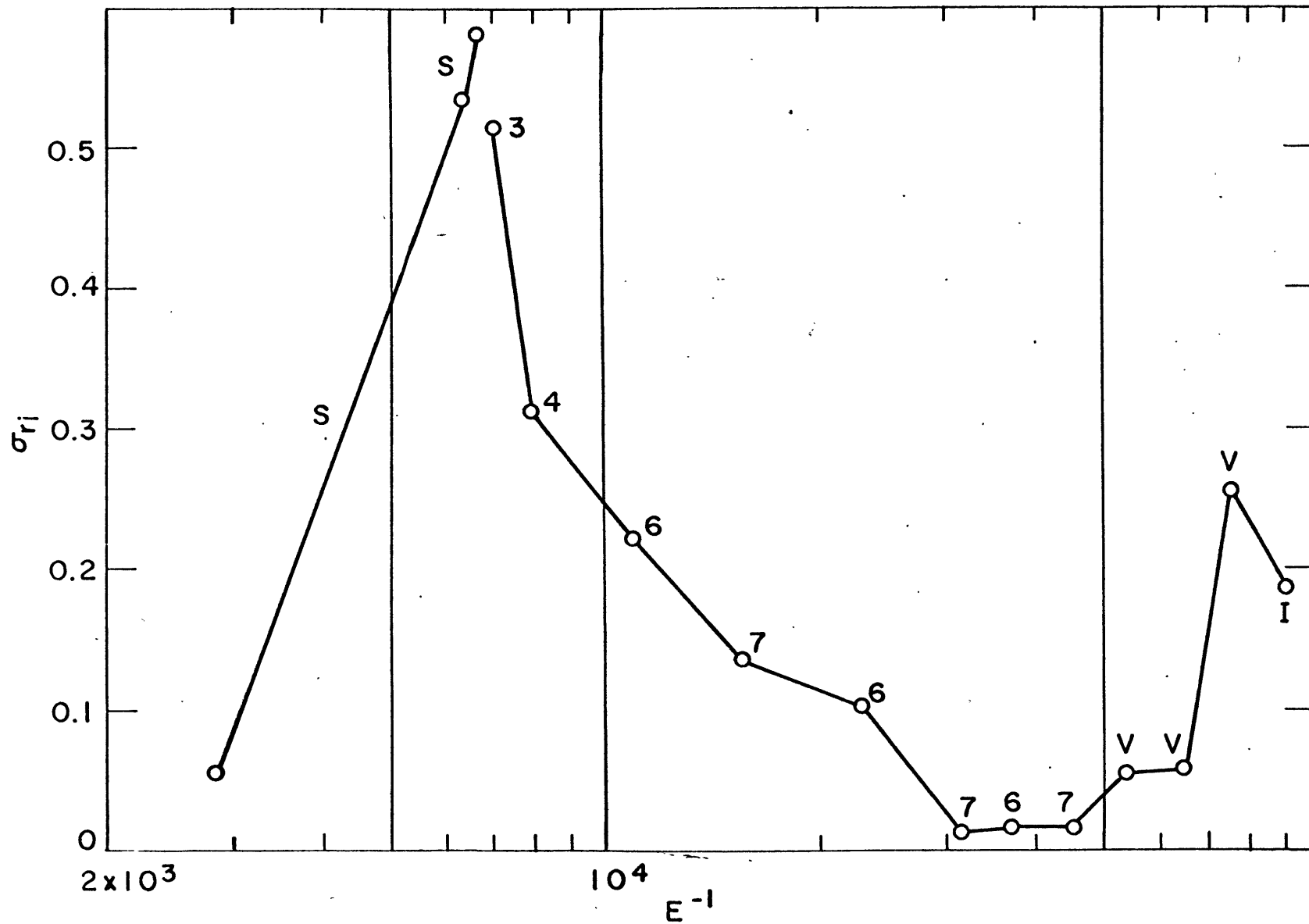


Figure 14b

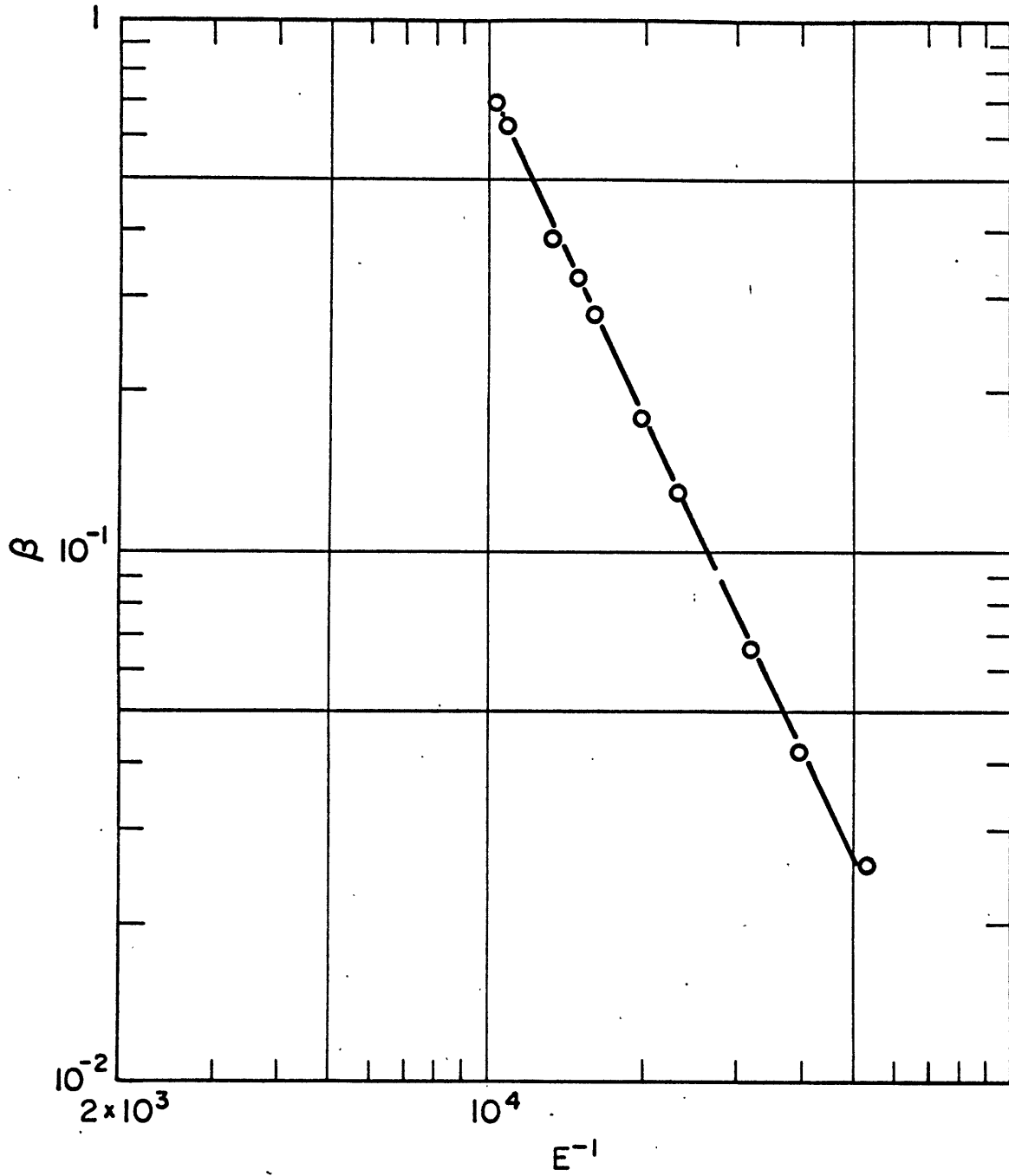


Figure 15

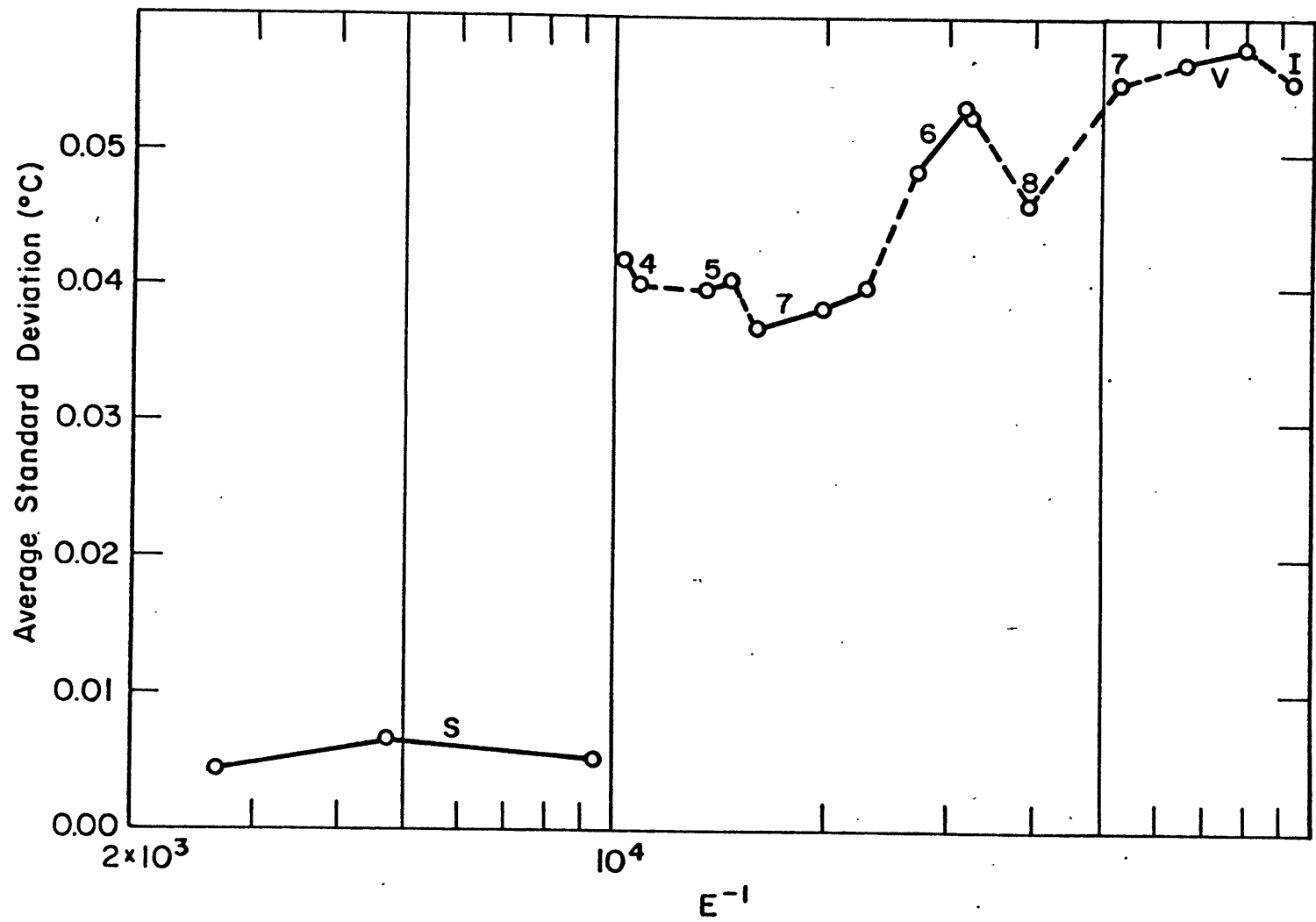


Figure 16

TABLE III

Experimental Parameters for $\Delta T = 2.53^\circ\text{C}$

Run No.	State	E^{-1}	σ_z	σ_r	σ_{rz} Central	RAPE erg cm ⁻³	ZAPE erg cm ⁻³	TAPE erg cm ⁻³
55	S	0.000	0.633					
48	S	0.497	0.855	0.456	0.661	0.1664	0.0048	0.1712
49	3	0.551	0.804	0.336	0.580	0.1023	0.0310	0.1333
50	6 ¹	2.228	0.746	0.220	0.017	0.0336	0.0402	0.0738
51	7 ¹	3.186	0.776	0.244	0.039	0.0422	0.0375	0.0797
53	6 ¹	3.777	0.810	0.260	0.029	0.0490	0.0372	0.0862
54	V	4.524	0.816	0.276	0.058	0.0571	0.0374	0.0945
52	V	5.331	0.803	0.248	0.072	0.0508	0.0430	0.0938

- 1 This wave number was inferred from the phase of the wave at the different vertical thermocouple arrays determined from a calcomp plot of the data.

TABLE IV

Values of Σ and B_{crit} for the 42 Inch Annulus

Wave Number	$\Sigma = \frac{m}{\pi} \frac{(b-a)}{b+a}$	B_{crit}
1	0.0789	0.5669
2	0.1579	0.5283
3	0.2368	0.4745
4	0.3158	0.4153
5	0.3947	0.3579
6	0.4737	0.3062
7	0.5526	0.2615
8	0.6316	0.2239
9	0.7105	0.1924
10	0.7894	0.1663
11	0.8684	0.1447
12	0.9473	0.1266
13	1.0263	0.1115
14	1.1052	0.0987
15	1.1842	0.0879
16	1.2631	0.0787
17	1.3421	0.0708
18	1.4210	0.0640
19	1.4999	0.0581
20	1.5789	0.0530
21	1.6573	0.0484
22	1.7368	0.0445

Wave
Number

$$\Sigma = \frac{m}{\pi} \frac{(b-a)}{b+a}$$

Bcrit

23	1.8157	0.0410
24	1.8947	0.0378
25	1.9736	0.0350
26	2.0526	0.0325
27	2.1315	0.0303
28	2.2104	0.0283
29	2.2894	0.0265
30	2.3683	0.0248

tends to become concentrated near the lower portion of the fluid at the cold wall. Since the contour interval increases from Run 73 to Run 69, it also supports this conclusion.

The volume averaged available potential energy (Lorenz (1955)) of the fluid for each state can be determined from the mean temperature field and the standard deviation. The ^{total} available potential energy is proportional to the variance of the temperature along a geopotential surface. This is shown in the Appendix II to be:

$$TAPE_1 = \iiint_{Volume} g \rho_m \alpha (T'')^2 \left(\frac{\partial \bar{T}}{\partial z} \right)^{-1} d\tau$$

where

$$T(r, \theta, z) = \bar{T}(r, z) + T''(r, \theta, z) ,$$

$$\rho = \rho_m (1 - \alpha(T - T_m))$$

\bar{T} is the average temperature over a geopotential surface, and T_m and ρ_m are the mean temperatures and density of the fluid, respectively. If we assume that the time average of the thermocouple output is equivalent to an azimuthal average, we can then set:

$$T(r, \theta, z) = \overline{T(r, \theta, z)} + T^1(r, \theta, z)$$

The variance along a geopotential surface is then

$$T'' = \left(\overline{T(r, \theta, z)} - \bar{T}(r, z) + T^1(r, \theta, z) \right)$$

and the ^{total} available potential energy per unit volume is:

$$TAPE = \frac{2\pi g \rho_m \alpha}{Volume} \iint (\overline{T} - \bar{T})^2 \left(\frac{\partial \bar{T}}{\partial z} \right)^{-1} r dr dz$$

$$+ \frac{g \rho_m \alpha}{Volume} \iiint (T^1)^2 \left(\frac{\partial \bar{T}}{\partial z} \right)^{-1} r dr d\theta dz$$

since $\int T'(\bar{T} - \tilde{T}) \left(\frac{\partial \bar{T}}{\partial z}\right)^{-1} d\theta = 0$ by our assumption, and we neglect the higher order correlation with $\left(\frac{\partial \bar{T}}{\partial z}\right)^{-1}$ by computing $\left(\frac{\partial \bar{T}}{\partial z}\right)^{-1}$ from the time averaged temperature field. The first term of the right hand side measures the radial available potential energy per unit volume.¹ This can be calculated from the time averaged temperature field interpolated to the geopotential surfaces. The second term represents the zonal available potential energy per unit volume,² which can be calculated from the standard deviation of the sample.

The calculated values of these quantities, along with their sum or total available potential energy, are shown in Figure 17a and 17b. for the runs at $9.12C^{\circ}$ and $5.09C^{\circ}$, respectively. The values for the runs at $2.53C^{\circ}$ are included in Table III. In Figure 17 the radial available potential energy² (RAPE) increases rapidly in the symmetric regime. The value drops abruptly at the transition to the wave regime and tends to decrease within this regime. The radial potential energy also tends to decrease within the wave numbers and increase slightly at the transition between wave numbers, with the exception of Runs 44 and 46, where it increases within the wave number. This value increases again with rotation rate in the vacillating and irregular regimes. The line of best fit to all points in the wave regime for RAPE with $\Delta T = 9.12C^{\circ}$ is:

$$\text{RAPE} = (0.6581 \pm 0.1510) - (0.1303 \pm 0.0348) \log E^{-1}$$

(units: ergs/cm³)

This does indicate a significant decrease or radial available potential energy with increasing E^{-1} .

The zonal available potential energy (ZAPE) reflects the

See following page for footnotes 1 and 2.

1. The radial available potential energy per unit volume as defined in this text is the available potential energy per unit volume of the azimuthally averaged fluid. This corresponds in the meteorological context to the zonal available potential energy per unit volume. The zonal available potential energy per unit volume as defined in this text corresponds to the eddy available potential energy in the meteorological context.

2. The values of the radial, zonal and total available potential energy are recorded in terms of unit volume. However, since the volume of the array is always constant, this will not be stated explicitly in the proceeding.

variation of the average standard deviation in that it tends to increase with increasing rotation rate for the wave, vacillating and irregular regime points. The line of best fit to all points in the wave regime for ZAPE with $\Delta T = 9.12^{\circ}\text{C}$ is;

$$\text{ZAPE} = (-0.3024 \pm 0.0867) + (0.0944 \pm 0.0200) \log E^{-1}$$

(units: ergs/cm³)

The line of best fit for the total available potential energy, TAPE, for the wave regime under the same conditions is;

$$\text{TAPE} = (0.3553 \pm 0.1699) - (0.0357 \pm 0.0392) \log E^{-1}$$

(units: ergs/cm³)

Thus, the total available potential energy remains almost constant within the wave regime and increases with increasing rotation rate for the symmetric and vacillating flows.

The same pattern is not quite as evident for the runs at $\Delta T = 5.09^{\circ}\text{C}$ in Figure 18. However, if as indicated in Figure 17a, the radial available potential energy changes within each wave number, then there are not enough samples taken for Figure 17b to indicate the variation accurately. The same argument would hold for the runs at $\Delta T = 2.53^{\circ}\text{C}$ in Table III where the radial available potential energy actually shows a tendency to increase in the wave regime.

There is no accurate manner with which the kinetic energy of this flow can be calculated due to a lack of some reference level from which to integrate the thermal wind equation. However, the fact that the slope of the isotherm in the center of the fluid decreases with increasing rotation rate, whereas, the value of σ_r defined at the edges of the thermocouple array remains constant, would indicate that the slope of the isotherms

Figure 17. Radial, zonal and total available potential energy per unit volume; $T = 9.12^{\circ}\text{C}$.

Legend

- Lower plot; radial available potential energy per unit volume.
- ⊙ Zonal available potential energy per unit volume.
- Upper plot; total available potential energy per unit volume.

Figure 18. Radial, zonal and total available potential energy per unit volume; $T = 5.09^{\circ}\text{C}$.

Legend

- Lower plot; radial available potential energy per unit volume.
- ⊙ Zonal available potential energy per unit volume.
- Upper plot; total available potential energy per unit volume.

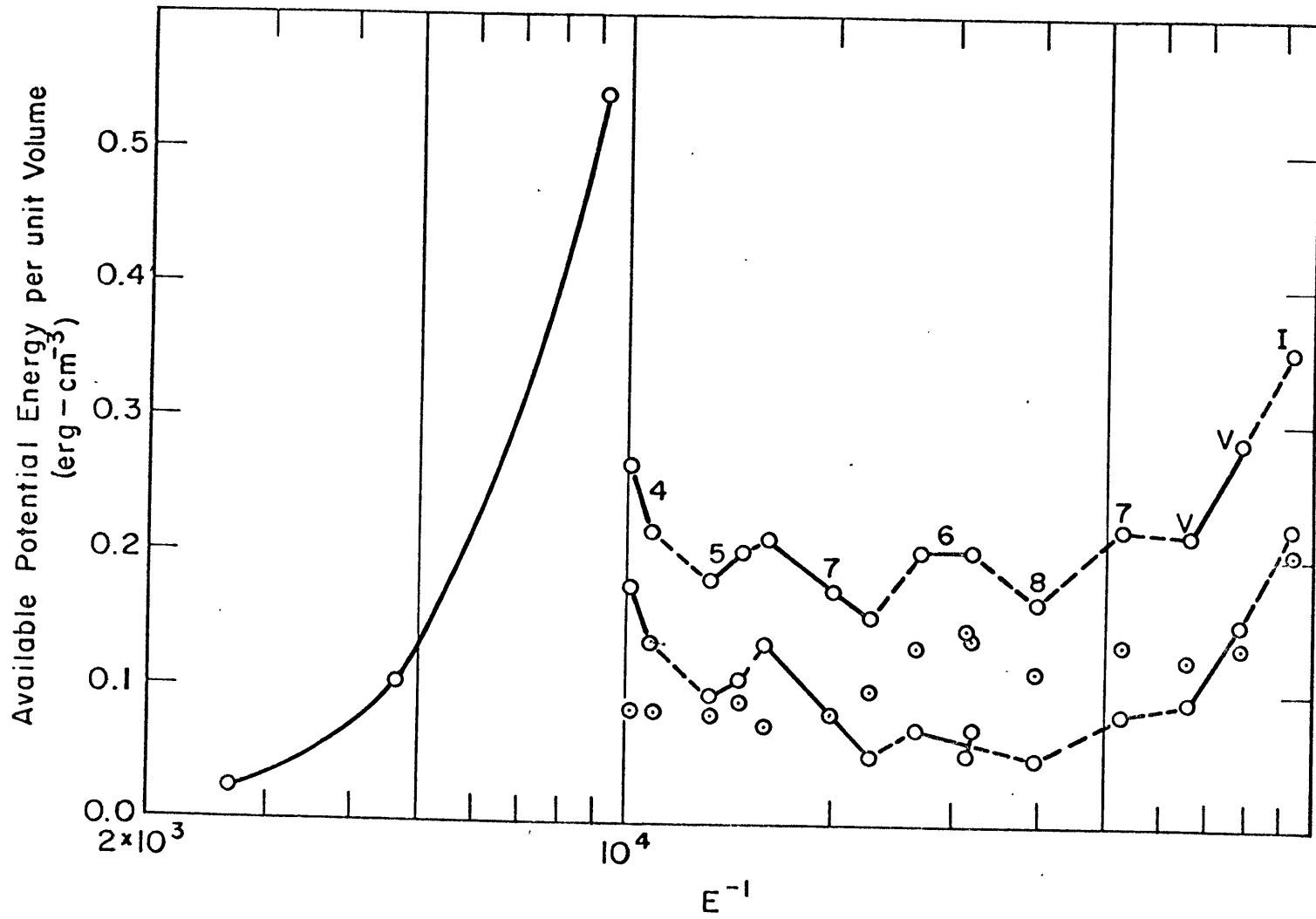


Figure 17

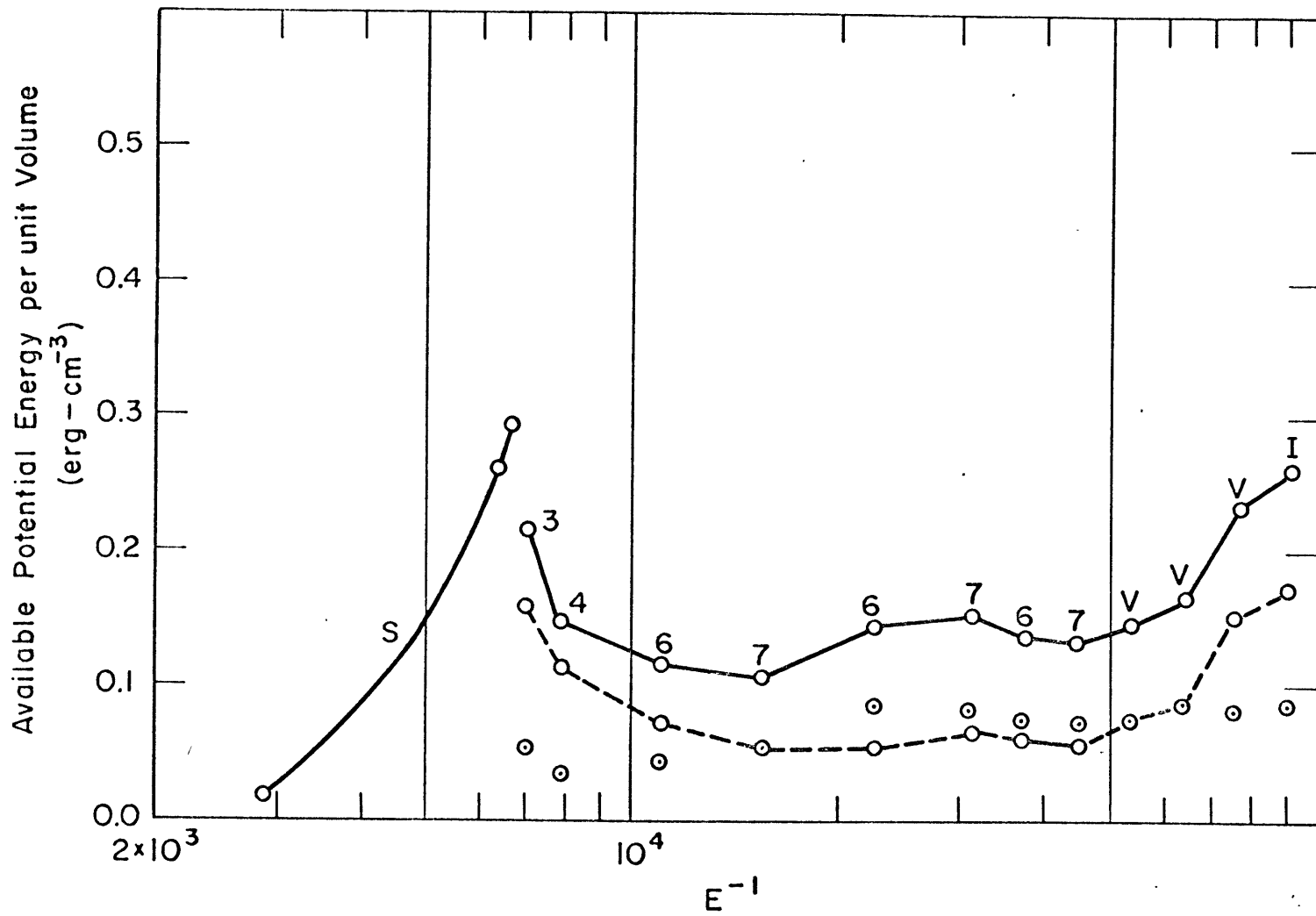


Figure 18

near the edges of the fluid must increase with increasing rotation. This means that the kinetic energy of the fluid computed from the thermal wind would increase. This process has been shown to occur in wave amplitude vacillation by Pfeiffer, et al. (1966), when the rotation rate of the apparatus was constant.

Spectral analysis

Further insight into the structure of the convection in the wave, vacillating and irregular flow can be obtained from a time series analysis of the temperature oscillations. The results of the analysis should indicate the frequency structure, ^{amplitude,} the coherence and radial and vertical phase variations of the mode. To this end, the power spectrum, complex cospectrum and coherence of all the thermocouples in the array, with respect to thermocouple T (3,3) (see Figure 9), have been computed for all the runs in the regular wave, vacillating and irregular regime for $\Delta T = 9.12^{\circ}\text{C}$ and Runs 25, 26, 65, 63b, 66 and 67 at $\Delta T = 15.09^{\circ}\text{C}$. The computations were done using a fast Cooley Tukey Fourier transform subroutine written by Dr. Ralph Wiggins^{at}, MIT. Further details of the computations are given in Appendix II.

The power spectrum results for thermocouple T(3,3) for Run 42 are shown in Figure 19. The 95% confidence level shown is calculated using Fisher's (1929) test of significance in harmonic analysis. This level represents the maximum amplitude one could expect 95% of the time from a harmonic analysis of a completely random set of data with the same standard deviation as the actual sample (see Nowroozi, 1967). The typical power spectrum

in the wave regime is characterized by a sharp peak at the dominant frequency and a smaller peak near the third harmonic of the frequency. The power spectrum curve for the vacillating, Run 71, and irregular, Run 69, flows are shown in Figure 20. The peak power for Run 71 occurs at a much lower frequency and has a broader peak than any in the wave regime. In the irregular flow the power is split between two frequency components at a higher frequency than that in the vacillating flow and one low frequency component. Some care must be exercised in the interpretation of the low frequency components less than 0.0087 sec^{-1} as these represent estimates of wave amplitudes based on waves that occur less than 10 times in the original sample. Thus, we cannot really state whether the low frequency component in Run 69 is real or not.

Figure 21 is a plot of the period at which the maximum power occurs for each run at 9.12C° in the regular wave, vacillating and irregular regimes. This indicates that the period of the disturbance tends to increase with increasing rotation rate in the wave regime. This increase is even more pronounced in the vacillating regime. This is followed with a decrease in period to the irregular regime point.

The contours of constant cospectrum amplitude at the period of maximum power for the wave regime are shown in Figure 22.

These indicate the same characteristic variations as the contours of the standard deviation. At low rotation rates the wave disturbance is concentrated near the upper surface near the cold wall. As the rotation rate is increased the wave disturbance moves into the center of the fluid and broadens to cover a larger

Figure 19. Power spectrum; Run 42, thermocouple T(3,3).

Figure 20. Power spectrum; Runs 71 and 69, thermocouple T(3,3).

Figure 21. Period at maximum power versus E^{-1} ; $\Delta T \approx 9.12^\circ\text{C}$.

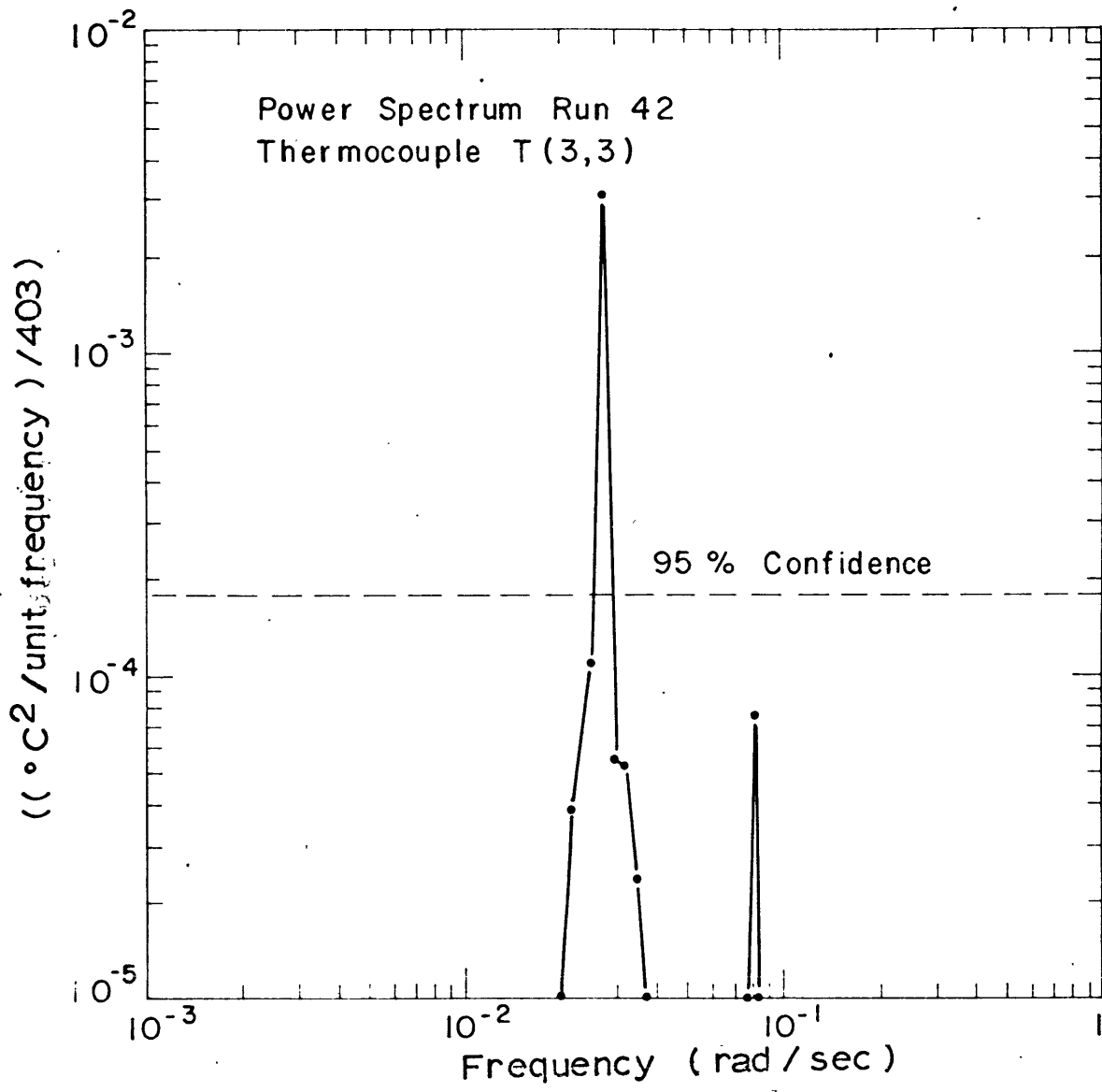


Figure 19

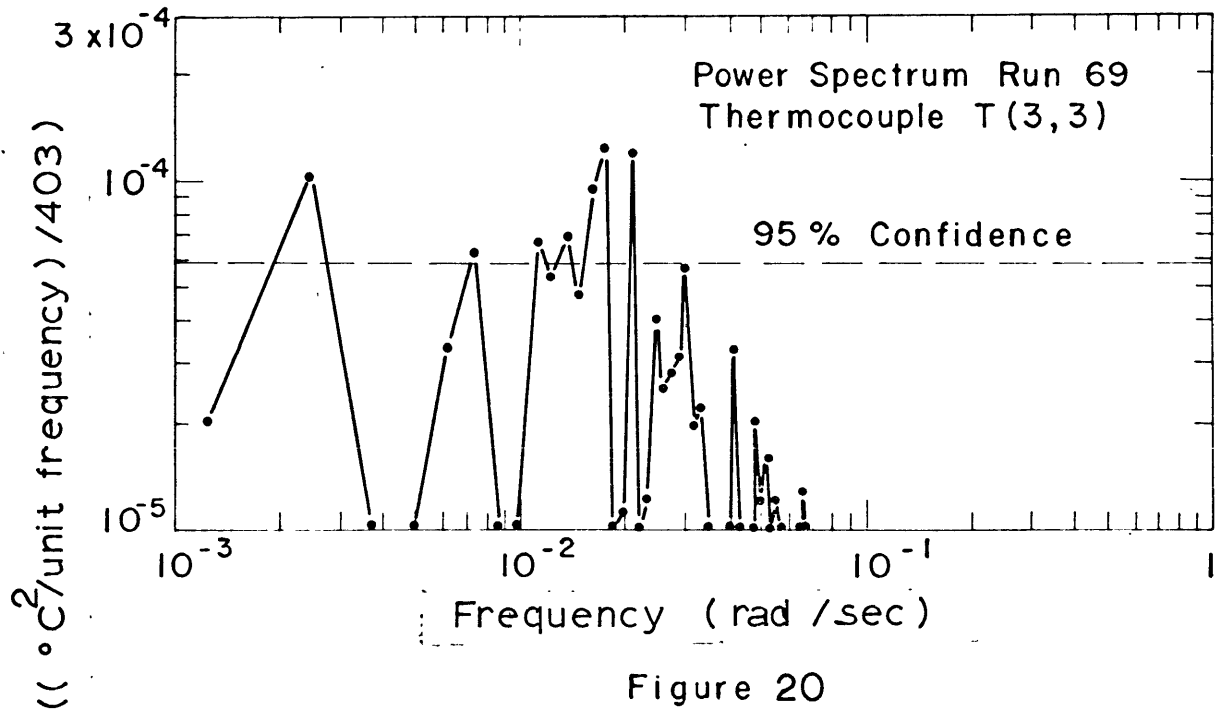
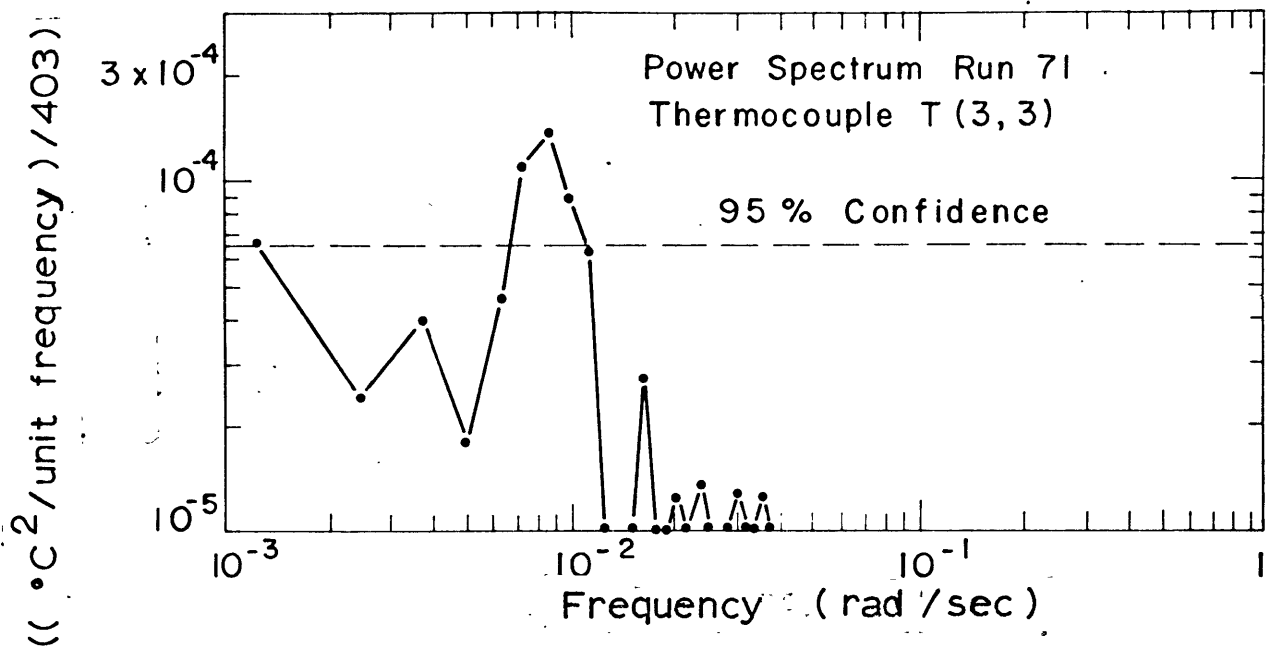


Figure 20

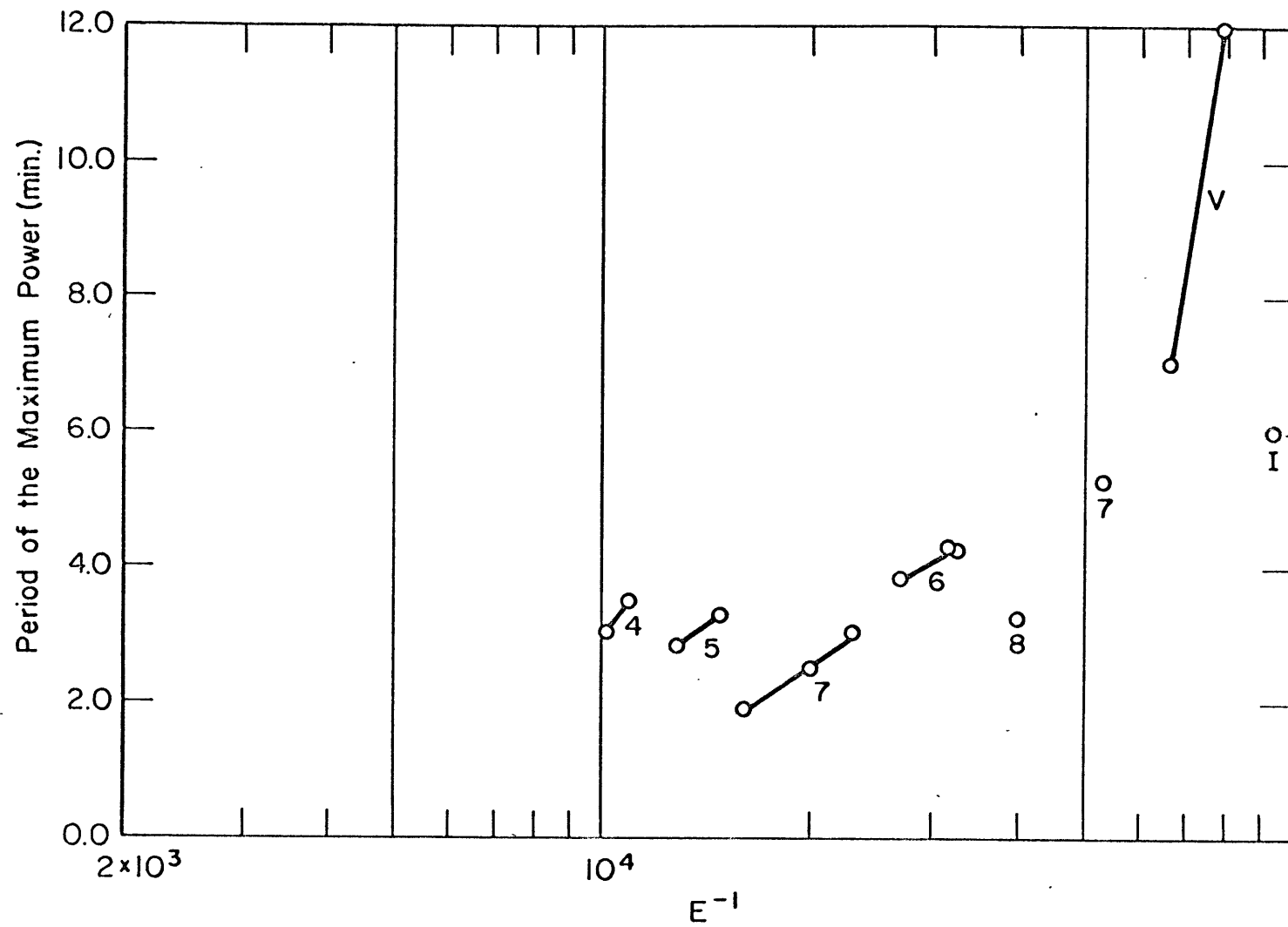


Figure 21

volume of the fluid. The contours of constant phase, with respect to thermocouple T (3,3), and projected to this azimuth using the observed wave number, are also shown in Figure 22. These indicate that the wave tends to lead near the upper section of the warm wall and lags near the lower section of the cold wall. There also appears to be a region of maximum lag in the middle sections of the fluid for Runs 36 and 42. The phase lines for Run 38 do not show this variation. There is much less overall phase variation for Run 38 than in the other two, since the contour interval is approximately one half that of the other two runs.

A better idea of the vertical phase variation can be obtained from a vertical plot of the radially averaged phase for each run as shown in Figure 23. This plot indicates that the wave leads in the upper half of the fluid with a maximum lead, just above the midlayer of the fluid, and it lags in the lower section of the fluid with a maximum lag just below the midpoint of the fluid. The difference between the maximum and minimum phase tends to decrease with increasing rotation rate in the wave regime. The coherence of each thermocouple at the point of maximum power, with respect to thermocouple T (3,3), is greater than 0.9 for all runs except for a few isolated cases near the boundaries of the array.

The contours of constant cospectrum amplitude for the point of maximum power are represented along with those of constant coherence for Runs 73, 71, and 69 in Figure 24. The contours of the cospectrum amplitude do not represent the exact characteristics as indicated for the contours of standard devia-

tion, since the contour intervals decrease from 7.4×10^{-5} at Run 73 to 3.2×10^{-5} at Run 71 and 2.7×10^{-5} at Run 69. Thus, it is not clear from this figure that the disturbance becomes more concentrated in the lower region of the fluid near the cold wall as rotation rate increases. This discrepancy occurs because the standard deviation is an indication of the power at all frequencies. However, the conclusion drawn from the standard deviation amplitudes can be rejustified by considering the contours of cospectrum amplitude for the other spectral peak indicated in Run 69. (This contour plot not shown). This plot has the same characteristic contour plot as shown for Run 69 in Figure 24. Thus, the sum of the two modes does indicate that the disturbance has become more concentrated near the lower section of the cold wall.

There was no obvious phase variation to the cospectrum values for these runs which would indicate a wave number. Thus, it was not possible to project the phase variation back to the azimuth of thermocouple T (3,3). Further, the coherence for these runs decreases rapidly away from the vertical thermocouple array T (3,3), and therefore, the results of the phase variation could not be very meaningful. The lines of constant coherence indicate this decrease. They also indicate that the overall coherence decreases with increasing rotation rate. This decrease is even more pronounced than shown in the plot since the contour intervals also increase from Run 73 to Run 69.

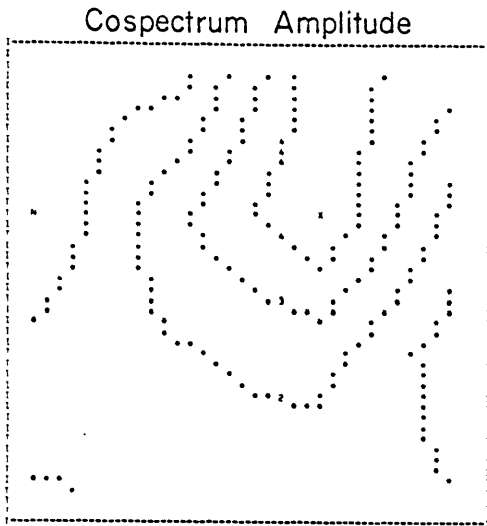
Figure 22. Contours of maximum cospectrum values and phase; Runs 36, 42, and 38.

Run No.		Min. Val.	Max. Val.	Contour Interval
36	Cospectrum	0.00006	0.00231	0.00045
	Phase	-2.15	1.04	0.64
42	Cospectrum	0.00039	0.00302	0.00053
	Phase	-2.04	0.72	0.50
38	Cospectrum	0.00034	0.00142	0.00022
	Phase	-1.59	0.006	0.31

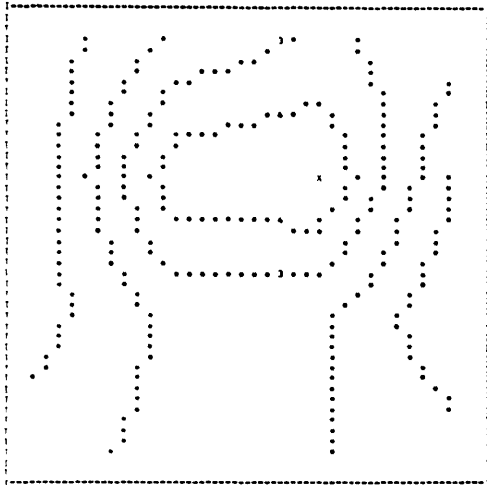
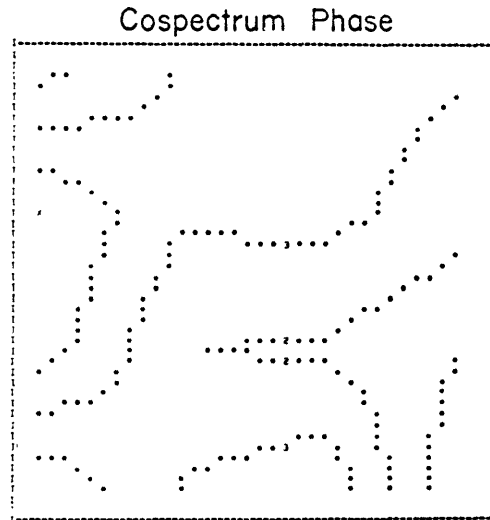
Figure 23. Average vertical phase variation; wave regime, $\Delta T = 9.12^{\circ}\text{C}$.

Figure 24. Contours of maximum cospectrum values and coherence; Runs 73, 71 and 69.

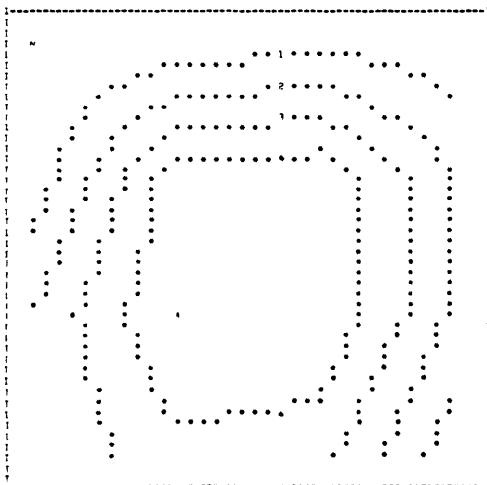
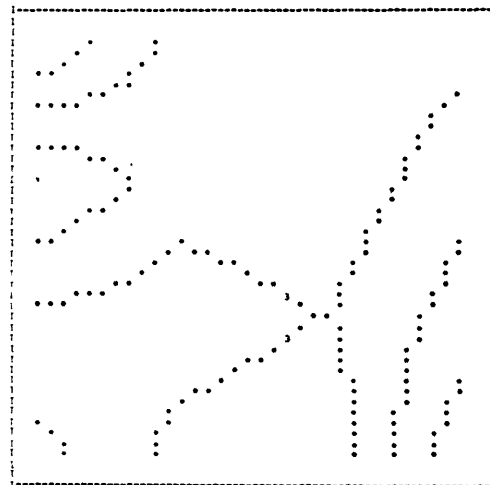
Run No.		Min. Val.	Max. Val.	Contour Interval
73	Cospectrum	0.00006	0.00044	0.00007
	Coherence	0.452	0.999	0.11
71	Cospectrum	0.00001	0.00018	0.00003
	Coherence	0.526	0.999	0.09
69	Cospectrum	0.00001	0.0014	0.00003
	Coherence	0.213	0.999	0.16



Run 36



Run 42



Run 38

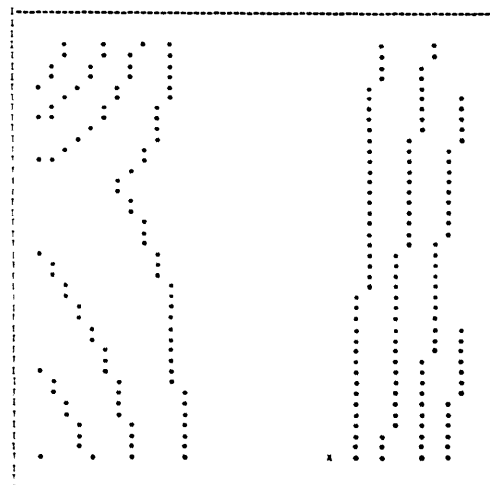


Figure 22

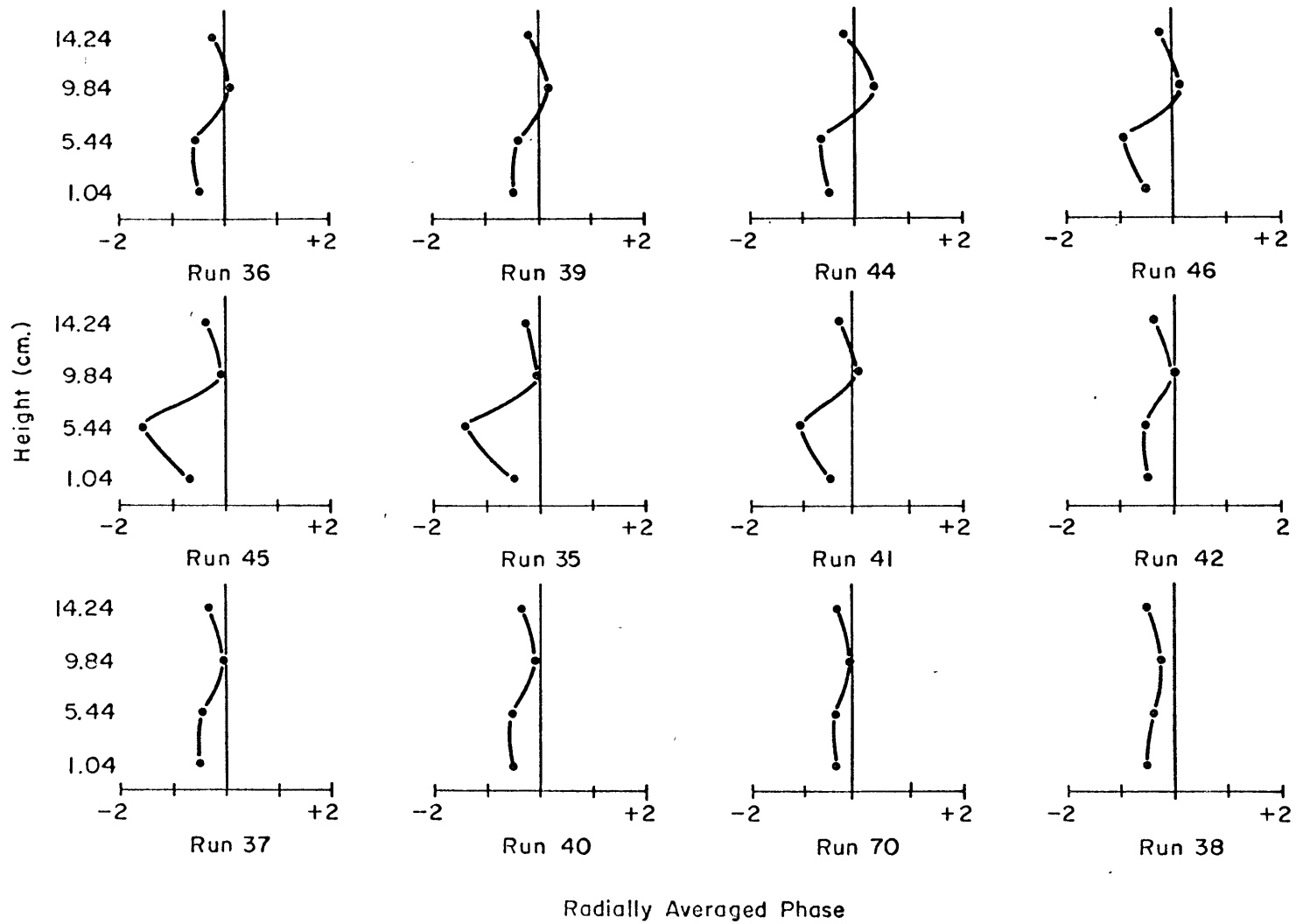
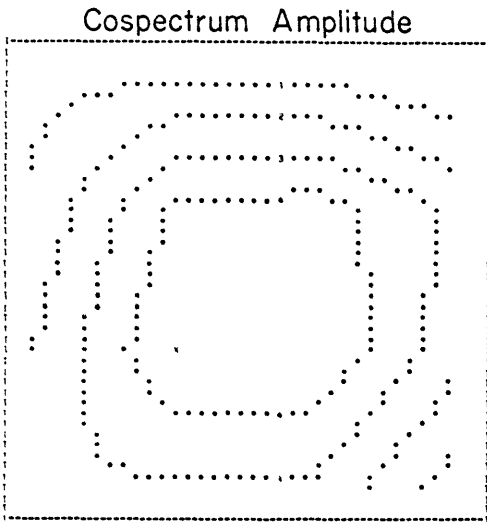
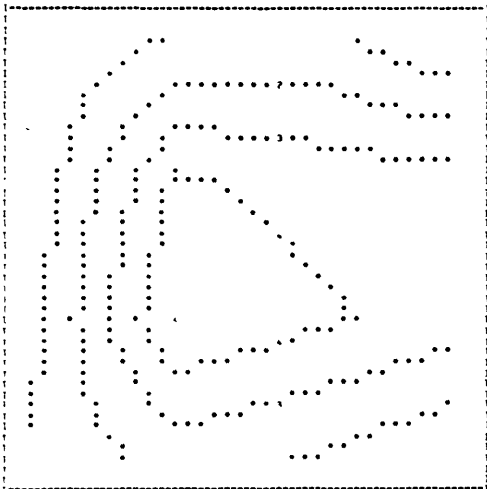
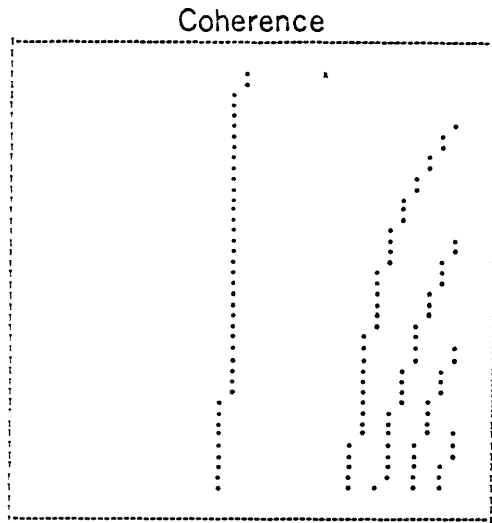


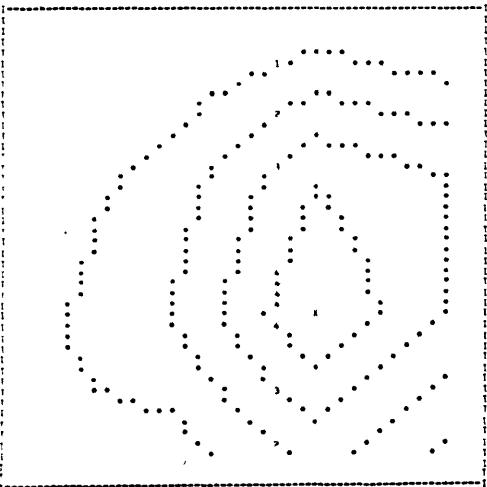
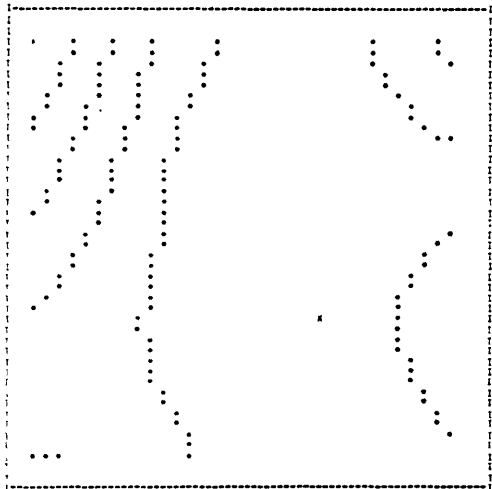
Figure 23



Run 73



Run 71



Run 69

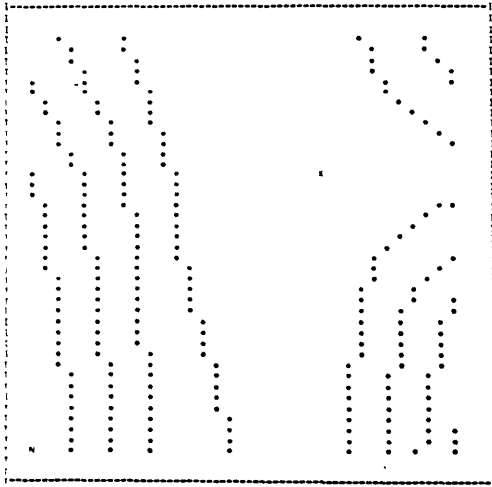


Figure 24

CHAPTER V

SIDE WALL BOUNDARY LAYERS AND EFFECT OF
THE THERMOCOUPLES ON THE FLUID

It has been noted previously that the side wall boundary layer scale thickness is:

$$l^4 = \frac{\nu k d}{g \alpha \Delta T}$$

l is of the order 0.2 cm. to 0.3 cm. for the range of these experiments. This means that the thermocouples for most runs are separated from the boundary by three times the boundary layer thickness. However, some of the contours of standard deviation showed a slight asymmetry in that the values reached a minimum either near the upper surface of the warm wall or near the lower region of the cold wall. For this reason, a short series of experiments were designed to determine if the side wall boundary layers biased the results of the previous work significantly.

The first experiment tried to determine the temperature variation at 1 cm. from the bottom of the convecting fluid with $\Omega = 0.0$ and $\Delta T = 8.3^\circ\text{C}$. This was accomplished by moving a single thermocouple probe mounted in a 0.062" stainless steel needle in 0.1 cm. increments through the boundary layer. The results of this experiment are indicated in Figure 25. The amplitude of the hump on the warm wall is 0.1°C , and it occurs 3 mm. from the wall. Since the boundary layers grow with increasing vertical distance from the source or sink of heat,

the cold wall hump occurs at a greater distance from the wall. The amplitude of the hump is approximately 0.3°C , and it occurs 5 mm. from the wall. These measurements, since only a single probe was used, have a relative accuracy of $\pm 0.03^{\circ}\text{C}$.

It was, of course, impossible to perform these measurements accurately when the apparatus was rotating. Consequently, another experiment was performed with a horizontal string of thermocouples suspended between the two walls at 3.24 cm. depth from the free surface of the fluid. These thermocouples were located at 0.27, 0.45, 0.63, 0.84, 1.09, 1.34 and 1.61 cm. from the cold wall and 0.30, 0.60, 0.83, 1.08, 1.40, 1.74, 2.08 and 2.59 cm. from the warm wall. The upper level of the fluid was chosen since the upper region near the warm wall is where the nonlinear effects in the boundary layer are greatest.

The experimental procedure was exactly the same as used in recording the data from the thermocouple array. Runs were taken with ΔT set approximately at 9.12°C for the values of E^{-1} of 0.0, 0.924×10^4 , 1.587×10^4 , 2.747×10^4 , 6.140×10^4 , and 7.665×10^4 . The results for mean temperature and standard deviation for the run with $E^{-1} = 2.747 \times 10^4$ are plotted in Figure 26. The nondimensional temperature scale is twice that of the scale in Figure 25, but the horizontal distance scale is the same in both cases. Figure 26 indicates a region of slightly colder temperatures at 1.74 cm. from the warm wall with an amplitude of 0.09°C . This region occurs at the same position for all runs taken but with slightly smaller amplitudes. The cold wall does not indicate the characteristic increase in temperature, because it occurs too close to the wall to be

detected by the above thermocouple array.

Because this experiment uses several probes, the relative accuracy of the reading will be $\pm 0.07^{\circ}\text{C}$, and, consequently, these observed variations are just on the verge of being significant. These experiments, although not accurate enough, nor spaced closely enough, to indicate the structure of the boundary layers, do, however, indicate that the preceding results are not strongly biased by the proximity of the thermocouples to the boundary layers.

Another consideration and addition to the problem of the boundary layers is how much ^{do} the thermocouples disturb the flow of the fluid. When dye is placed upstream of the thermocouple in the zonal velocity maximum of the symmetric regime, it appears to separate slightly in the wake of the thermocouple. This separation is laminar and does not last for more than 3 cm. distance downstream. The local Reynolds number at this point is less than or equal to five. The Reynolds number for all the other thermocouples is significantly less than five. This, in addition to the fact that no thermocouple lies in the downstream wake of the other thermocouples, leads the investigator to believe that the effect is not significant in the present context of the data.

Figure 25. Side wall boundary layer temperature; $\Omega = 0.0$,
 $\Delta T = 8.3^{\circ}\text{C}$, 1 cm. from bottom.

Figure 26. Side wall boundary layer temperature;
 $\Omega = 0.549 \text{ sec}^{-1}$, $\Delta T = 8.85^{\circ}\text{C}$, 3.24 cm. from
top.

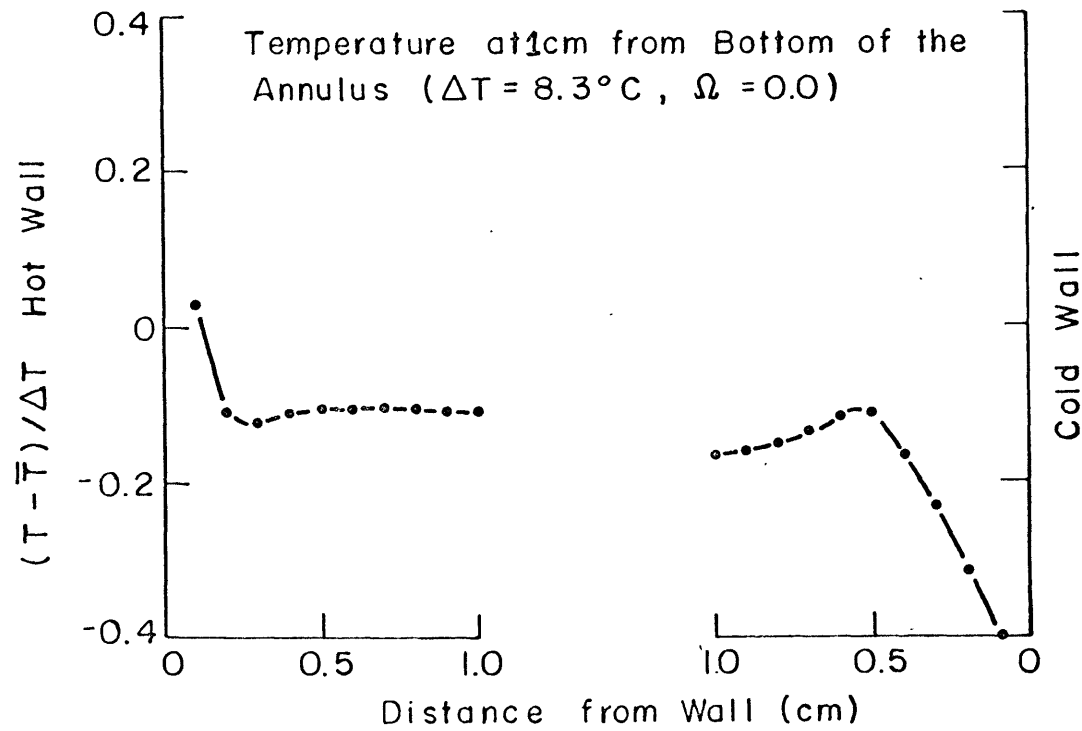


Figure 25

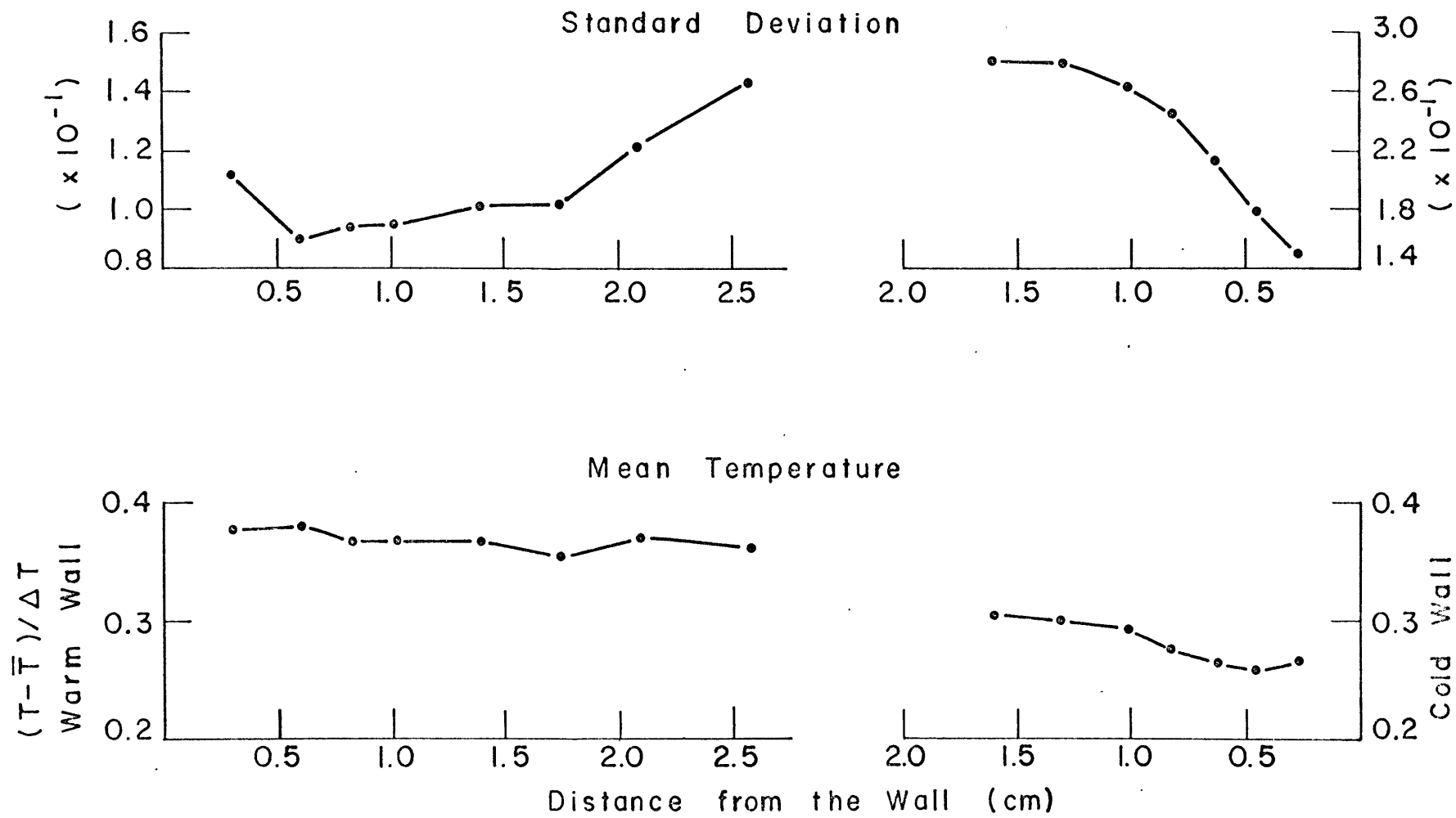


Figure 26

CHAPTER VI

SUMMARY AND SUGGESTIONS FOR FUTURE WORK

The positions of the various convecting regimes and the interior temperature structure of a rotating annulus of liquid have been investigated. The principal distinctions between this work and the previous work are the use of an annulus with a large gap width, and also that detailed temperature measurements were obtained in the various regimes. The results indicate that the critical value of π_{4c} at the transition between the upper symmetric regime and the wave regime has a tendency to increase slightly with increasing values of π_5 for $\pi_5 \geq 2.75 \times 10^7$. This result, however, was not statistically significant from being independent of π_5 in this range. The point at which the flow becomes irregular does not occur until high rotation rates are reached when the gap width is large or until π_5 is greater than 7.259×10^9 .

The vertical stability of the fluid increases in the symmetric regime and decreases slightly in the wave regime with increasing rotation rate. When this value is used to calculate the Eady number, it is found that B exceeds the critical value necessary for instability. The larger values of B at the point of instability may be due to the fact that the part of the zonal velocity which is even about the mean radius of the gap acts to destabilize the symmetric flow. The observed wave number, n , generally, does not correspond to the wave number with the theoretical maximum rate of growth. It is suggested that this result is due to the increase of the viscous dissipation within

the fluid as the wave number increases, which, in turn, will decrease the growth rate of those waves with the larger wave number.

The total available potential energy of the fluid increases with increasing rotation rate in the symmetric, vacillating and irregular regimes. This value is almost constant with a slight tendency to decrease with increasing rotation in the wave regime. The radial available potential energy decreases with increasing rotation rate_{in the wave regime}. The thermal amplitude of the wave and, consequently, the zonal available potential energy increases with increasing rotation rate.

The position of the maximum wave amplitude in the regular wave regime seems to be slightly more concentrated in the upper half of the fluid. The maximum amplitude in the vacillating and irregular flows tends to concentrate in the lower half of the fluid. The phase of the wave in the regular wave regime leads in the upper half of the fluid and lags in the lower half. The vertical difference in the phase decreases with increasing rotation rate.

The period of the wave tends to increase with increasing E^{-1} in the wave regime, and at a much faster rate in the vacillating regime. The spectrum of the oscillations in the irregular regime appears to be split into at least two components. The coherence in this regime tends to decrease rapidly with distance from the thermocouple.

The results presented here lend to interesting speculation on future experiments. It would be quite valuable to obtain the transition line between the symmetric and regular wave

regime using an annulus with an even larger gap width. These results would produce a more significant estimate of the dependence of π_{4c} on π_5 . Experiments with the larger gap width would also indicate the behavior of the transition lines from the regular wave to the vacillating regime and from the vacillating to the irregular regimes. In the same context it appears essential that some information be obtained for moderate values of π_5 using an apparatus with slightly smaller gap widths than in the present experiment. The results of this latter work should be combined with the previous results of Fowles and Hide (1965) and the present work to determine the behavior of the transition to the irregular regime throughout this range of π_5 .

It would also be useful to obtain the temperature structure of the convecting fluid when the upper surface is in contact with a rigid lid. Under these conditions the flow in the symmetric regime is more symmetric in depth. The results just outside the boundary layer could be used as a comparison to the results obtained theoretically by McIntyre (1967). It also appears that a more detailed study of the structure of the boundary layer in all regimes for both a free upper surface and a rigid upper surface should be made. This study would also lead to more information as to how the boundary layers affect the flow, especially in the vacillating and the irregular regimes.

Accurate velocity measurement at various depths and radii would lead to greater understanding as to the nature of the stability of the symmetric flow. The measurements would have to be spaced so that any horizontal parabolic variation of the

zonal velocity could be detected in addition to the stronger linear horizontal shear which occurs in these experiments. These measurements, in conjunction with the measurement of potential energy, would also indicate the total energy balance occurring in the annulus regimes. Angular momentum transport and heat transport within each regime should also be calculated.

Finally, perhaps the most obvious experiment, is the determination of the statistical properties of the vacillating and irregular regimes. This study will require a long series of samples from a much closer network of sensors than used in the present experiment. The increase in the number of sensors used increases the possibility that the sensor will disturb the flow. In addition to this effect, there is the mechanical problem of attaining the large and stable rotation rates necessary to produce the irregular flow when an annulus with a large gap width is used.

REFERENCES

- Barcilon, V., 1963: "Thermally driven motion of a stably stratified fluid in a rotating annulus", Ph.D. dissertation, Harvard University.
- Barcilon, V., 1964: "Role of the Ekman layers in the stability of the symmetric regime obtained in a rotating annulus", J. Atmos. Sci. 21, 291-299.
- Bless, S.J., 1965: "The effect of a radial barrier on thermally-driven motions in a rotating fluid annulus", B.S. thesis, Department of Physics, M.I.T.
- Bowden, M., 1961: "An experimental investigation of heat transfer in a rotating fluid", Ph.D. dissertation, University of Durham, Newcastle upon Tyne, England.
- Bowden, M., Eden, H.F., and Hide, R., 1966: "An experimental study of the effect of a radial wall on thermal convection in a rotating annulus of liquid", in preparation.
- Bowden, M., and Eden, H.F., 1965: "Thermal convection in a rotating fluid annulus: temperature, heat flow and flow field observations in the upper symmetric regime", J. Atmos. Sci. 22, 185-195.
- Bowden, M., and Hide, R., 1968: "Experimental study of heat transfer by thermal convection in a rotating annulus of liquid: general survey", in preparation.
- Brindley, J., 1960: "Stability of flow in a rotating viscous incompressible fluid subjected to differential heating", Phil. Trans. Roy. Soc. London A 253, 1-25.
- Brindley, J., 1964: "Thermal convection in a rotating fluid annulus: a critical review of existing theory", Scientific Report No. 13, Hydrodynamics of Rotating Fluids Project, Department of Geology and Geophysics, M.I.T.
- Charney, J.G., 1947: "The dynamics of long waves in a baroclinic westerly current", J. Meteor. 4, 135-163.
- Charney, J.G., and Stern, M.E., 1962: "On the stability of internal baroclinic jets in a rotating atmosphere", J. Atmos. Sci. 19, 159-172.
- Cooley, J.W., and Tukey, J.W., 1965: "An algorithm for the machine computation of complex fourier series", Math. of Comp. , 297-301.
- Davies, T.V., 1953: "Large scale atmospheric flow patterns in the laboratory", Aero, Res. Coun. FM 1896, 15, 872, pp.

- Davies, T.V., 1956: "The forced flow due to heating of a rotating liquid", Phil. Trans. Roy. Soc. London A 249, 27-64.
- Davies, T.V., 1959: "On the forced motion of a deep rotating liquid", J. Fluid Mech. 15.
- Eady, E.T., 1949: "Long waves and cyclone waves", Tellus 1, 33-52.
- Eden, H.F., 1964: "Apparatus for investigating the temperature field due to convection in a rotating annulus of fluid", Technical Report No. 3, Hydrodynamics of Rotating Fluids Project, Department of Geology and Geophysics, M.I.T.
- Eden, H.F., and Piasek, S.A., 1967: "The effect of rotation on the free convective flow in a vertical cylindrical annulus", in preparation.
- Faller, A.J., 1957: "A laboratory model of the general circulation of the atmosphere", Ph.D. dissertation, M.I.T.
- Fisher, R.A., 1929: "Test of significance in harmonic analysis", Proc. R. Soc., A 125, 54-59.
- Fowles, W.W., 1964: "Apparatus for investigating the regimes of thermal convection in a rotating annulus of liquid", Technical Report No. 5, Hydrodynamics of Rotating Fluids Project, Department of Geology and Geophysics, M.I.T.
- Fowles, W.W., and Hide, R., 1965: "Thermal convection in a rotating annulus of liquid: effect of viscosity on the transition between axisymmetric and non-axisymmetric flow regimes", J. Atmos. Sci. 22, 541-558.
- Fultz, D., 1950: "Experimental studies of a polar vortex", Technical Report No. 1, USAF Contract AF 19 (122)-160, from Department of Meteorology, University of Chicago.
- Fultz, D., 1951: "Experimental analogues to atmospheric motions" in Compendium of Meteorology, 1235-1248.
- Fultz, D., 1952: "On the possibility of experimental models of the polar front wave", Scientific Report No. 4, USAF Contract AF 19 (122)-160, from Department of Meteorology, University of Chicago.
- Fultz, D. (ed.), 1956: "Studies in experimental hydrodynamics applied to large-scale meteorological phenomena", Final Report, Parts I and II, USAF Contract AF 19 (122)-160, from Department of Meteorology, University of Chicago.
- Fultz, D., 1956: "A survey of certain thermally- and mechanically-driven fluid systems of meteorological interest", in Fluid Models in Geophysics (ed. R.R. Long), U.S. Government, Washington, D.C., 27-63.
- Fultz, D., 1958: "Studies in experimental hydrodynamic analogues of the atmosphere", Final Report to USAF

- Geophysics Research Directorate, Contract AF 19(604)-1292.
(As quoted in Bowden and Eden, 1965).
- Fultz, D., Long, R.R., Owens, G.V., Bohan, W., Kaylor, R., and Weil, J., 1959: "Studies of thermal convection in a rotating cylinder with some implications for large-scale atmospheric motions", Meteorological Monograph 4. Boston: American Meteorological Society.
- Fultz, D., 1961: "Developments in controlled experiments on large-scale geophysical problems", Advances in Geophysics 7, 1-103.
- Fultz, D., 1964: "Research on hydrodynamic analogues of large-scale meteorological phenomena", Final Report to Air Force Cambridge Research Laboratories, OAR, USAF, Bedford, Mass.
- Haurwitz, B., 1961: "Thermally driven circulations in a rotating fluid system", Scientific Report No. 2, Contract AF 19(604)-5488, from High Altitude Observatory, University of Colorado.
- Hide, R., 1953: "Some experiments on thermal convection in a rotating liquid", Ph.D. dissertation, Cambridge University.
- Hide, R., 1953: "Fluid motion in the earth's core and some experiments on thermal convection in a rotating liquid" in Fluid Models in Geophysics (ed. R.R. Long), U.S. Government, Washington, D.C., 101-116.
- Hide, R., 1958: "An experimental study of thermal convection in a rotating liquid", Phil. Trans. Roy. Soc. London A 250, 442-478.
- Hide, R., 1963a: "Thermal convection in a rotating annulus: notation and dimensionless parameters", Scientific Note No. 1, Hydrodynamics of Rotating Fluids Project, Department of Geology and Geophysics, M.I.T.
- Hide, R., 1963b: "The theory of the effect of boundary layer friction on baroclinic instability of a rotating liquid", unpublished ms.
- Hide, R., 1963c: "On the transition between the upper symmetrical regime and the steady wave regime of thermal convection in a rotating annulus", Scientific Report No. 3, Hydrodynamics of Rotating Fluids Project, Department of Geology and Geophysics, M.I.T.
- Hide, R., 1964a: "Experiments on baroclinic instability and vacillation: a review", abstract published in Trans. A.G.U. 45, 142-143.
- Hide, R., 1964b: "The viscous boundary layer at the free

- surface of a rotating baroclinic fluid", Tellus 16, 523-529.
- Hide, R., 1965: "The viscous boundary layer at the free surface of a rotating baroclinic fluid: effects due to the temperature dependence of surface tension", Tellus 17, 440-442.
- Hide, R., 1966: "Review article on the dynamics of rotating fluids and related topics in geophysical fluid dynamics", B. Amer. Met. Soc. 47, 873-885.
- Hide, R., 1967: "On the vertical stability of a rotating fluid subject to a horizontal temperature gradient", J. Atm. Sci. 24, 6-9.
- Hide, R., 1967: "Theory of axisymmetric thermal convection in a rotating fluid annulus", The Physics of Fluids 10, 56-68.
- Hide, R., Bowden, M., Eden, H.F., Fowles, W.W., Ibbetson, A., and Titman, C.W., 1961: "Research on thermal convection in rotating fluids and on rotating barotropic fluids", Technical Summary Report, Contract AF61(052)-216, Geophysics Research Directorate, Cambridge (as quoted in Bowden and Eden, 1965).
- Hide, R., Bowden, M., Eden, H.F., Fowles, W.W., Ibbetson, A., and Titman, C.W., 1962: "Research on thermal convection in rotating fluids and on rotating barotropic fluids", Final Report, Contract AF61(052)-216, Geophysics Research Directorate, Cambridge.
- Hunter, C., 1967: "The axisymmetric flow in a rotating annulus due to a horizontally applied temperature gradient", J. Fluid Mech. 27, 753-778.
- Kuo, H.L., 1954: "Symmetrical disturbances in a thin layer of fluid subject to a horizontal temperature gradient and rotation", J. Met. 11, 399-411.
- Kuo, H.L., 1955: "On convective instability of a rotating fluid with a horizontal temperature contrast", J. Marine Res. 14, 14-32.
- Kuo, H.L., 1956a: "Energy releasing processes and stability of thermally driven motions in a rotating fluid", J. Met. 13, 82-101.
- Kuo, H.L., 1956b: "Forced and free axially symmetric convection produced by differential heating in a rotating fluid", J. Met. 13, 521-527.
- Kuo, H.L., 1957: "Further studies of thermally driven motions in a rotating fluid", J. Met. 14, 553-558.
- Lorenz, E.N., 1953: "A proposed explanation for the existence

of two regimes of flow in a rotating symmetrically heated cylindrical vessel", Fluid Models in Geophysics (ed. R.R. Long), U.S. Government Printing Office, Washington, D.C., pp.73-80.

- Lorenz, E.N., 1960: "Maximum simplification of the dynamic equations", Tellus 12, 243-254.
- Lorenz, E.N., 1962: "Simplified dynamic equations applied to the rotating basin experiment", J. Atmos. Sci. 19, 39-51.
- Lorenz, E.N., 1963: "The mechanics of vacillation", J. Atmos. Sci. 20, 448-464.
- McIntyre, M.E., 1967: "The axisymmetric convective regime for a rigidly-bounded rotating annulus", in preparation.
- Nowroozi, A.A., 1967: "Table for Fisher's test of significance in harmonic analysis", Geophys. J.R. Astr. Soc. 12, 517-520.
- Pedlosky, J., 1964a: "The stability of currents in the atmosphere and the ocean, Parts I and II", J. Atmos. Sci. 21, 201-219, 342-353.
- Pedlosky, J., 1964b: "An initial value problem in the theory of baroclinic instability", Tellus 16, 12-17.
- Pedlosky, J., 1965: "On the stability of baroclinic flows as a functional of the velocity profile", J. Atmos. Sci. 22, 137-145.
- Pedlosky, J., 1966: Lecture notes and problem sets given in a course titled Special Problems in Applied Mathematics, M.I.T.
- Pfeffer, R.L., and colleagues, 1965: "A new concept of available potential energy", Final Report, U.S. Weather Bureau Grant WBG 45, Report 66-1, Department of Meteorology, Florida State University.
- Phillips, N.A., 1963: "Geostrophic motion, Rev. of Geophys. 1, 123-173.
- Piacsek, S., 1966: "Thermal convection in a rotating annulus of liquid: numerical studies of the axisymmetric regime of flow", Ph.D. dissertation, M.I.T.
- Riehl, H., and Fultz, D., 1957: "Jet streams and long waves in a steady rotating dishpan experiment: structure and circulation", Quart. J. Roy. Met. Soc. 83, 215-231.
- Riehl, H., and Fultz, D., 1958: "The general circulation in a steady rotating dishpan experiment", Quart. J. Roy. Met. Soc. 84, 389-417.
- Robinson, A.R., 1959: "The symmetric state of a rotating fluid

- differentially heated in the horizontal", J. Fluid Mech. 6, 599-620.
- Rogers, R.H., 1959: "The structure of the jet stream in a rotating fluid with a horizontal temperature gradient", J. Fluid Mech. 5, 41-59.
- Rogers, R.H., 1962: "The effect of viscosity near the cylindrical boundaries of a rotating fluid with a horizontal temperature gradient", J. Fluid Mech. 14, 25-41.
- Rossby, H.T., 1964: "Operating instructions for the digital data acquisition system", Laboratory Note No. 3, Hydrodynamics of Rotating Fluids Project, Department of Geology and Geophysics, M.I.T.
- Schulman, E.E., 1967: "The baroclinic instability of a mid-ocean circulation", Tellus 19, 292- .
- Smith, A.R., 1958: "The effect of rotation on the flow of a baroclinic liquid", Ph.D. dissertation, Cambridge University (as quoted in Fowles and Hide, 1965).
- Starr, V.P., and Long, R.R., 1953: "The flux of angular momentum in rotating model experiments", Geophys. Res. Pap. 24, 103-113.
- Williams, G.P., 1967: "Thermal convection in a rotating fluid annulus: Part 1. the basic axisymmetric flow", J. Atm. Sci. 24, 144-161.
- Williams, G.P., 1967: "Thermal convection in a rotating fluid annulus: Part 2. classes of axisymmetric flow", J. Atm. Sci. 24, 162-174.

APPENDIX 1

DESIGN AND CONSTRUCTION OF THE 42 INCH ANNULUS

Several years of previous experimental work on thermal convection in a rotating annulus have made it desirable to obtain accurate and detailed measurements of the thermal structure and the velocity structure of the various convecting regimes. In addition, the results also indicated the desirability of obtaining the state of the flow at large values of Ekman numbers or when the percentage of total fluid under the effect of the viscous side wall boundary was reduced from that of previous experiments. The former investigation can only be done when the dimensions of the sensor used or its disturbance to the flow are much smaller than the physical scale of the apparatus. The current version of the 42 inch annulus at the Rotating Fluid Dynamics Laboratory at M.I.T. was designed with these experiments in mind. This apparatus will be set up in the Meteorological office at Bracknell, Berkshire in the United Kingdom, under the direction of Dr. Raymond Hide. A prototype of the apparatus was originally built by Dr. Fowlis. In the interest of obtaining greater accuracy and more versatility this prototype was redesigned and rebuilt with the exception of the turntable, the turntable stand and the circulation units. This apparatus conforms to the following specifications:

1. The walls of the convection chamber are concentric to the axis of rotation within ± 0.005 inches.
2. The gap width (b-a) is uniform with ± 0.0075 inches, and consequently a false bottom with an O ring seal is water-tight so lighting can be placed below the convection chamber and the position of the bottom varied.

3. The turntable is level within ± 0.5 min. over the area of the convection chamber.
4. The stability of the rotation rate of the apparatus is $\pm 0.089\%$ (standard deviation).
5. The false bottom of the convection chamber is flat to within ± 0.005 inches.

The remaining section of the appendix will describe the design and construction of the apparatus which is shown schematically in Figure 7A.

Turntable and drive mechanism

The turntable is a $\frac{1}{2}$ inch flat ground steel plate with ^a 42 inch outside diameter. This is mounted on a 22.5 inch diameter four point contact radial and thrust ring bearing. (Kaydon Engineering Corp. No. B-8090-1). The bearing is bolted on the underside to a $\frac{1}{2}$ inch steel ring which in turn is fastened to a welded triangular frame made of one inch square tubular steel. The frame is supported with three steel legs with individual leveling screws on each. When correctly mounted the edge of the turntable runs with a vertical deviation of ± 0.005 inches with respect to the plane of rotation at a distance of 21 inches from the axis of rotation.

A hollow stainless steel shelf is fastened underneath the table concentric to the axis of rotation. This has been turned at the top to 6.500 inches to support the eight coin silver power slip rings (Airflyte Electronics Corp. part # CSR-342). Below the slip rings, it has been turned to 6.543 inches in order to make a positive, concentric mount for a reamed Browning 72 teeth pulley. The four channel fluid slip rings are mounted

inside this shaft.

The table is driven by a $\frac{1}{2}$ h.p. 220 volt synchronous motor with a Graham variable speed transmission. This is coupled to the table by an 18 or 36 notch Browning one inch pulley on the transmission, a one inch wide Browning notched belt, and the 72 notch gear on the turntable shaft. The Graham transmission could be modified to supply a maximum output speed of 20 rpm. as an N30W60 series or of 48 rpm. as a N29W23 series. Experiment runs 1-56 were run with the former unit which means that the turntable required about $\frac{1}{3}$ the total output power of the drive. Experiment runs 57-73 were made with the N29W23 and the turntable required approximately one-half the total output power of the transmission unit.

The average standard deviation calculated from 39 different runs was 0.086%. This includes all the standard runs of Experiment Number 1 with the exception of four runs whose deviations were at least three times larger than the standard deviation of the sample. These large errors were probably due to improper setting of the Beckman timing triggers and associated circuitry.

Convection chamber and baths

On the top of the turntable six 3.5 x 2 x 17 inch canvas phenolic support spacers are mounted at 60 degree intervals. A $\frac{1}{2}$ inch thick by 40 inch diameter phenolic plate is mounted on top of these spacers. Each spacer is carefully shimmed so that the top of the plate runs true in the vertical to ± 0.0025 inches

and is level to within ± 0.5 min. near the mounting points for each cylinder. The copper cylinders which form the wall of the convection chamber are fastened to this plate with six $5/16$ inch stainless steel bolts. $1/8$ inch Burna-N O rings placed in grooves in the base plate under each cylinder serve as the seal for each bath.

Three copper cylinders were made for the annulus so that different gap widths could be used. These cylinders were made from copper casting done at the Mystic Valley Foundry, Somerville, Mass. The castings were carefully turned and faced by General Ship and Engine Works, Boston, Mass. The final dimensions and tolerances of each of the three cylinders are given in Table V. In this experiment only cylinders II and III were mounted with final concentricities of ± 0.0025 inches and ± 0.005 inches, respectively. The maximum variation of the gap width is ± 0.0075 inches. It is interesting to note that careful alignment and tightening of cylinder III actually improved the tolerances of the gap width.

The bottom of the convection chamber is made from a circular disk of one inch type II plexiglas. O ring grooves for $3/16$ inch Neoprene O rings are milled on the inner and outer edges to form a water^otight seal between each cylinder. This is supported six inches above the phenolic base by seven six inch milled phenolic blocks. When carefully installed the vertical deviation of the bottom with respect to the plane of rotation is ± 0.005 inches. Radial grid lines are drawn every 5 degrees and azimuthal grid lines are drawn every 3 cm for a 120 degree

sector on the underside of the false bottom. These are covered with diffusing paper. Three 9 inch fluorescent lights are mounted under this sector for lighting in dye studies.

The outer boundary of the outside bath is formed with a one inch thick by 18 inch high and 38 inch inside diameter plexiglas cylinder. This was faced on both top and bottom, and the top inside edge turned to be concentric for a depth of one inch to accommodate an O ring seal. The inner bath consists of the inside volume of the inner cylinder. Both baths are then closed with a 3/4 inch plexiglas type II lid with 1/8 inch Burna-N O ring grooves on each sealing surface. The outer and inner bath capacities of the apparatus with cylinders III and II mounted are 28.5 gallons and 18.0 gallons, respectively.

The walls of the convection chamber are maintained at an almost constant temperature by circulating water through the baths. The temperature and flow rate of the circulating water is maintained with two Haake Circulators Type N.B.S. These have a temperature range from 0°C. to 50°C. with a setting increment of 0.025°C. Under full normal operating conditions the temperature of the inflowing water to each bath varies by less than 0.1°C. and has a flow rate of 2.4 gallons/minute. In the experiment the temperature of the colder bath was maintained below room temperature by using two coolers in parallel with the temperature control circuit of the circulator. The mean temperature of the baths was adjusted to room temperature.

The baths are constructed so that this water is released into the baths through any combination of four circulation

rings. These rings are made from $\frac{1}{2}$ inch rolled copper tubing with $72 \frac{1}{8}$ inch holes drilled in them such that the circulating water is forced directly toward the wall. The circulation tubes are mounted $1 \frac{1}{2}$ inches from each wall at the heights of 1, 6, 12, and 17 inches from the phenolic base. They are suspended by means of slots cut in six $1/16$ inch copper fins mounted on the bath side of each copper cylinder. Each fin consisted of two blades where each blade extends into the bath 3 inches.

In general more heat is removed from the baths near the bottom of the warm wall and more heat is added near the top of the cold wall; consequently, the optimum circulation pattern is to add the fresh fluid near the lower two circulations in the warm bath and extract the fluid from the top of this bath. The reverse is true for the cold bath. The bath liquid is directed towards the wall in order to help create more turbulent boundary layers and consequently decrease the temperature drop occurring between the bath and the convection chamber wall.

The temperature of each wall could be monitored with 24 copper constantan thermocouples. These were constructed from Leads and Northrup # 30-55-3 wire, threaded through clear flexible tubing and sealed at the ends. Each thermocouple was positioned 0.1 inch from the edge of the convection chamber wall. The 24 thermocouples are mounted in three sets of five vertical positions and three sets of three vertical positions. The set of five thermocouples are mounted at $1 \frac{1}{2}$, 6, 9, 12 and $16 \frac{1}{2}$ inches in height from the phenolic base and at 120 degree intervals. The set of three thermocouples are mounted at $1 \frac{1}{2}$,

9, $16\frac{1}{2}$ inches in height and 120 degree intervals, the latter separated from the former by 60 degrees. These thermocouples can be read individually or the thermocouples spanning the convection chamber can be summed so that an average temperature difference between the warm and cold wall can be obtained.

The vertical temperature variation in the wall due to the preferential removal of heat is indicated in Figure 8. This is a variation of $\pm 3\%$ of ΔT . Since this effect is just the opposite on the cold wall the deviation in the impressed temperature difference at any one height is much less than this variation. There is also a noticeable variation in the local temperature of the wall as a wave lobe passes that point. This amounts to a maximum local variation of $\pm 2.5\%$ of ΔT . The azimuthal average of this variation is zero.

Convection chamber thermocouples

After several different methods of suspending movable thermocouples in the bath were tried, unsuccessfully, it was decided to use thermocouples rigidly suspended from the upper lid and the false bottom. This allows the use of very small thermocouple wire, thus causing a minimum disturbance to the fluid. These thermocouples can also be positioned accurately. This is accomplished by having four $5/16$ inch reamed holes at 1.02 cm, 5.42, 9.82 and 14.22 cm from the equivalent edge of the outer cylinder cut in the false bottom, each hole being separated by 60 degrees in azimuth. In this way several $5/16$ inch plugs with a shallow grease ring cut in each to prevent capillary action can be used to plug up the hole and support one

end of the thermocouple array. Several such plugs were made with 0.005 inch Omega Engineering constantan thermocouple wire suspended from a sealed .025 inch center hole. The copper leads were soldered to the constantan wire at ≈ 0.025 cm. scrape in the constantan wire made at 1.02, 5.42, 9.82, 14.22 cm. from the top of the plug. The other end of the constantan lead was securely fastened at the top from a milled spacing block with a 0.025 inch hole for positioning. When tightened and set in place the position of each thermocouple junction should be known in the vertical direction by ± 0.025 cm and in the radial direction by ± 0.033 cm. This uncertainty introduces a maximum error of $\pm 0.012^{\circ}\text{C}$. with an impressed temperature difference of $10^{\circ}\text{C}^{\circ}$ in the upper symmetrical regime near the transition.

The constantan lead from each of the convection chamber thermocouples is connected to a reference junction in an ice bath on the turntable made from a wide mouth dewer flask filled with ice and water. All of the readings are then relative to this reference point, and only 17 leads are needed to obtain the temperature of the 16 thermocouples in the bath.

The copper leads from each thermocouple and the reference junction are connected to either a 15 pin or a nine pin cannon plug. These can then be connected to the cannon plugs which lead to the 36 silver plated thermocouple slip rings. These slip rings are connected to the recording apparatus using a five foot patch cord. In the same manner the individual leads or the two leads indicating the sum of the temperature difference for the wall thermocouple can be connected to the slip rings.

Electrical recording and measuring systems

Three different systems were used to record the thermocouple voltages. These are a four channel Beckman Instruments analog recorder, a Leads and Northrup potentiometer and a digital data ^{acquisition} system. Each system can be connected directly to the 37 lead cannon plug patch cord or to a 24 position double deck thermocouple selector switch. The connections to the analog recorder and digital data acquisition systems are indicated in Figure 7b.

The Beckman Instruments Dynograph type SII four channel recorder can be used to obtain an analog record of any four signals. A separate switching box allows an absolute reference for each channel to be set with the digital voltmeter. The recorder has a maximum sensitivity of 1 uv/div with a noise level less than 1 uv. rms. The Leads and Northrup potentiometer is generally used in connection with the selector switch for individual thermocouple readings during calibration.

The digital data acquisition system consists of a stepping switch and logic circuit, a preamplifier, digital voltmeter and a paper tape punch adapter and punch. The stepping switch (Sigma Cohn) is a twenty position triple deck switch driven by a Sigma Cohn cyclopulser unit. The upper deck is used for the thermocouple signals while the lower deck is required to program the logic circuit. The upper deck has been carefully insulated and shielded, and it contains one reference zero position on each side.

The logic circuit was designed by Mr. Don Sordillo of M.I.T.

with the use of Digital Data Corporation flip chip modules. The circuit is shown schematically in Figure 27. The R 302 (A2) is the flip flop unit and the W601 is the pulse conversion unit which together signal the cyclopulser to start to step the stepping switch. This moves the switch one position with a period of the time constant of the R 302 (A2) circuit. This is initiated by grounding pin E of R 111 (A1) with a microswitch. The cycle is stopped when a signal of 3 volts is applied to pin P of the R 302 (A2). A separate logic circuit exists for programming the digital voltmeter. It consists of the flip flop unit R 302 (B2), a pulse shaping unit R111 (B3) and a conversion unit W 600 (B4). The unit is triggered at the same time the stepping switch steps. It is programmed so that the digital voltmeter will read the signal τ ms. after the stepping switch is positioned. τ is the variable time constant of the R 302 (B2) and was generally set at 300 ms. This read signal can be suppressed by programming the lower deck of the stepping switch to connect pin P of the R 302 (B2) to ground.

During the experiments the logic system was set to step through 20 positions continuously every 9.8 seconds. Nineteen readings were recorded consisting of one zero reference, the 16 thermocouples in the array, and two zero references. The maximum sample time, determined by the length of the paper tape, was approximately two hours.

Discussion of error

The maximum error due to the measurement of the dimensions of the convection chamber occurs in the determination of the

depth. This measurement is accurate to $\pm 0.5\%$ of the reading whereas, the gap width is known to within $\pm 0.01\%$. The rotation rate is approximately constant at $\pm 0.089\%$ (standard deviation). The largest error in the determination of the dimensionless parameters is then due to the variation of the wall temperature which, as noted previously, can introduce an error of $\pm 3\%$ of ΔT . In addition to this the local temperature of the wall may vary by $\pm 2.5\%$ in the wave regime with a period of the wave. This effect is also noticeable in the determination of the average temperature difference between the walls when six waves are present and in phase with the six sets of wall thermocouples. The results of this measurement correspond to an average local temperature variation of $\pm 0.05^{\circ}\text{C}$. This effect was averaged out in the determination of ΔT and consequently should not strongly affect the mean results for the dimensionless parameters.

The determination of error for the temperature measurements has many factors and since all thermocouples were referenced to the same ice bath thermocouple, we will only discuss the relative accuracy of each measurement. The maximum error due to misalignment and incorrect spacing of the thermocouple is $\pm 0.01^{\circ}\text{C}$. The noise level of the Dana preamplifier is ± 0.05 uv or $\pm 0.012^{\circ}\text{C}$. The digital voltmeter which was set to read to the nearest uv introduces a maximum round off error of $\pm 0.025^{\circ}\text{C}$. Errors due to thermal differences across the cannon plugs and other junctions in the stepping switch can be estimated from the calibration results as ± 1 .uv or $\pm 0.025^{\circ}\text{C}$. An additional error in the calibrations will occur for the four

surface array thermocouples since the local temperature near the surface cannot be measured accurately enough. This error should be $\pm 0.025^{\circ}\text{C}$. Thus, the maximum error for the 12 thermocouples at depths greater than 5 cm is $+ 0.072$ and $- 0.047^{\circ}\text{C}$. The maximum error for the four thermocouples near the surface is $+ 0.097$ and $- 0.072^{\circ}\text{C}$. This latter error could have been reduced simply by filling the annulus chamber with more water during the calibration. In general the relative error will be less than this since most results depend on a time average of these quantities and the random errors introduced by the noise levels of the electronics will be reduced by a factor of $1/\sqrt{N}$ where N is the total number of samples taken. N is generally greater than 100.

Suggestions for future modifications

The apparatus runs very well in its present state. However, some additional improvements should be made. Some attempt should be made to improve the control of the wall temperature with the addition of several more circulation tubes in each bath. In addition several more thermocouples should be added to each wall in order to determine the actual temperature variation more accurately. The inside edge of the outer bath leaks slightly unless some silastic sealant is used for an additional seal. This can be stopped either by replacing the current $1/8$ inch Buna-N O ring with a larger and softer neoprene O ring, or by adding an additional $1/8$ inch O ring seal to the top. Finally, some modification must be made to the turntable drive so that more stable and larger rotation rates can be attained as necessary in the study of the irregular regime.

Figure 27. Stepping switch logic circuit.

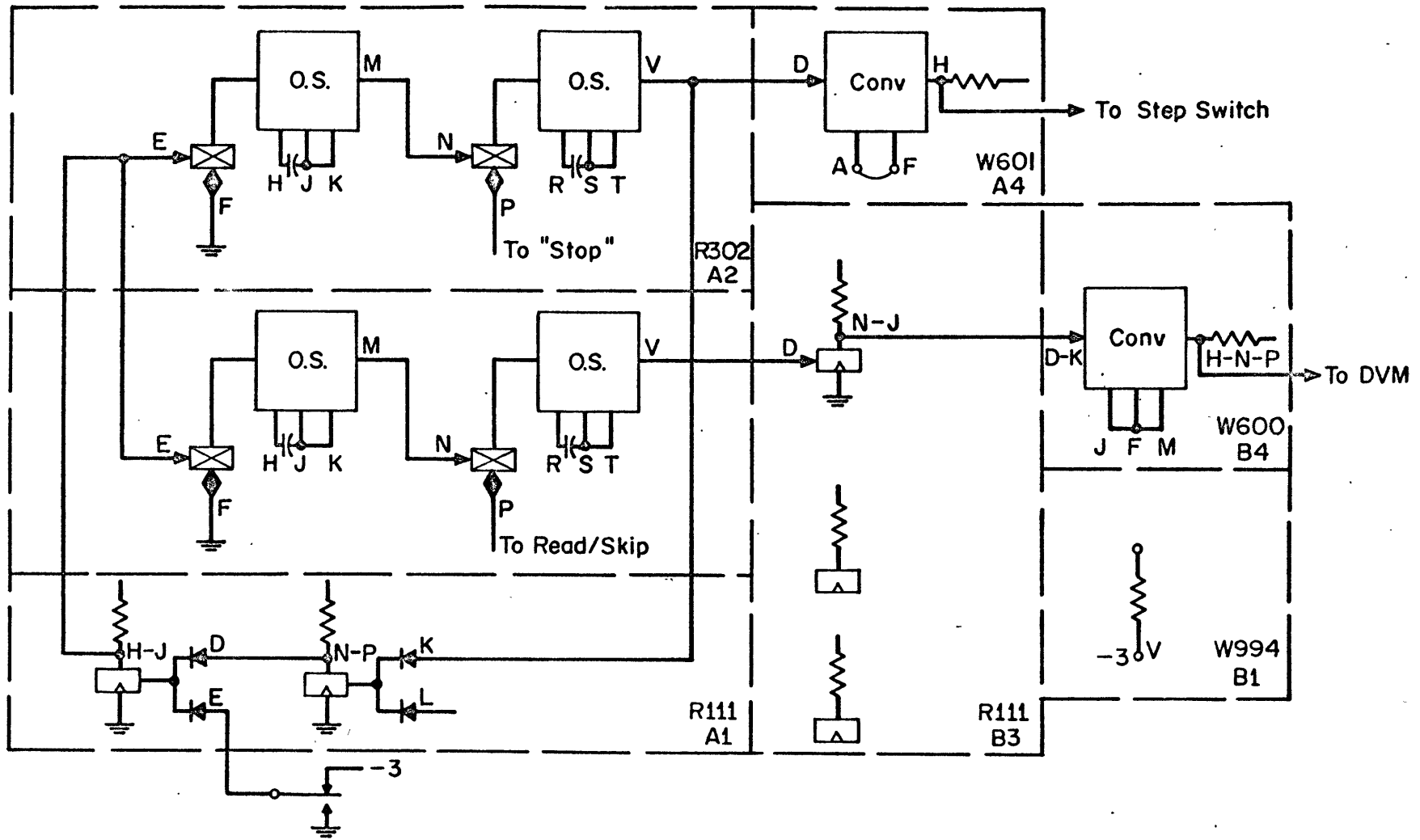


Figure 27

TABLE 4

Inner Cylinders		Wall Thickness	Height
O.D. (inches)	I.D. (inches)	(inches)	(inches)
I 9.982 \pm 0.001	8.966	0.508	17.997
II 18.239 \pm 0.001	17.200	0.520	18.000
Outer Cylinder			
III 31.237	30.272 \pm 0.008	0.432	18.000

APPENDIX 2

METHODS FOR THE CALCULATION OF EXTERNAL AND INTERNAL
EXPERIMENTAL PARAMETERS, AVAILABLE POTENTIAL
ENERGY AND TIME SERIES ANALYSIS

The purpose of this appendix is to define the formulae used to compute the external experimental parameters, the internal parameters of the flow, the potential energy of the flow and the manner in which the time series analyses were made. All of these calculations were done at the M.I.T. Computation Center except for a small section which was done at the computation center at the State University of New York at Albany.

The external parameters were calculated from the measured value of the mean temperature, T_m , determined by the average of the inflow and outflow temperatures of each bath, the mean rotation rate, Ω , computed from the mean of ten rotation periods, the mean temperature difference, ΔT , which was computed from the mean value of difference between the wall thermocouples, and the measured dimensions of the apparatus. Using this rotation, the mean density is:

$$\rho_m = 0.9976846 \times (1 - 0.000232218 \times (T_m - 22.5) - 0.000005052 (T_m - 22.5)^2) \quad \text{A.2.1}$$

to within 0.001% of the range covered in this experiment. The mean temperature difference is given by

$$\Delta T = \frac{\Delta E}{100} \times 2.473 - 0.00625 \times \left(\frac{\Delta E}{100}\right)^2 \quad \text{A.2.2}$$

where ΔE is the mean difference in uv of the wall thermocouples

output. This is accurate to within + 0.05% of ΔT over the range of the experiment. The density difference is then calculated by substituting $T_m + \Delta T/2$ and $T_m - \Delta T/2$ in the equation A.2.1 and subtracting ^{the two results}. The resulting value of $\Delta \rho$ is:

$$\Delta \rho = 0.9976846 (0.000232218 + 0.000010104) (T_m - 22.5) \quad \text{A.2.3}$$

* ΔT

The mean viscosity is given by

$$\nu_m = 0.01 (0.9640 - 0.0224 \times (T_m - 22.0)) \quad \text{A.2.4}$$

The nondimensional parameters are calculated using these values for the variables with $g = 980 \text{ cm/sec}^2$.

The temperature of the convecting fluid is determined from the output of the thermocouples, $E(I, J)$, in micro volts with the following formula:

$$\begin{aligned} \text{Temp} (I, J) &= 2.473 (E(I, J) - 900)/100 \quad \text{A.2.5} \\ &- 0.00625 ((E(I, J) - 900)/100)^2 + 22.80 \end{aligned}$$

The nondimensional temperature, Temp' , can be written as:

$$\text{Temp}' (I, J) = (\text{Temp} (I, J) - T_m)/\Delta T \quad \text{A.2.6}$$

The internal parameters were generally defined in terms of a volume average over the thermocouple array. The weight given to each thermocouple was determined by the volume of fluid its measurement could represent. Thus, the corner thermocouples values were weighted with $\frac{1}{4}$ and the other edge thermocouples were weighted with $\frac{1}{2}$ of the weight of the interior thermo-

couples. The average defined in this way extends only to the edge of the array. Let $R(I)$, $I = 1, 4$ denote the radial position of each vertical thermocouple array.

In this experiment $(R(I), I = 1, 4) = 37.405, 33.005, 28.605, 24.205$. Further, let the incremental distance dR and dz be written as: $\delta R(I)$ and $\delta Z(J)$ respectively:

$$(\delta R(I), I = 1, 4) = 2.2, 4.4, 4.4, 2.2$$

$$(\delta Z(J), J = 1, 4) = 2.2, 4.4, 4.4, 2.2$$

Then the volume integral of a quantity $A(I, J)$ whose I index represents the different radial positions and whose J index represents the different vertical positions is:

$$\iiint A r dr dz = 2\pi \sum_{I, J=1}^4 A(I, J) R(I) dR(I) dZ(J) \quad \text{A.2.7}$$

where we have implicitly assumed that $A(I, J)$ already represents some type of equivalent azimuthal average. In this manner we can compute the following:

$$\Delta T \sigma_z = \frac{d \cdot 2\pi}{\text{Volume}} \sum_{I=1}^4 (T(I, 4) - T(I, 1)) \cdot R(I) \cdot dR(I) \quad \text{A.2.8}$$

and

$$\Delta T \sigma_r = \frac{(b-a)2\pi}{\text{Volume}} \sum_{I=1}^3 \sum_{J=1}^4 T(I, J) - T(I+1, J) \cdot \frac{1}{2} (R(I) + R(I+1)) \cdot dR(I) dZ(J) \quad \text{A.2.9}$$

where the volume is $13.2 \times \pi \times (R^2(1) + R^2(4))$, i.e. the volume of the thermocouple array. The Eady number and Rossby number can then be computed from these values.

The potential energy of a stratified fluid of height d can be written as:

$$P.E. = \iiint_{\text{volume}} g \cdot \rho(x, y, z; t) Z d\tau \quad A.2.10$$

where Z represents the height above the level surface of the isopycnal surface of density ρ .

Using the equation of state for water, the density can be written as:

$$\rho = \rho_m (1 - \alpha(T - T_m)) \quad A.2.11$$

where the subscript m indicates the volume average of that quantity and T is the temperature at any point in the fluid.

Equation A.2.8 can be written as

$$PE = \frac{1}{2} \rho_m g \cdot \text{Volume} - g \rho_m \iiint (T - T_m) \alpha Z d\tau \quad A.2.12$$

where the triple integral is taken over the volume of the fluid and $d\tau$ represents the differential volume element. This integral can be evaluated by replacing Z by the sum of the heights Z_r and Z' where Z_r is the height of a geopotential surface along which the mean value of temperature is \tilde{T} and Z' is the deviation in height of the isotherm \tilde{T} from the surface Z_r at any point on the surface. With the assumption that the height Z' can be expressed as a Taylor series in temperature about the surface

$$\text{or } Z' = -T'_r \left(\frac{\partial T}{\partial Z} \right)^{-1} \quad A.2.13$$

where $T'_r = T_r - \tilde{T}$ and T_r is the temperature at any point on the surface, Z_r , Equation A.2.9 becomes

$$P.E. = \frac{1}{2} \rho_m g \cdot \text{Volume} - g \rho_m \iiint (\bar{T} + T' - T_m) \alpha z_r d\tau$$

$$+ g \rho_m \iiint \alpha (\bar{T} + T' - T_m) T' \left(\frac{\partial T}{\partial z} \right)^{-1} d\tau \quad A.2.14$$

Since the average of T' over the surface Z_r is zero, the above equation can be written as:

$$P.E. = \frac{1}{2} \rho_m g \cdot \text{Volume} - g \rho_m \iiint (\bar{T} - T_m) \alpha z_r d\tau$$

$$+ g \rho_m \iiint \alpha (T')^2 \left(\frac{\partial T}{\partial z} \right)^{-1} d\tau \quad A.2.15$$

The first term is the potential energy of a homogeneous fluid of density ρ_m . The second term is a correction to the first term due to the horizontally averaged vertical stratification. The last term represents the potential energy due to the inclination of the isotherms or isopycnals to the geopotential surface.

The available potential energy of the fluid can be defined, Lorenz (1955), as the difference between the potential energy of present fluid state and that which would result if all the isopycnal surfaces were made parallel to the geopotential surfaces (i.e. $T' = 0$). The resultant of this difference in Equation A.2.15 is

$$APE = \iiint g \rho_m \alpha (T')^2 \left(\frac{\partial T}{\partial z} \right)^{-1} d\tau \quad A.2.16$$

The available potential energy can be considered as the

sum of two terms, the radial available potential energy and the zonal available potential energy. The radial available potential energy is:

$$\text{RAPE} = \iiint g \rho_m \alpha (\bar{T} - \bar{T}')^2 \left(\frac{\partial T}{\partial Z} \right)^{-1} d\tau$$

and the zonal available potential energy is:

$$\text{ZAPE} = \iiint g \rho_m \alpha (T'')^2 \left(\frac{\partial T}{\partial Z} \right)^{-1} d\tau$$

where $T_p(r, \theta, Z_r; t) = \bar{T}(r, \theta, Z_r; t) + T''(r, \theta, Z_r; t)$

and the bar indicates a time average which is interpreted in this experiment as equivalent to the azimuthal average.

In the calculation the surface Z_r was chosen as that geopotential surface which crosses the radial mid point of each horizontal row of thermocouples. The value of the temperature along this surface was interpolated from the neighboring vertical values and the vertical temperature gradient $\frac{\partial T}{\partial Z}$ was estimated by the difference in temperature between the two vertical probes between which the surface Z_r passes. The volume average can then be computed as previously indicated.

Spectral analysis

The power spectrum, cospectrum and coherence for each run were obtained from a Fourier transform of the temperature matrix. The transform of the data is computed using a subroutine supplied and written by Dr. Ralph Wiggins of M.I.T. This routine uses an algorithm for fast computations of 2^h frequency

estimates similar to that described in Cooley and Tukey (1965).

The power spectrum values for each frequency estimate n are given by:

$$\phi_{aa}(n) = F_a(n) F_a(n)^*$$

where $F_a(n)$ is the transform of the data vector, * indicates the complex conjugate, and the subscript, a , indicates the specific thermocouple output used. The significance of the power spectrum level can be tested using a method proposed by Fisher (1929). This method determines a level with a confidence of N percent, below which all harmonic peaks would fall if calculated from a similar set of completely random data with the same standard deviation. Tables for the calculation of these levels for 99, 98, 95 and 90% confidence levels are given in Nowroozi (1967).

The complex cospectrum between two thermocouple outputs, a and b , for each frequency estimate is:

$$\phi_{ab}(n) = F_a^*(n) F_b(n)$$

The amplitude of the cospectrum is:

$$\left| \phi_{ab}(n) \right| = \left(\phi_{ab}(n) (\phi_{ab}(n))^* \right)^{\frac{1}{2}}$$

The phase, θ , of the cospectrum is:

$$\theta = \tan^{-1} \frac{\text{Im}(\phi_{ab}(n))}{\text{Re}(\phi_{ab}(n))}$$

The significance of the cospectrum values, ie, whether the peaks relate to the same physical process or not, can be checked

by determining if the phases of the neighboring frequencies are in the same relationship to each other. An estimate of the relationship is the coherency defined as:

$$\text{coherency}^{(n)} = \frac{1}{K+1} \sum_{J=N-K/2}^{n+K/2} \frac{\phi_{ab}(J)}{|\phi_{aa}(J)| |\phi_{bb}(J)|} \quad \text{A.2.17}$$

This quantity has a maximum value of unity when all the phases over the neighboring estimates are correlated.

In this text the Fourier transform for each thermocouple was calculated from a smoothed digital output. Each data record $X(J)$ was smoothed according to the formula:

$$X(j) = \frac{1}{4} X(J-1) + \frac{1}{2} X(j) + \frac{1}{4} X(J+1)$$

This filters out any oscillation with a period less than 20 sec. Sixty four estimates were made for each record and the power spectrum, cospectrum and phase calculated with reference to thermocouple T(3,3). The significance level was estimated in the manner indicated above. The coherency at each frequency estimate was calculated with $k = 2$ in Equation A.2.17 .

AUTOBIOGRAPHICAL NOTE

The author was born on January 3, 1941 in Boston, Massachusetts. He attended the Falmouth Massachusetts secondary school system. In 1962 he received a B.S. degree in Physics and Mathematics from Bates College, Lewiston, Maine. He received an M.S. degree from the Department of Meteorology and Oceanography at New York University, New York in 1967. In September 1964 he enrolled as a graduate student in the Department of Geology and Geophysics at Massachusetts Institute of Technology.

He received the Chemical Rubber Company achievement award in Physics from Bates College in 1960. He also received the Tidewater Oil Company fellowship for his first year of graduate study at ^{the} Massachusetts Institute of Technology.

The author is currently an assistant professor of Atmospheric Sciences at the State University of New York at Albany. He is a member of the M.I.T. chapter of the Society of Sigma Xi. He is married and has two children.